MECHANISMS OF ALKA-CATALYZED AND ACID-CATALYZED 2’-DEOXYINOSINE HYDROLYSIS

TOWARDS THE MECHANISMS OF ALKA-CATALYZED AND ACID-CATALYZED 2’-DEOXYINOSINE HYDROLYSIS: INVESTIGATIONS INTO LEAVING-GROUP ACTIVATION AND TRANSITION STATE STRUCTURE

By VINCENT AZHIKANNICKAL, B.Sc.

A Thesis Submitted to the School of Graduate Studies in Partial Fulfilment of the
Requirements for the Degree Doctor of Philosophy
McMaster University

McMaster University DOCTOR OF PHILOSOPHY (2015) Hamilton, Ontario

(Chemical Biology)

TITLE: Towards the Mechanism of AlkA-Catalyzed *N*-Glycoside Hydrolysis: Investigations into Leaving-Group Activation and Transition state Structure

AUTHOR: Vincent Azhikannickal, B.Sc. (University of Waterloo)

SUPERVISOR: Professor Paul Berti NUMBER OF PAGES: xviii, 168

Lay Abstract

When DNA, the genetic material in all living things, is chemically damaged, the health of the cell and its daughter cells is affected. To protect against DNA damage, proteins are produced by all cells to repair DNA. These proteins usually perform chemical reactions on a single type of damage in DNA, but *Escherichia coli* AlkA (3-methyladenine DNA glycosylase II) reacts with several types of damage. To study how AlkA participates in these varied reactions, its behaviour was examined under different conditions. The results show that it does not closely interact with the nucleobase of the damaged DNA. Additional aspects of the reaction in the presence and absence of AlkA were studied using an experimental method in which AlkA reacts with radioactive DNA. Attempts to use this method did not yield data that were reproducible enough to reveal an even more detailed picture of this reaction.

Abstract

Escherichia coli AlkA (3-methyladenine DNA glycosylase II) is a DNA repair enzyme that can excise both damaged and undamaged nucleobases. To determine whether AlkA's excision of neutral purines is facilitated by general-acid catalysis (i.e., protonation of the nucleobase), pH vs. k_{cat} and pH vs. $k_{\text{cat}}/K_{\text{M}}$ profiles for hypoxanthine excision were generated. Each profile revealed acid catalysis and a single pK_{a} of 5.7 ± 0.1 and 5.1 ± 0.2, respectively. Mutants of ionizable and hydrogen-bonding active site residues – Y273F, W272F, Y222F, R244M, and R22M – demonstrated at most a 4-fold reduction in hypoxanthine excision, so these residues were not involved in purine protonation. A dependence on buffer concentration was observed in the mutants at pH 7 and in wild-type AlkA at pH 7 and 8 but not at pH < 7. Solvent deuterium kinetic isotope effects (KIEs) at pH 6 and 7 showed that proton transfer was rate-limiting at pH 7 when [DNA] > K_{M} (K_{M} = 1.0 μM). AlkA could not bind adenine, hypoxanthine, and nicotinamide along with a transition state-mimicking pyrrolidine DNA. Therefore, AlkA does not interact specifically with the nucleobase to protonate it. To determine the structure of AlkA's transition state, methods for primary and secondary KIE measurement were developed, but none of the methods produced precise KIE values (95% confidence interval < 0.005). To determine the structure of the transition state of the cognate non-enzymatic reaction, the acid-catalyzed

hydrolysis of 2’-deoxyinosine 5’-monophosphate, the 1’-^{3}H, 4’-^{3}H, 5’-$^3H_2$, 1’-^{14}C, and 7-^{15}N KIEs were measured and were 1.25 ± 0.02, 0.94 ± 0.01, 0.99 ± 0.02, 0.997 ± 0.004, and 0.99 ± 0.05, respectively. Despite being consistent with an oxacarbenium ion-like transition state, these values would not be precise enough to distinguish between potential transition state models.

Acknowledgements

To Dr. Paul Berti, thank you for all your support, guidance, and understanding over these past 6+ years.

To my committee members, Dr. Fred Capretta and Dr. Alba Guarne, thank you for your constructive feedback.

To my parents, my sister, and brother-in-law, thank you for supporting me in so many ways. I’m so blessed to have such a loving family.

Naresh, Simanga, Vlad, Shan, Maren, Lisset, and Rasa, thank you for making the experience in this lab a wonderful one. I only hope my future co-workers are as amazing as you all are.

Ryan, thank you for always listening to me and helping me through my struggles, both personal and academic.

Table of Contents

List of Figures and Tables

List of Abbreviations and Symbols

1-aza	1-aza-1,2-dideoxy-4a-carba-D-*erythro*-pentofuranose
1-aza-DNA	DNA containing 1-aza-1,2-dideoxy-4a-carba-D-*erythro*-pentofuranose
1-aza-RNA	RNA containing 1-aza-1,2-dideoxy-4a-carba-D-*erythro*-pentofuranose
3MeA	3-methyladenine
7MeG	7-methylguanine
A	adenine
AAT	*E. coli* aspartate aminotransferase
ADA	*Aspergillus niger* adenylic acid deaminase
AMP	adenosine 5'-monophosphate
AP	apurinic/apyrimidinic
APRT	adenine phosphoribosyltransferase
ATP	adenosine triphosphate
B. halodurans	*Bacillus halodurans*
B. subtilis	*Bacillus subtilis*
BER	base-excision repair
BSA	bovine serum albumin
BTP	1,3-bis[tris(hydroxymethyl)methylamino]propane
C	cytosine
CI	confidence interval
CPM	counts per minute
dCTP	2'-deoxycytidine 5'-triphosphate
dIMP	2'-deoxyinosine 5'-monophosphate
dITP	2'-deoxyinosine 5'-triphosphate
DMS	dimethyl sulfate
DNA	deoxyribonucleic acid
DP5P	4,5-dihydroxy-pent-2-enal 5-phosphate
DTT	dithiothreitol
dTTP	2'-deoxythymidine 5'-triphosphate
dUTP	2'-deoxyuridine 5'-triphosphate
dUTPase	2'-deoxyuridine 5'-triphosphatase
DSB	double-strand break
εA	1,N^6-ethenoadenine
εC	3,N^4-ethenocytosine
E. coli	*Escherichia coli*
EDTA	ethylenediaminetetraacetic acid

EMSA	electrophoretic mobility shift assay
FADH$_2$	reduced flavin adenine dinucleotide
FPLC	fast protein liquid chromatography
G	guanine
$\Delta G^{\ddagger}$	Gibbs free energy of activation
G6PDH	*Leuconostoc mesenteroides* glucose-6-phosphate dehydrogenase
hAPE1	human apurinic/apyrimidinic endonuclease I
HCA	human carbonic anhydrase
HhH	helix-hairpin-helix
HK	*S. cerevisiae* hexokinase
HPLC	high-performance liquid chromatography
*Hs*OPRT	human orotate phosphoribosyltransferase
Hx	hypoxanthine
IAG-NH	inosine-adenine-guanine nucleoside hydrolase
IU-NH	inosine-uridine nucleoside hydrolase
KIE	kinetic isotope effect
k_{cat}	catalytic turnover constant
K_{d}	dissociation constant
$K_{\mathrm{i,app}}$	apparent inhibition constant
K_{M}	Michaelis constant
k_{non}	rate constant for non-enzymatic depurination
k_{st}	single-turnover rate constant
LMW	low molecular weight
MK	rabbit muscle myokinase
MMLV-RT	Moloney murine leukemia virus reverse transcriptase
MNNG	*N*-methyl-*N*'-nitro-*N*-nitrosoguanidine
MNU	*N*-methyl-*N*-nitrosourea
MTA	5'-methylthioadenosine
MTAN	5'-methylthioadenosine/*S*-adenosylhomocysteine nucleosidase
MTAP	5'-methylthioadenosine phosphorylase
NAD$^+$	nicotinamide adenine dinucleotide
NADH	reduced nicotinamide adenine dinucleotide
NADP$^+$	nicotinamide adenine dinucleotide phosphate
NADPH	reduced nicotinamide adenine dinucleotide phosphate
NaHEPES	sodium 4-(2-hydroxyethyl)-1-piperazineethanesulfonate
NER	nucleotide-excision repair
$O_2^{\bullet -}$	superoxide
OGT	*O*^{6}-methylguanine DNA methyltransferase
OH•	hydroxyl radical
OMP	orotidine 5'-monophosphate
OPRT	orotate phosphoribosyltransferase

PAGE	polyacrylamide gel electrophoresis
PCNA	proliferating cell nuclear antigen
PEP	phosphoenolpyruvate
P. falciparum	*Plasmodium falciparum*
6PGDH	*S. cerevisiae* 6-phosphogluconic dehydrogenase
PK	rabbit muscle pyruvate kinase
PLP	pyridoxal 5’-phosphate
PMP	pyridoxamine 5’-phosphate
PNP	purine nucleoside phosphorylase
PRI	spinach phosphoriboisomerase
PRPPase	phosphoribosyl pyrophosphate synthetase
pyr-DNA	pyrrolidine-containing DNA
RNA	ribonucleic acid
ROS	reactive oxygen species
RTR	ribonucleoside triphosphate reductase
S. pneumoniae	*Salmonella pneumonia*
SAM	*S*-adenosylmethionine
S. pombe	*Schizosaccharomyces pombe*
SSB	single-strand break
SDKIE	solvent deuterium kinetic isotope effect
t_R	retention time
T	thymine
TBAS	tetrabutylammonium sulfate
TBE	tris-borate EDTA
THF	tetrahydrofuran
TIM	yeast triose phosphate isomerase
TLS	translesion synthesis
Tris-HCl	tris(hydroxymethyl)aminomethane hydrochloride
T. vivax	*Trypanosoma vivax*
UV	ultraviolet
WT	wild-type

Declaration of Academic Achievement

All work described herein was performed by the author, with the following exceptions. Generation of mutant plasmids for R244M and Y222F were performed by Hanna Zhao. Radiolabelled dIMPs were both wholly synthesized by the author and from dAMP synthesized by Joe McCann.

Chapter 1. Introduction

1.1 The biological imperative for DNA repair

A cell's survival and the viability of its progeny depend on the chemical integrity of the nucleobases in its DNA. Because the cell's catalytic and structural proteins are encoded in the sequence of these bases, oxidation, dimerization, deamination, and alkylation can alter their coding properties, introducing mutations into messenger RNA during transcription and potentially heritable mutations into daughter strands during DNA replication. Even worse, such damage may lead to replicational or transcriptional stalling. However, the overall toxicity of a particular lesion is not only dependent on the type of lesion but also on the number of lesions, the sites of damage, and timing of the damage-producing events.[1]

1.2 Types and sources of damage

1.2.1 Radiation and oxidation

Ionizing radiation can lead to oxidative damage through interactions with water to form the hydroxyl radical, OH•.[2,3] OH• can also be produced during the reaction of superoxide, a byproduct of oxidative phosphorylation, or hydrogen peroxide with Fe^{2+} or Cu^{+}.[4-6] Ultraviolet light also produces singlet oxygen when its energy is transferred to oxygen via endogenous photosensitizers such as flavins and NADH/NADPH.[3] OH• and singlet oxygen react indiscriminately with DNA at near the diffusional rate limit to oxidize purines and pyrimidines.[7] Oxidation of adenine (A) or guanine (G) to form 8-hydroxy radicals causes ring opening to formamidopyrimidines, which direct A incorporation by DNA polymerase I.[8,9] 8-Oxoguanine is a major G oxidation product; it pairs with A instead of cytosine (C), leading to a transversion mutation if not repaired.[10] Pyrimidine oxidation products include 5-hydroxypyrimidines, pyrimidine glycols, and hydantoins. Thymine (T) can also be oxidized to form 5-hydroxymethyluracil and 5-formyluracil, which cause transition and transversion mutations.[2,11] OH• can produce single-strand and double-strand breaks (SSBs and DSBs, respectively), both of which are lethal if unrepaired.[7,11,12]

Ultraviolet (UV) radiation can cause dimerization of stacked pyrimidines, producing cyclobutane pyrimidine dimers and pyrimidine (6-4) pyrimidone photoproducts.[13] These lesions blocked *Escherichia coli* DNA polymerase I *in vitro*.[14] DNA synthesis can continue downstream, but this leaves a gap in the daughter strand.[15] If post-replication repair of the parental strand is initiated by an endonuclease that nicks 5’ to the pyrimidine dimer, then a DSB will be produced.[15]

1.2.2 Deamination

Deamination of C, A, and G residues produces uracil, hypoxanthine (Hx) and xanthine, respectively; uracil pairs with A and Hx pairs with C, causing transition mutations.[16] C is the most labile, but is generally protected from hydrolytic deamination in double-stranded DNA until local transient "breathing" motions expose it to water.[17,18] A, C, and G can undergo nitrosative deamination, in which nitrous anhydride (Figure 1.4A), N_2O_3, reacts with exocyclic amino groups to form an N_2OH group.[17] Deamination is completed following dehydration of the N_2OH group and nucleophilic aromatic substitution by water.[17] N_2O_3 is produced from condensation of two molecules of nitrite, NO_2^-, which can be produced from the nitrate reductase-catalyzed reduction of nitrate, NO_3^-, or from oxidation of nitric oxide, NO•, which can be produced from the nitrite reductase-catalyzed reduction of NO_2^-.[19]

1.2.3 Alkylation and cross-linking

Alkylation by endogenous and exogenous agents can occur at the exocyclic oxygen atoms of G, T, and C residues and the N1, N3, and N7 atoms of purines (Figure 1.1).[20] *O*^{6}-Methylguanine and *O*^{4}-methylthymine are mutagenic because *O*^{6}-methylguanine pairs with T and *O*^{4}-methylthymine pairs with G.[21,22] Neither 7-methylguanine (7MeG) (Figure 1.2A) nor 3-methyladenine (3MeA) (Figure 1.2B) is miscoding on its own, but the increased hydrolytic lability of their *N*-glycosidic bonds leads to depurination and the formation of toxic abasic sites.[23] For example, 3-methyl-2'-deoxyadenosine's half-life is 35 min, compared with 2'-deoxyadenosine's half-life of 35 years.[24,25] As well, 3MeA and 2,6-diamino-4-hydroxy-5*N*-methyl-formamidopyrimidine, the product of 7MeG's imidazole ring opening, can cause replicational stalling.[26,27] Unlike the other methylbases, *O*^{2}-methylthymine (Figure 1.2S) and presumably *O*^{2}-methylcytosine (Figure 1.2T) do not miscode.[28]

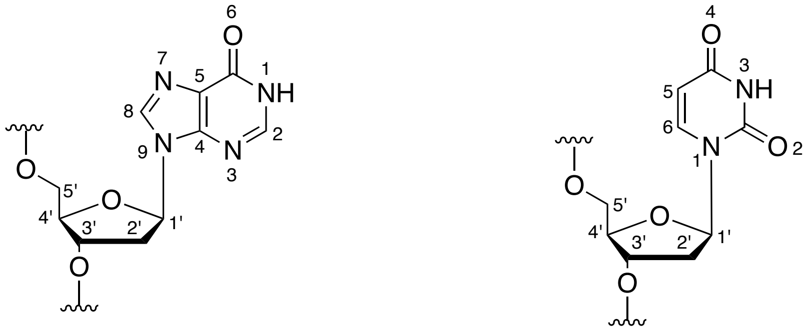

A **B**

Figure 1.1. Atom numbers in purine and pyrimidine 2'-deoxyribonucleosides
A) inosine B) uridine

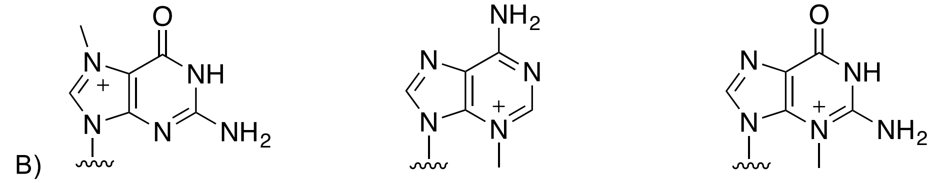

7-methylguanine (7MeG) 3-methyladenine (3MeA) 3-methylguanine (3MeG)

A **B** **C**

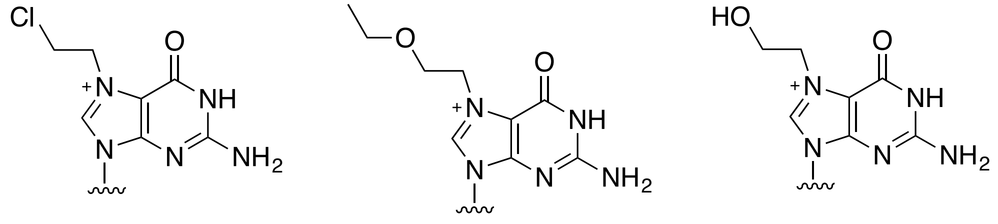

7-(2-chloroethyl)guanine 7-(2-ethoxyethyl)guanine 7-(2-hydroxyethyl)guanine

D **E** **F**

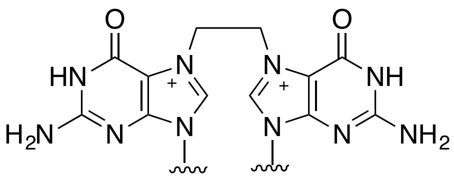

1,2-bis(7-guanyl)ethane

G

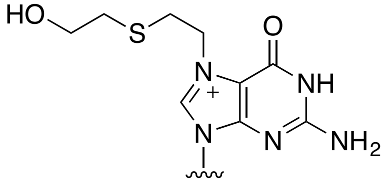

7-hydroxyethylthioethylguanine

H

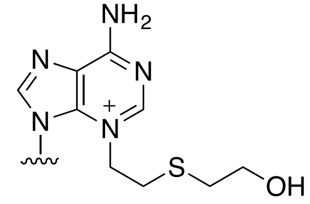

3-hydroxyethylthioethyladenine

I

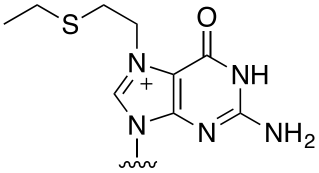

7-ethylthioethylguanine

J

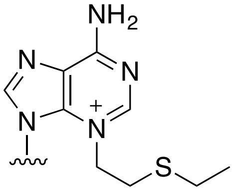

3-ethylthioethyladenine

K

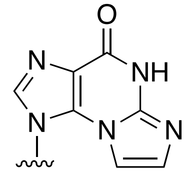

N^2,3-ethenoguanine

L

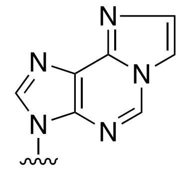

1,N^6-ethenoadenine

M

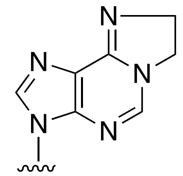

1,N^6-ethanoadenine

N

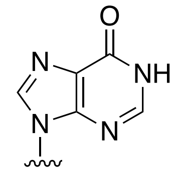

hypoxanthine (Hx)

O

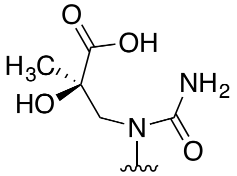

N-(2-deoxy-*β*-D-erythro-pentofuranosyl)-*N*-3-(2R-hydroxyisobutyric acid)-urea

P

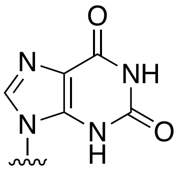

xanthine

Q

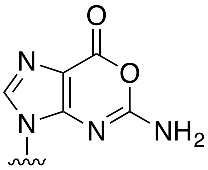

oxanine

R

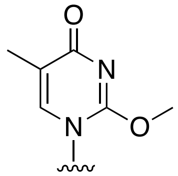

O^2-methylthymine

S

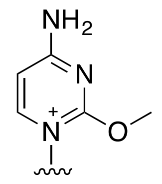
O^2-methylcytosine
T

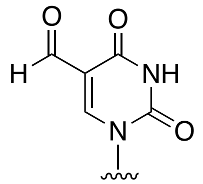
5-formyluracil
U

Figure 1.2. Modified bases that are AlkA substrates

The biological methyl donor *S*-adenosylmethionine (SAM) (Figure 1.3J) can non-enzymatically methylate N7 and N3 of A and G residues.[29] However, in *E. coli*, increasing the intracellular concentration of SAM via overexpression of SAM synthetase did not appreciably increase the G:C-to-A:T mutation rate in either WT cells or cells deficient in both the repair proteins Ada (see Section 1.5) and O^6-methylguanine methyltransferase (OGT) (see Section 1.3.4).[30] Environmental and industrial methylating agents include dimethyl sulfate (DMS) (Figure 1.3G) and methyl halides, which are produced by both living and decaying biomass and by wood-rotting fungi.[31,32]

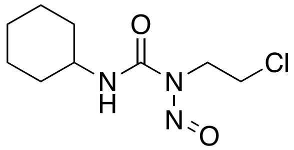
A

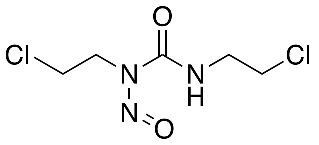
B

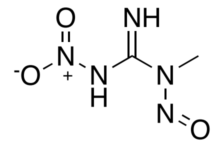
C

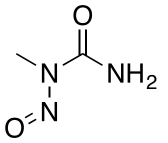
D

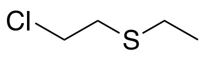
E

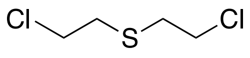
F

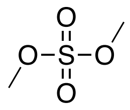

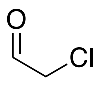

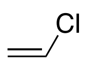

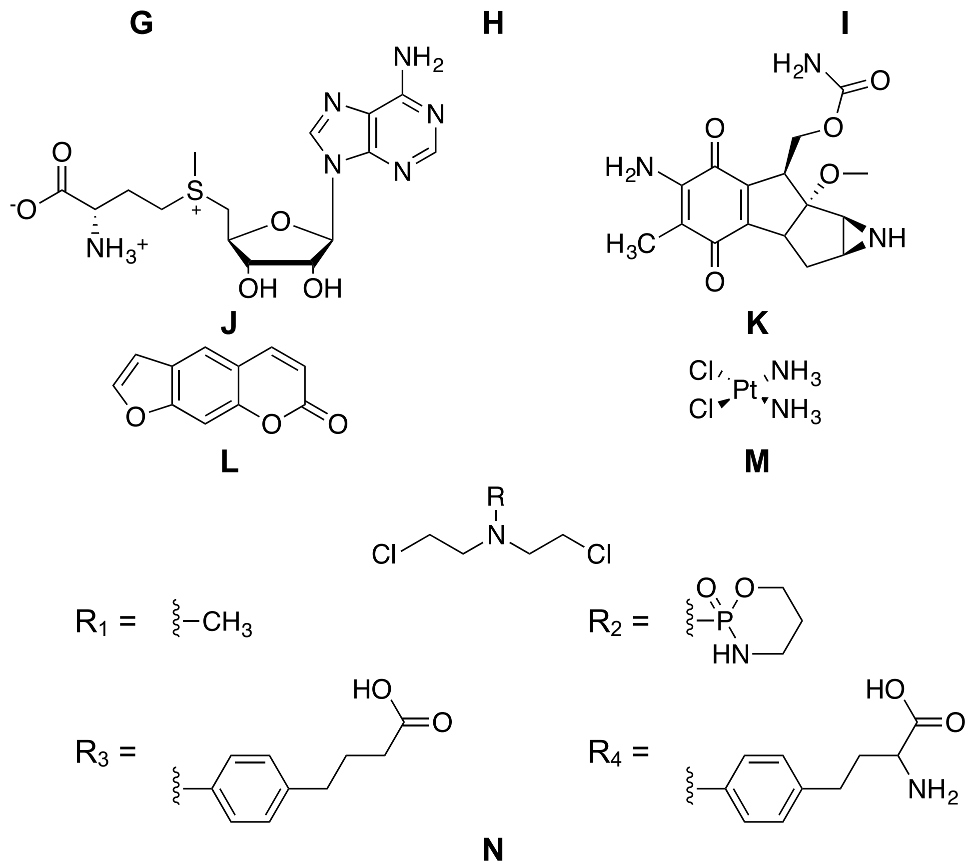

Figure 1.3. DNA alkylating and cross-linking agents
A) 1,3-bis(2-chloroethyl)-1-nitrosourea (BCNU) B) *N*-(2-chloroethyl)-*N*'-cyclohexyl-*N*-nitrosourea (CCNU) C) *N*-methyl-*N*'-nitro-*N*-nitrosoguanidine (MNNG) D) *N*-nitroso-*N*-methylurea (MNU) E) chloroethyl ethyl sulfide F) bis-(2-chloroethyl)sulfide G) dimethyl sulfate H) chloroacetaldehyde I) vinyl chloride J) *S*-adenosylmethionine K) mitomycin C L) psoralen M) cisplatin N) nitrogen mustards in clinical use: R_1 = mechloroethamine, R_2 = cyclophosphamide, R_3 = chlorambucil, R_4 = melphalan

Amino acids and other free amines can be *N*-nitrosated in the presence of NO_2^-, producing potent alkylating agents (Figure 1.4).[33] Nitrosative alkylation occurs non-enzymatically under acidic conditions (below pH 5.0), but intact *E. coli* A10 cells were found to synthesize *N*-nitrosomorpholine at pH 7.2; attempts to isolate the source of the nitrosation activity failed as the activity was lost in lysed cells.[33,34] However, *E. coli* mutants incapable of synthesizing molybdopterin guanine dinucleotide had lower mutation frequencies when grown in the presence of NO_2^-.[35] Exogenous *N*-nitroso compounds include the antineoplastic agents 1,3-bis(2-chloroethyl)-1-nitrosourea (BCNU) (Figure 1.3A) and *N*-(2-chloroethyl)-*N*'-cyclohexyl-*N*-nitrosourea (CCNU) (Figure 1.3B).

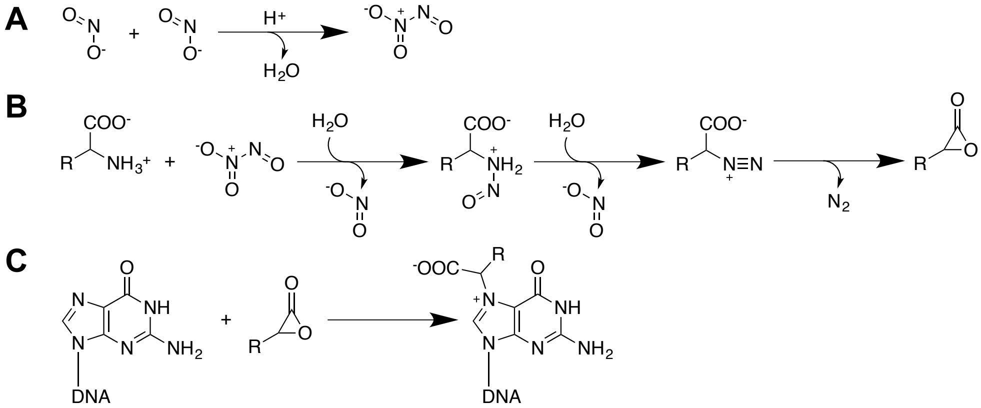

Figure 1.4. DNA alkylation by NO_2^-
Pathway proposed by García-Santos et al.[33] A) N_2O_3 formation by NO_2^- dehydration B) α-amino acid *N*-nitrosation by N_2O_3, followed by lactonization of the *N*-nitroso product. C) Attack on the lactone by a nucleophilic O or N of a DNA base (guanine shown here) to form the DNA adduct

DNA bases can also be alkylated by lipid peroxidation end-products. During lipid peroxidation, a methylene hydrogen of an unsaturated fatty acid is abstracted by a radical; the carbon-centered radical then reacts with oxygen to form a peroxy radical.[36,37] The propagation and termination steps yield varied products that include aldehydes such as malondialdehyde and *trans*-4-hydroxy-2-nonenal.[36,37] These species can react with A, C, and G residues to form a number of adducts, including 1,N^6-ethenoadenine (εA, Figure 1.2H), 3,N^4-ethenocytosine (εC), N^2,3-ethenoguanine (Figure 1.2G), and 1,N^2-ethenoguanine.[37,38] In *E. coli*, N^2,3-ethenoguanine can cause transition mutations and 1,N^6-ethenoadenine can cause transition and transversion mutations.[39,40] Vinyl chloride (and its metabolites chloroethylene oxide and 2-chloroacetaldehyde) and ethyl carbamate can also produce these etheno adducts.[37]

A bifunctional alkylating agent can react with two bases, joining them to form an intrastrand or interstrand cross-link. Intrastrand cross-links can be repaired by nucleotide-excision repair (NER) (see Section 1.3.2) or bypassed altogether.[41,42] Interstrand cross-links, however, are cytotoxic because they prevent strand separation during DNA replication and transcription, blocking cell division and protein synthesis.[42] Aldehydes produced from lipid peroxidation can produce these cross-links, as can nitrous anhydride via a mechanism similar to that of nitrosative deamination (see Section 1.2.2), except the nucleophile is the exocyclic amino group of a guanine on the opposite strand.[38,43] Cross-linking agents, such as nitrogen mustards, platinum-containing compounds, psoralens, and mitomycins, are used clinically in cancer chemotherapy (Figure 1.3K-N).[41]

1.3 Modes of DNA repair

1.3.1 Recombinational repair

Homologous DNA can supply a contiguous portion of DNA to a DSB site via recombination. In one model of prokaryal recombinational DSB repair, the RecBCD complex or the individual proteins RecQ, RecJ, RecF, RecO, and RecR unwind and degrade the broken DNA from the two 5' ends of the break, leaving behind single strands on the 3' end.[44] RecA is recruited to the site. With the assistance of RecA, the single-stranded tails pair with complementary regions on each strand of a homologous duplex.[44] RuvAB and a DNA polymerase allow synthesis to continue from the tails until the end of the homologous region is reached; the newly extended strands are joined to the 5' ends of the break, producing two crossover structures called Holliday junctions.[44] The two duplexes are separated by the endonuclease RuvC, which acts specifically on Holliday junctions.[44,45] Repair of SSBs was also observed to be RecA-dependent.[46] An alternative non-recombinational process for DSB repair called non-homologous end-joining exists in eukaryotes and some prokaryotes (though not *E. coli*), in which two broken ends hybridize with each other over short regions of complementarity (1 to 4 nucleotides); this produces overhangs that must be clipped.[47,48] A DNA polymerase extends the strands and DNA ligase seals the nick.[47]

Prokaryal cross-link repair can also occur by homologous recombination. The UvrABC system of nucleotide-excision repair (NER) (see Section 1.3.2) produces nicks on the 5' and 3' sides of the cross-link, leaving a gap in one strand.[41] Using RecA, the gap is filled by a single-stranded portion of a homologous duplex; this produces a gap in the invading strand, which is filled using its intact complement as the template.[41] The two strands are no longer cross-linked, but the cross-link adduct remains on one strand, which is then fully removed by NER (see Section 1.3.2).[41]

1.3.2 Nucleotide-excision repair (NER)

NER removes a nucleotide patch that contains a damaged area. In prokaryotes, NER is carried out by the UvrABC system, which recognizes DNA damage through kinks, bends, pairing disruptions, or changes in DNA dynamics.[49] Consequently, larger adducts tend to be excised more quickly than smaller ones, but there is an upper limit to the size of the adduct.[49,50] The process begins with an ATP-bound UvrA dimer, which, in a manner that is dominated by hydrophobic forces and independent of sequence, binds to DNA and unwinds it (unwinding is not ATP-dependent).[50] One or two ATP-bound UvrB molecules then bind to the $UvrA_2$-DNA complex; UvrA-bound ATP is hydrolyzed and dissociates, leaving behind a UvrB-DNA complex.[50] UvrB probes the unwound DNA to verify that damage exists at that site.[50] If damage exists, two conformational changes occur:

the first occurs after UvrB-bound ATP is hydrolyzed and the second occurs after another molecule of ATP is bound.[50] This final conformation allows UvrC to bind to the UvrB-DNA complex and to hydrolyze the phosphodiester bonds 5' and 3' to the sites of damage.[50] The release of the nucleotide stretch between these nicks is mediated by the helicase UvrD and the resultant gap is normally filled by DNA polymerase I.[50]

NER can be used instead of homologous recombination for cross-link repair. In this case, a gap is produced on one strand by UvrABC and error-prone translesion synthesis (TLS) using DNA polymerase II, IV, or V fills in the gap.[41,51] UvrABC excises the nucleotide/cross-link adduct on the second strand and DNA polymerase I fills in the gap using the TLS-synthesized strand as the complement.[41] It has been suggested that an adduct's rigidity may determine whether NER is triggered instead of recombinational repair, as NER was observed to repair nitrogen-mustard and ethyl interstrand cross-links and but not psoralen ones.[41,52,53]

1.3.3 Mismatch repair

In *E. coli*, a process called methyl-directed mismatch repair repairs replication errors. A nucleotide erroneously incorporated during DNA replication is excised, along with ≈1000 neighbouring nucleotides.[54] The strand containing the misincorporated nucleotide is recognized because, prior to DNA replication, the A of the palindromic GATC sequence is methylated on both strands, but during replication, the daughter strand is temporarily non-methylated.[55] If the daughter strand has a mismatch, MutS and MutL bind to the mismatch, activating MutH to make an incision 3' or 5' to the mismatch on the daughter strand opposite a methylated GATC sequence.[55] Orientation-specific exonucleases (RecJ, or exonucleases I or VII) make an incision at the mismatch site, liberating a stretch of nucleotides that encompasses the mismatch.[54] DNA polymerase III holoenzyme and single-stranded DNA binding protein restore the missing nucleotides and correct the mismatch in the process, with DNA ligase then sealing the nick.[54]

Deamination of 5-methylcytosine in 5'-C($^{5\text{-me}}$C)YGG-3' (Y = A or T) produces T and leads to a T:G mismatch.[56] Vsr endonuclease hydrolyzes the C↑T phosphodiester bond in the resultant duplex 5'-CTYGG-3'.[57] Both the 5' to 3' exonuclease and polymerase activities of DNA polymerase I are required for full repair, so presumably it binds to the nick, removes the existing nucleotides via its exonuclease activity, and correctly replaces them with its polymerase activity.[58,59] MutS and MutL also appear to participate in this process, as their absence almost (but not completely) eliminates repair *in vivo*.[59,60] Repair tract lengths were found to be on the order of 10 nucleotides *in vivo*.[61,62] This site-specific cytosine methylation is performed by Dcm and has been associated with regulation of gene expression during the stationary phase.[63] Methylation at this site also prevents the restriction enzyme *EcoR*II, which recognizes the same site as Dcm, from cleaving genomic DNA.[64]

1.3.4 Direct reversal

The extraneous bonds or functional groups on a damaged base can be removed directly via direct reversal. Pyrimidine dimers can be separated by a photolyase using electrons from an enzyme-bound reduced flavin adenine dinucleotide ($FADH_2$); light stimulates the electron transfer from $FADH_2$ via deazaflavin or folate.[65] O^6-Methylguanine can be converted back to G by Ada (see Section 1.5) and OGT.[65]

1.3.5 Base-excision repair (BER)

Base-excision repair (BER) enzymes remove the damaged base by a BER enzyme, followed by removal of the abasic site by a nuclease, and repair of the gap. BER enzymes are *N*-glycosylases; they hydrolyze the *N*-glycosidic bond linking the damaged base to 2'-deoxyribose, liberating the damaged base and leaving behind an abasic site (Figure 1.5).

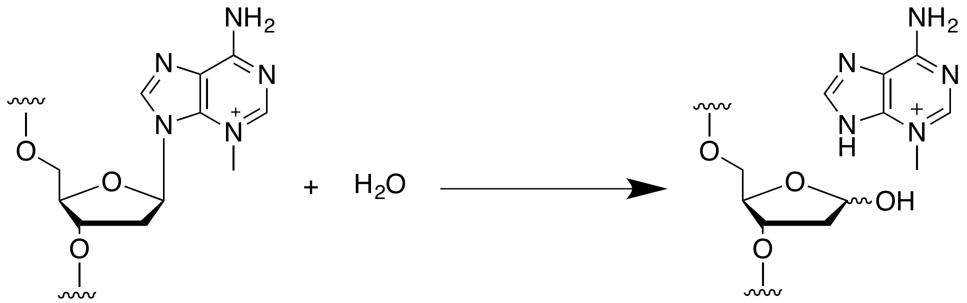

Figure 1.5. The BER hydrolysis reaction

Abasic sites are mutagenic and cytotoxic. Their cytotoxicity was demonstrated by the non-viability of *E. coli* K12 mutants deficient in 2’-deoxyuridine 5’-triphosphatase (dUTPase) and endonuclease III, an enzyme that removes abasic sites. The dUTPase deficiency caused dUTP to accumulate and be incorporated into DNA. The abasic sites produced by uracil DNA glycosylase (UDG), which excises uracil from DNA, went unrepaired, leading to cell death.[66]

Abasic sites block replication by DNA polymerase I *in vitro*.[67,68] They can also cause transcriptional stalling, though translesion RNA synthesis can occur. However, this introduces mutations into the transcripts because abasic sites are non-coding.[69] The *E. coli* pathway for abasic-site removal begins with a class II AP (apurinic/apyrimidinic) endonuclease that nicks the phosphate backbone 5’ to an abasic site, producing a nick with a 3’-OH end and a 5’-PO_4^{2-} end attached to 2’-deoxyribose. Exonuclease III and IV are responsible for ≈90% and ≈10%, respectively, of the total AP endonuclease activity.[70,71] The abasic site can be removed by a DNA deoxyribophosphodiesterase that hydrolyzes the phosphodiester bond 3’ of the abasic site (Figure 1.6B) or a class II AP endonuclease that performs β-elimination on the 2’-deoxyribose group (Figure 1.6A).[72] Alternatively, some BER enzymes have AP lyase activity and can perform β-elimination themselves; bifunctional BER enzymes in *E. coli* include formamidopyrimidine DNA glycosylase and endonuclease VIII, which excises damaged pyrimidines.[73,74] A class II endonuclease then completes the removal of the abasic site. A DNA polymerase replaces the lost nucleotide and DNA ligase seals the nick (Figure 1.6C).[75]

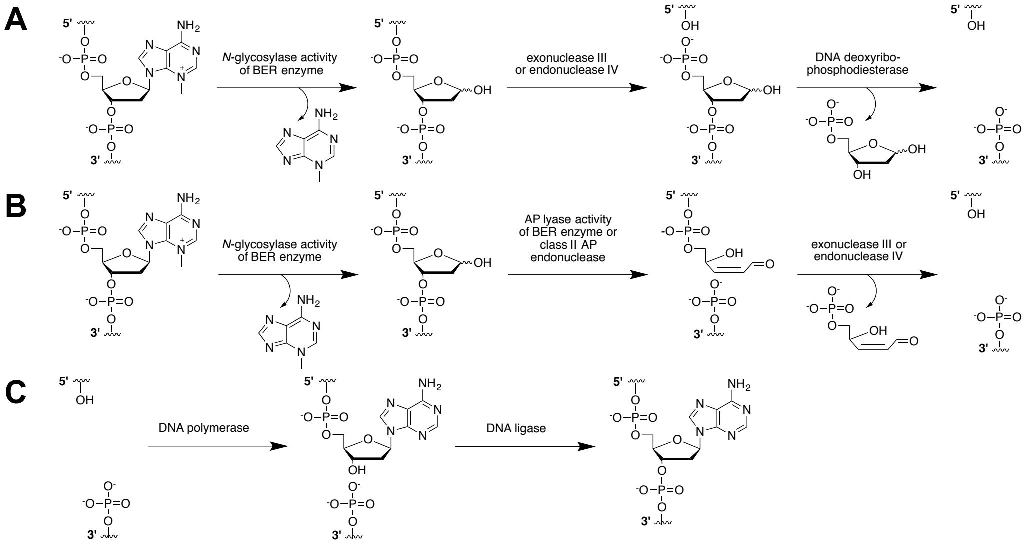

Figure 1.6. BER pathways in *E. coli*

A) Hydrolysis of the *N*-glycosidic bond, followed by β-elimination by an AP lyase and nicking 5’ to the abasic site B) Hydrolysis of the *N*-glycosidic bond, followed by nicking 5’ to the abasic site by exonuclease III/endonuclease IV and nicking 3’ to the abasic site by DNA deoxyribophosphodiesterase C) Gap filling and sealing by DNA polymerase and DNA ligase

1.4 Base excision repair enzymes as *N*-glycosylases

All BER enzymes are *N*-glycosylases; that is, they hydrolyze the *N*-glycosidic (C−N) bond of the damaged base to create an abasic site.[76] Other enzymes that act on *N-glycosidic bond*s include nucleoside hydrolases and nucleoside phosphorylases, which are involved in nucleoside recycling, toxins like diphtheria, cholera and pertussis toxins, which cleave the *N-glycosidic bond* of NAD^+ while ADP-ribosylating their target proteins, and ricin and saporin, ribosome-inactivating proteins which depurinate ribosomal RNAs. The mechanisms of these enzymes have been studied extensively, along with the analogous acid-catalyzed nucleoside hydrolyses.[77-83]

1.4.1 Non-enzymatic nucleoside hydrolysis

Early investigations into the mechanism of purine nucleoside hydrolysis consisted of rate measurements for non-enzymatic reactions at several pHs and with neutral and *N*-substituted (cationic) purine nucleosides. At that time, purine nucleoside hydrolysis was thought to follow one of two proposed pathways: one in which a purine imine produced after O4’ protonation is hydrolyzed (Figure 1.7A), or one in which in which purine protonation is followed by purine expulsion and C1’ attack (simultaneous or sequential) by water (Figure 1.7B). [84,85] The salient observation in these studies was that neutral purine hydrolysis rates increased 10-fold with a decrease in 1 pH unit at pHs below 4 (i.e., plots of log *k* vs. pH were linear, with slope = 1).[25,86] The pH vs. rate profiles fit a model consistent with the latter pathway in which there is equilibrium protonation before rate-limiting C−N bond cleavage.[86]

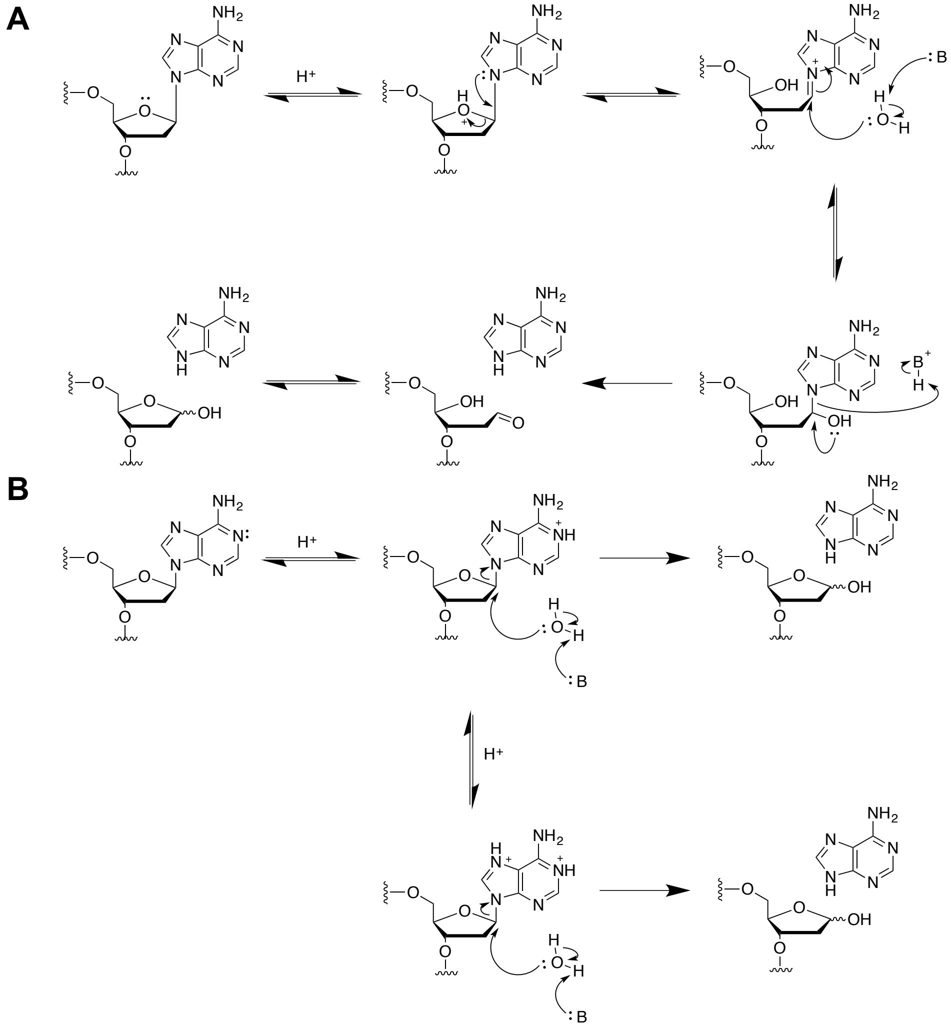

Figure 1.7. Initially proposed mechanisms for purine nucleoside hydrolysis
A) O4’ is protonated. The ribose ring opens and an imine is formed between the purine N9 and the ribose carbonyl C1’. Imine hydrolysis produces the free purine and ribose in the ring-opened form. B) The purine is mono- or diprotonated. C1’ is directly attacked by water. Purine departure can precede C1’ attack by water (see Section 1.8). Adapted from ref [25].

Adenosine (Figure 1.8A) and 1-methyladenosine (Figure 1.8B) rates were unaffected by increasing acetate buffer concentrations.[85] For pH-dependent reactions, rates that are independent of buffer concentration are indicative of specific-acid catalysis; in this case, the rate is dependent only on the hydronium-ion concentration (that is, the pH). When a reaction is accelerated by increasing buffer concentration, it is said to be general-acid-catalyzed because the rate depends on the buffer concentrations at a given pH value. According to the Brønsted linear free-energy relationship, the extent of proton transfer can be obtained from the slope of the line produced by plotting log k_{obs} against the reaction buffer pK_a.[87] Because adenosine and 1-methyladenosine hydrolysis did not exhibit general-acid catalysis, those reactions were not likely to proceed via the imine-based mechanism of *N*-arylglucosylamine hydrolysis, for which general-acid catalysis was observed.[25,86,88]

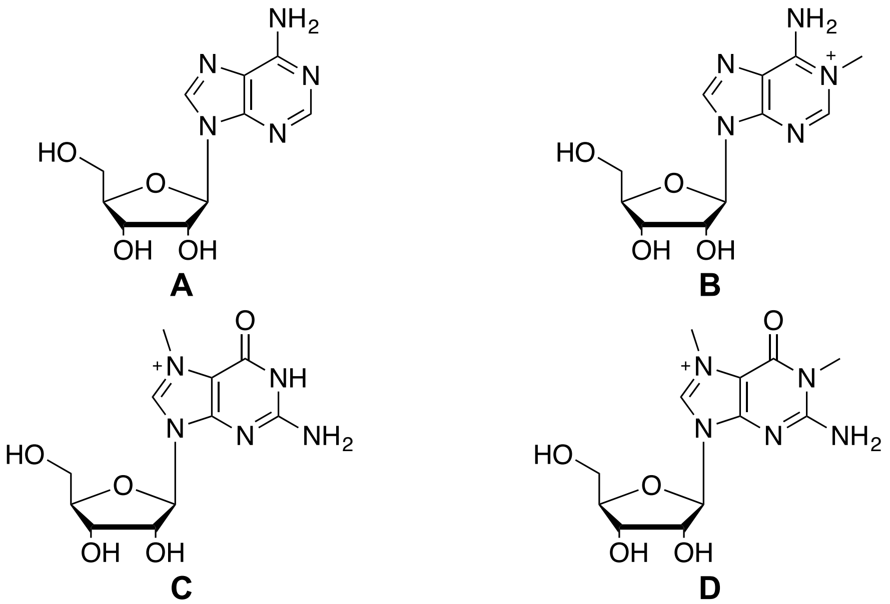

Figure 1.8. Methylated adenosines and guanosines

Support for the purine-protonation mechanism came from the fact that the cationic *N*-alkylpurines 7-methylguanosine (Figure 1.8C) and 1,7-dimethylguanosine (Figure 1.8D) were hydrolyzed with rates equal to that of guanosine from pH 1 to 2, and that 7-methylguanosine was also hydrolyzed with a rate equal to that of guanosine in 1 to 7 M $HClO_4$. [25,89] Adenosine and 1-methyladenosine were hydrolyzed with similar rates at pH 1.[85] Cationic leaving groups are more labile because the C−N bond in the reactant is weakened due to electron-withdrawing effects of the positive charge and because the leaving group, which becomes neutral after departure, is more stable than the anionic purine that would result from uncatalyzed departure.

These kinetic data showed that protonation imparted the same hydrolytic lability to nucleosides that *N*-alkylation does, but they did not show where protonation occurs.[85] The infrared spectrum of guanosine at low pH could not distinguish between N7 or N3 protonation, but protonated N7 was observed in the crystal structure of guanine hydrochloride.[90,91] The pK_a values of guanosine's N1, N3, and N7 atoms are 9.2, -2.4, and 2.1, respectively, so guanosine would become cationic only upon N7 protonation in acidic solution.[25,92] Similarly, both the adenosine infrared spectrum at pH < 3 and the crystal structure of adenosine hydrochloride showed that N1 was protonated.[90,91] The pK_a values for adenosine monoprotonation at N1 and N7 are ~4 and 2.2, respectively.[93]

1.4.2 Enzymatic N-*glycoside hydrolysis mechanisms*

With a couple of notable exceptions, like *E. coli* UDG, *S. pneumoniae* 5'-methylthioadenosine nucleosidase (MTAN), and human MTAN, the vast majority of *N*-glycosylases promote leaving group departure by protonating the nucleobase.[94-96] Because a cationic purine can leave as a neutral species when the C−N bond in a nucleoside is cleaved, enzymes can increase C−N bond reactivity toward water by protonating the purine moiety. This behaviour was found in *Crithidia fasciculata* IU-NH (IU-specific nucleoside hydrolase), a non-specific nucleoside hydrolase involved in purine salvage.[97] Its pH vs. k_{cat} profiles for inosine hydrolysis revealed two pK_as, at 7.1 and 9.1, and its pH vs. k_{cat}/K_M profiles revealed two similar pK_as, 7.3 and 8.7.[98] Because inosine's pK_as, 1.06 and 8.76, are not in that range, these were enzyme pK_as.[92] The pK_a of 9 from the pH vs. k_{cat}

and pH vs. $k_{\mathrm{cat}}/K_{\mathrm{M}}$ profiles was absent from the pH vs. K_{i} profile of a transition state-mimic inhibitor, indicating that this ionization is only crucial for catalysis and not for inhibitor binding, and that the residue to which this ionization belongs must be protonated in the active form.[98] The H241A mutant had a ~2100-fold reduction in k_{cat} and ~7400-fold reduction in $k_{\mathrm{cat}}/K_{\mathrm{M}}$ toward inosine, but only a ~3-fold decrease in k_{cat} and ~5-fold decrease in $k_{\mathrm{cat}}/K_{\mathrm{m}}$ for *p*-nitrophenyl riboside.[97] The small reduction in H241A activity against *p*-nitrophenyl riboside established that the mutant could hydrolyze a glycosidic bond by non-specifically stabilizing an oxacarbenium ion-like transition state, but the large reduction in activity against inosine was evidence for the importance of protonating the leaving group and for H241's role as the general-acid catalyst.[97]

1.5 AlkA (3-methyladenine DNA glycosylase II)

E. coli AlkA, or 3-methyladenine DNA glycosylase II, is a monofunctional BER enzyme that is expressed as part of the adaptive response to alkylative stress and can rapidly excise the methylpurines 3MeA (Figure 1.2B), 3-methylguanine (3MeG, Figure 1.2C), and 7MeG (Figure 1.2A). AlkA is part of the *ada* regulon, which codes for three other proteins involved in DNA alkylation repair, AlkB, AidB, and Ada.[99] AlkB is an Fe^{2+}/α-ketoglutarate-dependent dioxygenase that oxidatively dealkylates 3-methylcytosine, 1-alkyladenines, and 1-hydroxyalkyladenines.[100-102] AidB is thought to directly repair alkylative damage as well because it binds FAD, flavodoxin, RNA, and DNA and can reduce MNNG-induced mutagenesis.[103-105]

Ada controls expression of the entire *ada* regulon.[99] Ada recognizes alkylative stress by transferring methyl groups from backbone *S*-methylphosphotriesters to its Cys38 residue.[106] Cys38-methylated Ada induces expression of AlkB, AidB, AlkA, and itself. Transfer of an additional methyl group from O^6-methylguanine or O^4-methylthymine to Cys321 enhances this behaviour.[105,107-109] Unmethylated Ada is much weaker at inducing expression of AlkA, AlkB, and itself (it was unable to induce AidB expression) and inhibits Ada expression at high concentrations.[110] Therefore, as methylphosphotriesters are removed and the *ada* genes are upregulated, the accumulation of unmethylated Ada gradually lowers *ada* regulon gene expression.[110]

The crystal structure of AlkA complexed with 1-aza-1,2-dideoxy-4a-carba-D-*erythro*-pentofuranose-containing DNA (1-aza-DNA) showed that AlkA is a member of the helix-hairpin-helix (HhH) evolutionary superfamily of proteins.[111] The HhH motif consists of two antiparallel α-helices joined by a hairpin-like loop, with considerable sequence variability among HhH proteins.[112] Structural alignment of several HhH proteins (including AlkA) yielded a G*h*G consensus sequence in the hairpin region, where *h* is a hydrophobic residue, and a central conserved hydrophobic residue in each of the helices.[112] This motif participates in non-sequence-specific DNA binding: main-chain nitrogen atoms in each motif are thought to interact with the DNA phosphate backbone.[112] Aside from DNA binding, the motif does not impart any common catalytic ability, as the chemistry performed by the DNA-binding members of the superfamily is varied: the family includes the BER enzymes *E. coli* MutY and endonuclease III, plus *E. coli* DNA polymerase β, *E. coli* NAD$^+$-dependent DNA ligase, and the *E. coli* Holliday junction DNA helicase subunit.[112]

1.6 AlkA is a broad-specificity enzyme

AlkA can bind to and excise several different purines and pyrimidines. The relevant steady-state parameters are the equilibrium constant K_s (or K_d), the kinetic parameters K_M, k_{cat}, and k_{cat}/K_M, and the single-turnover rate constant k_{st}. K_S (or K_d) is the dissociation constant of the E•DNA complex (i.e., the ES complex) and is equal to k_{-1}/k_1 (Figure 1.9).[113] From the Michaelis-Menten equation (equation 1.1), k_{cat} is the reaction rate at saturating substrate concentration ($[S]_0 >> K_M$), and is also the rate constant for the rate-limiting step.[114] The k_{cat} value reflects the slowest step of the reaction, which is generally the chemical step (k_{chem}) or product release (k_{rel}) for BER enzymes.[115-117] K_M is the Michaelis constant and is the substrate concentration at which the rate is half-maximal. In some circumstances, it can equal K_s, but this cannot be assumed to be true.[113] The specificity constant k_{cat}/K_M is a second-order rate constant that reflects all steps up to and including the first irreversible step; that is, up to and including

k_{chem} (Figure 1.9).[113] The single-turnover rate constant k_{st} is the rate observed when AlkA is present in excess of substrate.[118] This way, all substrate is bound to enzyme at once and product release is not required for complete substrate consumption; consequently, this rate constant only accounts for the steps after substrate binding up to and including the chemical step.[118]

$$\frac{v_0}{[\mathrm{E}]_0} = \frac{k_{\mathrm{cat}}[\mathrm{S}]_0}{[\mathrm{S}]_0 + K_M} \qquad \mathbf{(1.1)}$$

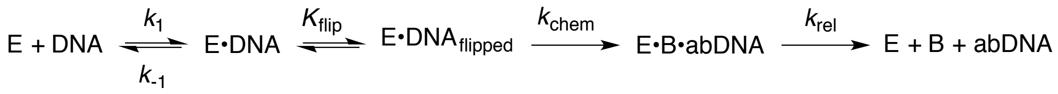

Figure 1.9. Model for AlkA-catalyzed base excision
E = AlkA, B = nucleobase, DNAflipped = DNA with nucleobase flipped out of the helix and into AlkA's active site, abDNA = abasic DNA product. K_{flip} is the equilibrium constant for nucleobase flipping, k_{chem} is the rate constant for *N*-glycoside hydrolysis (i.e., C-N bond cleavage and nucleophilic attack by water), and k_{rel} is the rate constant for product release.

For AlkA's eponymous substrate 3MeA in dimethyl sulfate (DMS)-treated calf thymus DNA, k_{st} and K_{d} for this lesion were 0.5 min^{-1} and 5 nM, respectively.[118-120] In *E. coli* adapted to alkylative stress by *N*-methyl-*N*'-nitro-*N*-nitrosoguanidine (MNNG, Figure 1.3C), 3MeG removal from DNA was attributed to AlkA.[121] *In vitro*, isolated AlkA excised 3MeG 2 to 3 times more quickly than 3MeA.[122] 7MeG was excised with $k_{\mathrm{cat}} = 0.05$ min^{-1} and $K_{\mathrm{M}} = 31$ nM.[123]

AlkA is also capable of excising alkylpurines with bulkier substituents (Figure 1.2D – K).[124-126] AlkA can excise etheno- and ethano-adducts to purines, but generally at significantly slower rates than 3MeA (Figure 1.2L – N).[127-130]

Deaminated purines are also substrates for AlkA. It can excise the A deamination product Hx (Figure 1.2O), with $k_{\mathrm{cat}} = 8.4 \times 10^{-3}\ \mathrm{min}^{-1}$ and $K_{\mathrm{M}} = 420$ nM at pH 7.8 and $k_{\mathrm{st}} = 2.9 \times 10^{-2}\ \mathrm{min}^{-1}$ at pH 6.[118,119] It can also excise the G deamination product xanthine (Figure 1.2Q), with $k_{\mathrm{cat}} = 4.8 \times 10^{-3}\ \mathrm{min}^{-1}$ and $K_{\mathrm{M}} = 53$ nM.[131] Xanthine's steady-state kinetic parameters are similar to those for 7MeG.[131] Oxanine (Figure 1.2R) excision was detected, but only after extended incubation time at high AlkA concentration.[131]

Despite their structural dissimilarity from alkylpurines, AlkA can also accept some damaged pyrimidines. O^2-Methylthymine (Figure 1.2S) and O^2-methylcytosine (Figure 1.2T) were excised approximately 2-fold faster than 3-methylpurines.[132] 5-Formyluracil (Figure 1.2U) excision proceeded with $k_{\mathrm{cat}} = 6.4 \times 10^{-3}\ \mathrm{min}^{-1}$ and $K_{\mathrm{M}} = 21$ nM, similar to those for the excision of 7MeG from a similar substrate.[123] AlkA can even slowly excise a ring-opened base produced from thymine C5-hydrate, *N*-(2-deoxy-β-D-erythro-pentofuranosyl)-*N*-3-(2R-hydroxyisobutyric acid)-urea (Figure 1.2P).[133]

AlkA-catalyzed excision of undamaged purines and pyrimidines has also been observed. Watson-Crick-paired G was released from a 2 kb fragment 2100-fold slower than 3MeA and 42-fold slower than 7MeG.[134] At pH 6, the k_{st}

values for A and G excision from mispairs were 6.9×10^{-3} min^{-1} and 5.2×10^{-3} min^{-1}, respectively. Excision from Watson-Crick pairs was ~50-fold slower: k_{st} for both bases was 1.3×10^{-4} min^{-1}.[118] Comparison of k_{st} values shows that A and G excision is 80- to 230-fold slower than excision of 3MeA and 7MeG.[118] Pyrimidine excision is slower than purine excision: under similar conditions, the k_{st} values for T, C, and uracil (all paired with C) were 2.8×10^{-5} min^{-1}, 4.7×10^{-4} min^{-1}, and 1.0×10^{-5} min^{-1}.[118] AlkA's excision of undamaged bases unnecessarily produces abasic sites, which is likely why constitutive AlkA expression leads to increased mutation rates.[134] This highlights the need for transcriptional control of such an indiscriminate enzyme.

AlkA appears to have *O*-glycosylase activity as well, hydrolyzing a variety of *O*-alkyl 2'-deoxyribosides (Figure 1.10).[135] In fact, the rate enhancement for β-methyl *O*-glycoside hydrolysis was over 300-fold greater than that for εA *N*-glycoside hydrolysis.[135] The enzymatic rate enhancement is defined as $k_{\text{st}}/k_{\text{non}}$, where k_{st} and k_{non} are the enzymatic and non-enzymatic rate constants, respectively, for the chemical step, i.e, *O*-glycoside cleavage.[135]

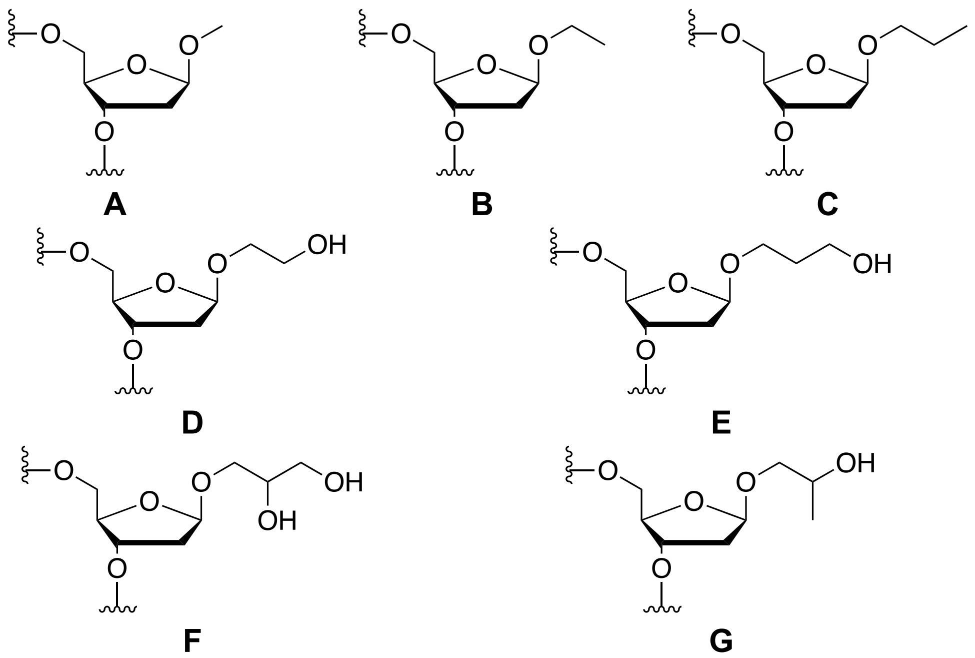

Figure 1.10. DNA *O*-glycosides that AlkA can hydrolyze

1.7 The mechanism of AlkA-catalyzed base excision

The first step in the proposed AlkA mechanism involves binding of the DNA substrate, then a base-flipping step that precedes *N*-glycosidic bond hydrolysis.[111] The crystal structure of AlkA•1-aza-DNA (Figure 1.11E) showed the sugar ring flipped into AlkA's active site. Weakening of the base pair in the damaged base mismatch would facilitate the flipping step.[111] Indeed, excision of mispaired normal purines and 7MeG in mismatches is faster than normal base pairs.[118] Extraneous functionalities on exocyclic or endocyclic O or N atoms on the Watson-Crick face would disrupt H-bonding and presumably facilitate flipping as well. Ease of flipping is not the sole determinant of excision efficiency, as shown by the differences in rates for the different mispaired purines, however.

Purines are generally excised faster than pyrimidines, though the purine ring system per se is not responsible for this preference, as AlkA can excise 5-formyluracil and O^2-methylpyrimidines as fast as some alkylpurines and can even excise acyclic substrates.[123,133-135]

The rate enhancement ($k_{\mathrm{st}}/k_{\mathrm{non}}$) was constant across several purines, namely Hx, 1,N^6-ethenoadenine, purine, 7MeG, G, and A, showing that AlkA is applying approximately the same amount of transition state stabilization across all substrates.[118] The differences in rates of C−N bond cleavage can be explained by differences in intrinsic reactivities of the scissile bases and would imply that AlkA is primarily stabilizing the common moiety among all the substrates, namely the oxacarbenium ion-like 2'-deoxyribose ring at the transition state.

Evidence for this stabilizing interaction comes from AlkA's affinities for oligonucleotides containing neutral and cationic sugar residues. AlkA binds to a DNA duplex containing a neutral tetrahydrofuran site (THF, Figure 1.11B) with $K_{\mathrm{d}} = 45$ nM, but with K_{d} values of 16 pM and 100 pM for DNA containing the cationic residues pyrrolidine (Figure 1.11E) and 1-aza (Figure 1.11D), respectively.[136,137] Its high affinity for the cationic species provides evidence that it stabilizes an oxacarbenium ion-like transition state (Figure 1.11C), one in which the extent of leaving-group (nucleobase) departure is greater than that of nucleophile bond formation.[76,111] The latter two species mimic the oxacarbenium ion via their cationic nitrogen atoms, but 1-aza is a better mimic because its positive charge is located at the same position as the oxacarbenium ion's (i.e., C1') (in donating electron density to C1’, the charge on O4’ increases to -0.03 from -0.33).[138]

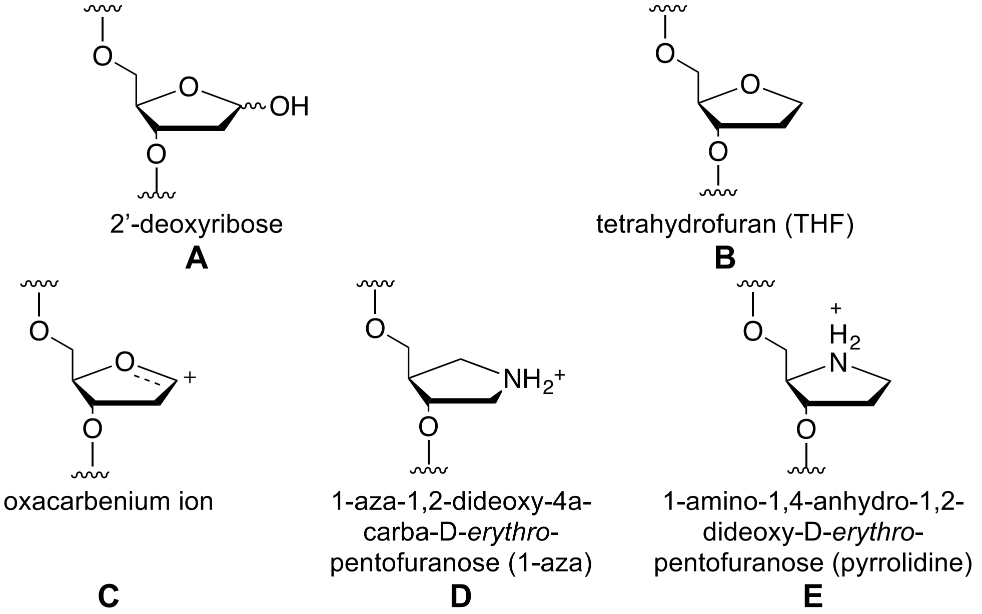

2’-deoxyribose
A

tetrahydrofuran (THF)
B

oxacarbenium ion
C

1-aza-1,2-dideoxy-4a-carba-D-*erythro*-pentofuranose (1-aza)
D

1-amino-1,4-anhydro-1,2-dideoxy-D-*erythro*-pentofuranose (pyrrolidine)
E

Figure 1.11. Sugar residues to which AlkA binds
A) 2’-deoxyribose (abasic site), one of the products of AlkA-catalyzed *N*-glycoside hydrolysis B) tetrahydrofuran (THF), identical to 2’-deoxyribose except C1’ is reduced C) oxacarbenium ion, the intermediate that forms when the nucleobase is fully departed D) 1-aza-1,2-dideoxy-4a-carba-D-*erythro*-pentofuranose (1-aza), an oxacarbenium-ion mimic E) 1-amino-1,4-anhydro-1,2-dideoxy-D-*erythro*-pentofuranose (pyrrolidine), another oxacarbenium-ion mimic

However, the pH dependence of AlkA-catalyzed excision suggests that AlkA could be protonating the nucleobase moiety to improve its leaving-group ability. Specifically, the rate of G excision falls as the pH increases from 6.5 to 7.9, while the rate of 7MeG excision is pH-independent.[134] A pH vs. k_{st} profile from pH 5 to 9 showed two ionizations for G and 1,N^6-ethenoadenine excision, but only one for 7MeG excision.[118] One of those ionizations can be assigned to D238. This residue is thought to stabilize the incipient positive charge at C1'. It is not thought to act as a general base that deprotonates water because there is not enough space in the AlkA•1-aza-DNA complex for water to fit between the D238 carboxylate and N1 of 1-aza.[111] Also, the D238N mutant is essentially inactive.[111]

The AlkA residue responsible for the second ionization is not known, but it is likely that this residue protonates N7 of purine substrates. Protonation and *N*-alkylation both facilitate hydrolysis by imparting a positive charge to the purine and allowing it to leave as a neutral species. Therefore, the most obvious strategy for catalyzing hydrolysis of unreactive *N*-glycosidic bonds is protonation.

1.8 Transition state analysis

There is evidence that the AlkA reaction proceeds via an oxacarbenium ion-like transition state, which implies one of two possible mechanisms.[111] In a D_N*A_N (S_N1) mechanism, nucleobase dissociation occurs first (the D_N step) and a discrete oxacarbenium ion intermediate appears (Figure 1.12A). Nucleophilic attack by water follows (the A_N step) and leads to product formation. In a dissociative A_ND_N mechanism, leaving group departure and nucleophile addition occur in one concerted step, with no discrete intermediate (Figure 1.12B). Because leaving group departure is far advanced over nucleophile addition, C1' has significant positive charge. These two mechanisms have distinct transition state structures, and determining AlkA's transition state structure would show whether the transition state is truly oxacarbenium ion-like and whether the leaving group is protonated at the transition state. As well, comparison of the enzymatic and cognate non-enzymatic transition states would illustrate how the enzyme is influencing the reaction trajectory.

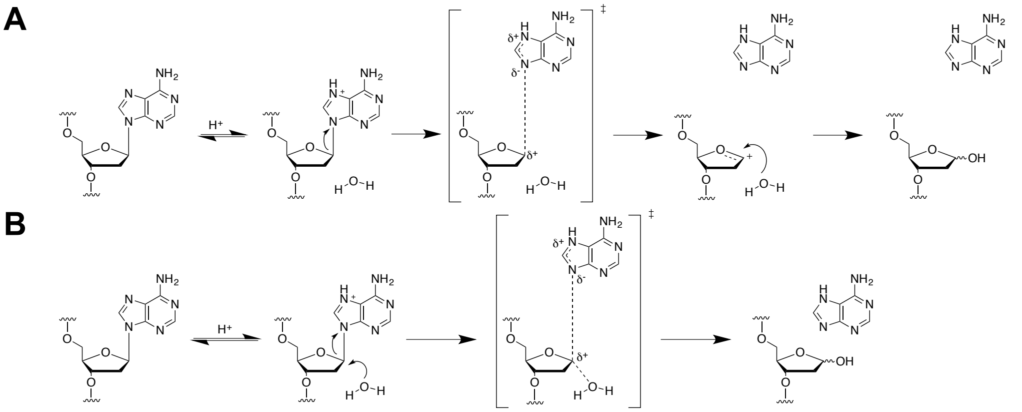

Figure 1.12. Possible mechanisms for AlkA-catalyzed *N*-glycoside hydrolysis
The transition state is in square brackets and denoted by the double-dagger symbol. A) D_N*A_N mechanism, in which an oxacarbenium ion forms after nucleobase departure. The transition state of interest is the transition state of oxacarbenium-ion formation; there is another transition state for nucleophile addition. B) Dissociative A_ND_N mechanism, in which C1' undergoes attack by water as the nucleobase departs. There is only one transition state, with C1' is partially bonded to both water and the nucleobase.

The transition state structure can be determined by measuring kinetic isotope effects (KIEs). KIEs are the differences in reaction rate that arise from an isotopic substitution in a reactant. They are expressed experimentally as the ratio of rates for the light versus the heavy isotopologues: $^{\text{light}}k/^{\text{heavy}}k$. KIEs are a fundamentally quantum phenomenon; they arise from three contributing factors: the changes in zero-point energies (ZPE), the excited-state energies (EXC), and the masses and moments of inertia (MMI) as a result of the isotopic substitution in the reactant and transition states (equation 1.2).[139]

$$\mathrm{KIE} = \mathrm{ZPE} \times \mathrm{EXC} \times \mathrm{MMI} \qquad \textbf{(1.2)}$$

Each term is a function of the vibrational frequencies in the transition state and reactant (equations 1.3, 1.4, and 1.5).[139]

$$\mathrm{ZPE} = \frac{\left[\prod_{i}^{3N-7} e^{\frac{-h({}^{\mathrm{light}}\nu_i - {}^{\mathrm{heavy}}\nu_i)}{2k_{\mathrm{B}}T}}\right]_{\mathrm{TS}}}{\left[\prod_{i}^{3N-6} e^{\frac{-h({}^{\mathrm{light}}\nu_i - {}^{\mathrm{heavy}}\nu_i)}{2k_{\mathrm{B}}T}}\right]_{\mathrm{reactant}}} \qquad \textbf{(1.3)}$$

$$\mathrm{EXC} = \frac{\left[\prod_{i}^{3N-7} \frac{1-e^{\frac{-h({}^{\mathrm{heavy}}\nu_i)}{k_{\mathrm{B}}T}}}{1-e^{\frac{-h({}^{\mathrm{light}}\nu_i)}{k_{\mathrm{B}}T}}}\right]_{\mathrm{TS}}}{\left[\prod_{i}^{3N-6} e \frac{1-e^{\frac{-h({}^{\mathrm{heavy}}\nu_i)}{k_{\mathrm{B}}T}}}{1-e^{\frac{-h({}^{\mathrm{light}}\nu_i)}{k_{\mathrm{B}}T}}}\right]_{\mathrm{reactant}}} \qquad \textbf{(1.4)}$$

$$\mathrm{MMI} = \frac{{}^{\mathrm{light}}\nu^{*}}{{}^{\mathrm{heavy}}\nu^{*}} \frac{\left[\prod_{i}^{3N-7} \frac{{}^{\mathrm{light}}\nu_i}{{}^{\mathrm{heavy}}\nu_i}\right]_{\mathrm{TS}}}{\left[\prod_{i}^{3N-6} \frac{{}^{\mathrm{light}}\nu_i}{{}^{\mathrm{heavy}}\nu_i}\right]_{\mathrm{reactant}}} \qquad \textbf{(1.5)}$$

In the preceding equations, h is the Planck constant, k_B is the Boltzmann constant, T is the temperature, and ν_i is the vibrational frequency of each normal mode, and ν^* is the imaginary frequency along the reaction coordinate. 3N-6 is the number of normal vibrational modes in the reactant. The transition state has

3N-7 normal vibrational modes, as the reaction-coordinate motion has an imaginary frequency and is not counted as a normal mode. The effects of isotopic substitution appear through changes in ν upon isotopic substitution. The value of ν is a function of the atomic masses, m_1 and m_2, in the bond and the force constant of the bond k (equation 1.6).[139]

$$\nu = \frac{1}{2\pi}\sqrt{\frac{k}{\frac{m_1 m_2}{m_1 + m_2}}} \qquad \textbf{(1.6)}$$

Generally, the major contributor to the KIE is the ZPE factor in equation 1.2, which arises due to changes in zero point energies. Zero point energy is the vibrational energy in a bond in its ground state at 0 K. Zero point energies depend on ν, which depends, in turn, on atomic masses. Heavy isotopes have lower zero point energies than lighter ones (equation 1.6). One can refer to an atom's vibrational environment as being "loose" or "tight", where a loose environment refers to weaker bonds (i.e., longer bond lengths) and reduced bending force constants and a tight vibrational environment refers to the opposite. If the transition state has a looser vibrational environment than the reactant, then the difference in the zero point energies will be smaller than that in the reactant, and the change in the free energy of activation for the heavy isotope (${}^{\text{heavy}}\Delta G^{\ddagger}$) will be greater than for the light isotope (${}^{\text{light}}\Delta G^{\ddagger}$). Therefore, ${}^{\text{light}}k$ will be greater than ${}^{\text{heavy}}k$, and the KIE will be greater than 1 (a normal KIE) (Figure 1.13A). If the transition state has a tighter vibrational environment than the reactant, then the difference in the ZPEs of the heavier and lighter isotopologues in the transition state will be smaller than that in the reactant, ${}^{\text{heavy}}\Delta G^{\ddagger} < {}^{\text{light}}\Delta G^{\ddagger}$, ${}^{\text{light}}k < {}^{\text{heavy}}k$, and KIE < 1 (an inverse KIE) (Figure 1.13B).

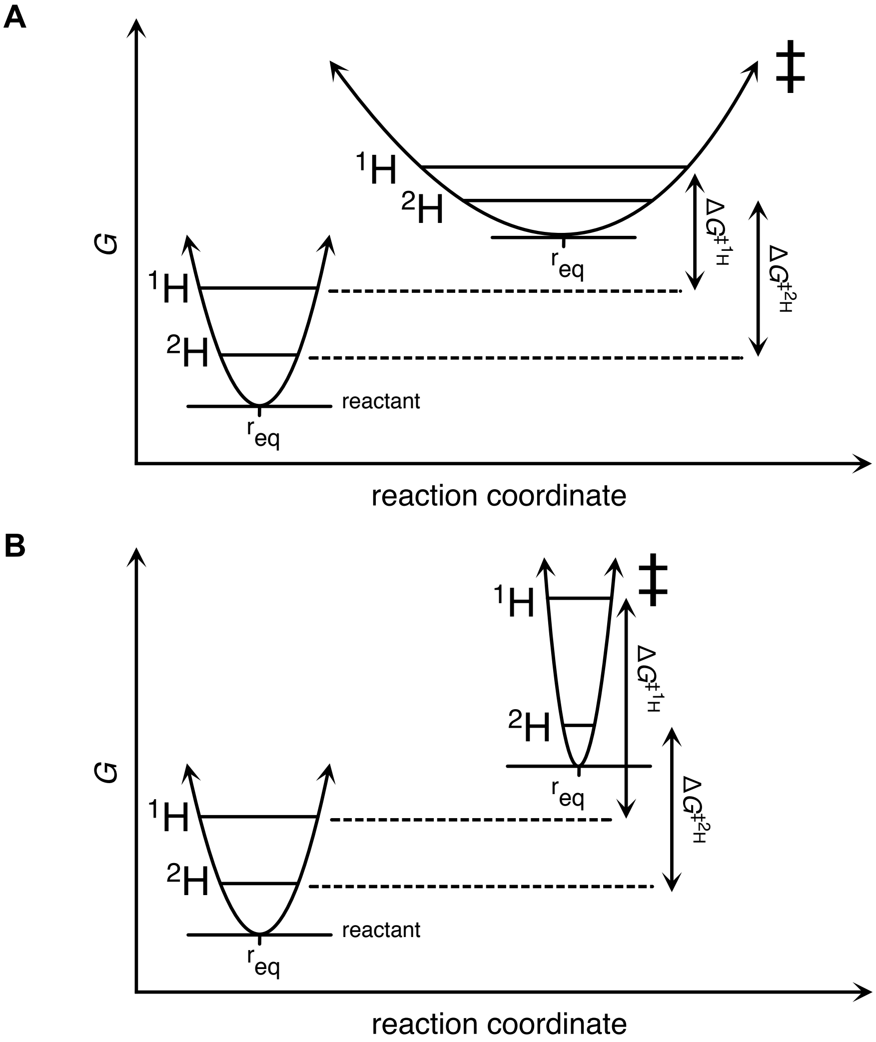

Figure 1.13. Change in the activation free-energy change (Δ$G^{\ddagger}$) upon replacing ^{1}H with ^{2}H in a C-H bond away from the reaction centre

r_{eq} = the equilibrium bond distance. The transition state is indicated by the double dagger. A) Transition state represents a looser vibrational environment. B) Transition state represents a tighter vibrational environment.

Primary KIEs refer to the atoms directly involved in bond breakage or formation in the reaction. In addition to the ZPE contributions, primary KIEs also contain a contribution from the reaction coordinate motion, which is reflected in the ratio of imaginary frequencies ($\nu^{*\text{light}}/\nu^{*\text{heavy}}$) in the MMI term (equation 1.5). The reaction coordinate, with its imaginary frequency, is not considered a normal vibrational mode and therefore is not part of the ZPE. Because imaginary frequencies are always higher for light versus heavy isotopes, the reaction coordinate contribution ($^{\text{light}}\nu^* / {}^{\text{heavy}}\nu^*$) is always normal.[139]

Structural changes can be propagated some distance through the molecule from the reaction center. These changes will be reflected in KIEs at atoms not directly involved in the chemical reaction; these KIEs are called secondary KIEs.

1.8.1 Competitive vs. non-competitive KIEs

KIEs can be measured competitively or non-competitively. In a competitive KIE, the two reactant isotopologues are present in the same mixture and both react simultaneously. The KIE is measured as the change in the abundances of the light and heavy isotopologues after the reaction is taken partway to completion. A competitive enzymatic KIE is a ratio of specificity constants, $k_{\text{cat}}/K_{\text{M}}$, for the light and heavy isotopes (equation 1.7).[140] The value of $k_{\text{cat}}/K_{\text{M}}$ reflects the pseudo-equilibrium between the free enzyme and substrate in solution and the first irreversible transition state ($E + S \rightleftharpoons ES^{\ddagger}$); therefore, the competitive KIE only accounts for steps up to and including the first irreversible step.

$$\mathrm{KIE} = \frac{{}^{\mathrm{light}}\left(k_{\mathrm{cat}} / K_{\mathrm{M}}\right)}{{}^{\mathrm{heavy}}\left(k_{\mathrm{cat}} / K_{\mathrm{M}}\right)} \tag{1.7}$$

In a non-competitive KIE measurement, the rates with each isotopologue are measured independently in separate reactions, and the KIE is calculated from the ratio of the two rates. If the KIE is measured under subsaturating conditions, it is a ratio of specificity constants (i.e., $k_{\mathrm{cat}}/K_{\mathrm{M}}$) as in equation 1.7, and reflects the same steps as a competitive KIE. Non-competitive KIEs measured under saturating conditions reflect the ratio of turnover constants (i.e., k_{cat}) (equation 1.8). The value of k_{cat} reflects the pseudo-equilibrium between the Michaelis complex and the transition state for the rate-limiting step ($\mathrm{E{\bullet}S} \rightleftharpoons \mathrm{ES}^{\ddagger}$); therefore, it accounts for steps only after substrate binding, including proton transfer, nucleophilic attack by water, and product release.

$$\mathrm{KIE} = \frac{{}^{\mathrm{light}}\left(k_{\mathrm{cat}}\right)}{{}^{\mathrm{heavy}}\left(k_{\mathrm{cat}}\right)} \tag{1.8}$$

1.8.2 Significance of individual KIEs

For purine nucleosides, the primary 1’-^{14}C KIE and 9-^{15}N KIEs are informative, as they reflect the leaving-group (C1’-N9) and incoming nucleophile (C1’-O) bond orders. They can show whether the transition state is oxacarbenium ion-like.[76] The 7-^{15}N KIE for purines indicates the extent of N7 protonation at the transition state.[76] The 2'(*S*)-^{2}H and 2'(*R*)-^{2}H KIEs report on the 2'-deoxyribosyl ring's conformation at the transition state, as their values reflect conformation-dependent hyperconjugation. Hyperconjugation is the donation of electron density from the C2'-H2' σ orbitals to the empty p orbital of C1' to stabilize the developing positive charge on C1' in an oxacarbenium ion-like transition state.[76] Hyperconjugation is conformation-dependent, so the 2'-^{2}H KIEs indirectly report on the sugar ring conformation at the transition state.[76] The 1'-^{3}H KIE reports on the vibrational freedom of H1'. Its vibrational freedom increases when there is an overall loss of bond order to C1' (as in dissociative transition states).[76]

1.8.3 Transition state structure determination

Solving the transition state structure from experimental KIE values requires creating computational models whose expected KIEs can be calculated. KIE computation is generally considered reliable for a given structure; thus, if a computational model is found whose calculated KIEs match the experimental values, that is considered the experimental transition state structure.

1.8.4 Transition state structures of base-excision enzymes and nucleoside hydrolases

The transition states of other BER enzymes have been determined. *E. coli* MutY is a BER enzyme that excises A from 8-oxoguanine:A mismatches. A suite of KIEs were measured at eight positions – 1'-^{14}C, 9-^{15}N, 7-^{15}N, 6-^{15}N, 1'-^{3}H, 2'(*S*)-^{2}H, 2'(*R*)-^{2}H, and 5'-$^{3}H_2$ – of an A residue mismatched with G in a 25-mer stem-loop DNA substrate.[141] Comparison of experimental KIEs to calculated KIEs from five computed transition-state models revealed a $D_N{*}A_N^{\ddagger}$ mechanism with reversible C1'-N9 bond cleavage that forms a discrete oxacarbenium-ion intermediate followed by irreversible attack at C1' by water.[141] Although less extensively than for MutY, the transition state of *E. coli* UDG was studied by measuring 1'-^{2}H, 1'-^{13}C, 2'(*S*)-^{2}H, 2'(*R*)-^{2}H KIEs of uracil excision from a DNA trinucleotide; the values demonstrated demonstrated an oxacarbenium ion-like transition state at which uracil possessed anionic character.[94]

The transition state was also determined for an RNA base-excision enzyme, ricin A-chain, which is a castor bean toxin that depurinates A4324 of 28S ribosomal RNA.[80] By measuring KIEs at similar positions to MutY for adenine excision from a 10-mer stem-loop RNA substrate, it was revealed the reaction proceeds via an oxacarbenium ion-like transition state and that reversible C-N bond cleavage is followed by an irreversible non-chemical step.[80]

In addition to these enzymes, transition states of nucleoside hydrolases and phosphorylases involved in purine/pyrimidine salvage and *de novo* synthesis have been determined. Some of these enzymes are potential anticancer or antibacterial targets; therefore, high-affinity inhibitors of these targets can be designed using the transition state as a template because enzymes reduce $\Delta G^{\ddagger}$ by stabilizing the transition state.[142] For example, immucillin-H and immucillin-G (Figure 1.15B and C) were designed from the transition state structure of bovine purine nucleoside phosphorylase (PNP), which catalyzes the nucleophilic attack of inosine, guanosine, and deoxyguanosine by phosphate (Figure 1.14).[143]

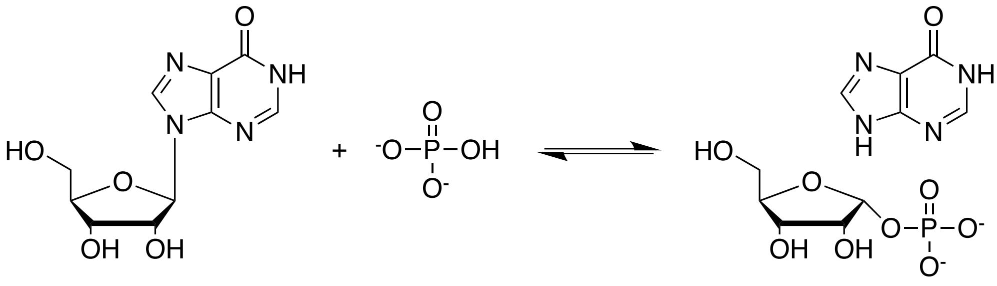

Figure 1.14. Reaction catalyzed by purine nucleoside phosphorylase (PNP)
Shown is the phosphorolysis of inosine, which produces ribose 1-phosphate and hypoxanthine.

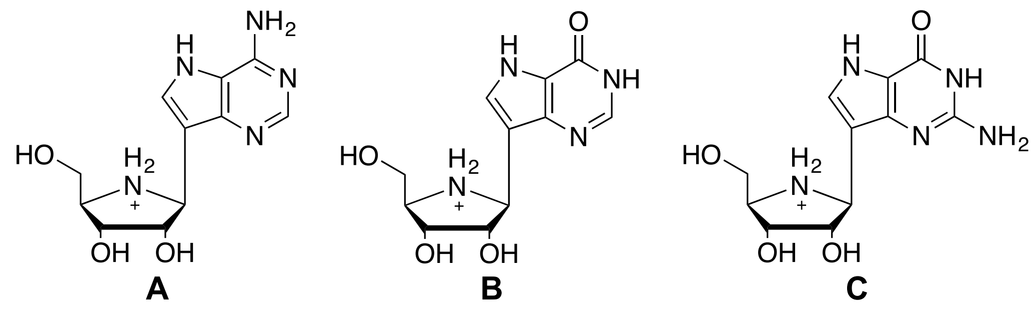

Figure 1.15. Immucillins
A) immucillin-A B) immucillin-H C) immucillin-G

Bovine PNP's transition state was protonated at N7 and exhibited oxacarbenium ion-like character, and the immucillins capture these properties by possessing cationic iminoribitol in place of ribose and by raising N7's pK_a as a result of C9 replacing N9; the K_i values of immucillin-H and immucillin-G were 23 pM and 29 pM, respectively.[143-145] Despite being designed from the bovine PNP transition state, both immucillin-H and immucillin-G demonstrated similar K_i values for human PNP (72 pM and 30 pM, respectively), the inhibition of which may be a strategy for treating leukemia and lymphoma.[143,146] Immucillin-H was also found to bind to PNP of the malaria parasite *Plasmodium falciparum*, but with lower affinity than the bovine and human PNPs (K_i = 860 pM).[147] Derivatives of immucillin-A (Figure 1.15A) bound to 5'-methylthioadenosine nucleosidases (MTANs, Figure 1.16) of the pathogenic bacteria *Salmonella enterica* and *Vibrio cholerae* with K_i values ranging from 300 pM to 3 pM.[148]

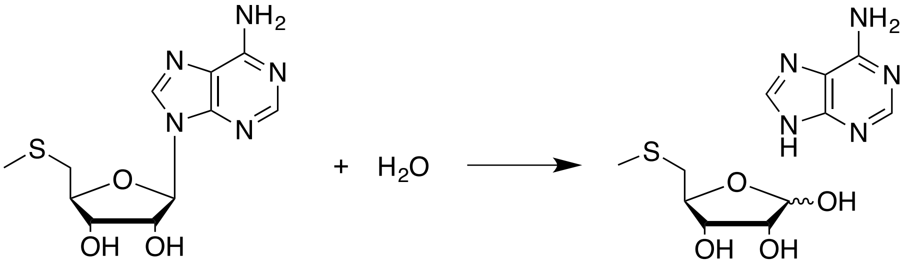

Figure 1.16. Reaction catalyzed by 5'-methylthioadenosine nucleosidases (MTANs)

1.9 Objectives of this work

This work describes the progress made in elucidating the transition state structures of AlkA-catalyzed Hx excision from DNA and of acid-catalyzed hydrolysis of 2'-deoxyinosine 5'-monophosphate (dIMP) using kinetic isotope effects (KIEs).

The present study seeks, in part, to identify how AlkA protonates the purine leaving group to activate it for departure. First, the source of the proton was examined. Besides D238, the ionizable or H-bonding active-site residues that could participate in protonation are Y273, W272, Y222, R244, and R22 (Figure 1.17).

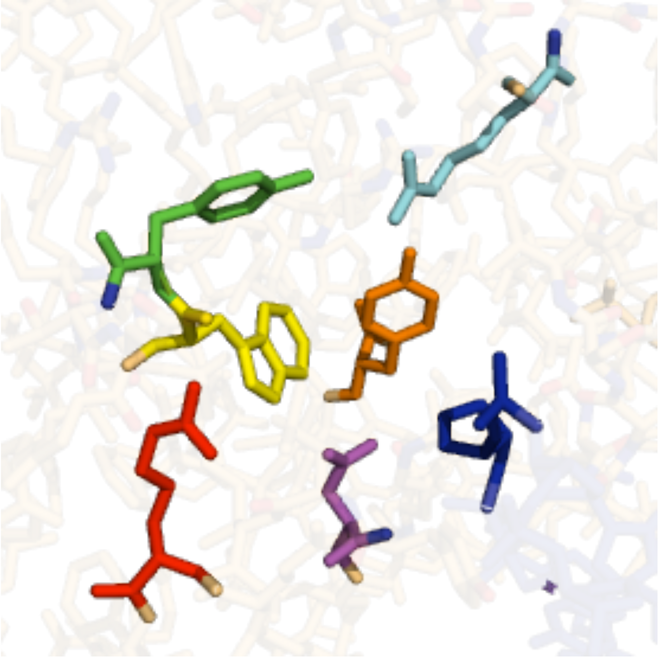

Figure 1.17. Candidate general-acid residues in AlkA's active site
Green = Y273, cyan = R22, red = R244, orange = Y222, yellow = W272, purple = D238, blue = pyrrolidine. Figure generated in PyMOL from PDB ID 1DIZ.[111]

These residues were mutated such that their ionization and/or H-bonding properties were eliminated. Then, the mutants' ability to excise Hx was studied; if any single residue is responsible for Hx protonation, then a dramatic loss in activity should be observed. This approach was used to identify H241 as the general acid for *Crithidia fasciculata* inosine-uridine nucleoside hydrolase (IU-NH), as the H241A mutant was over 2000-fold less active toward inosine but but only 3-fold less active for *p*-nitrophenyl *β*-D-ribofuranoside, a substrate not requiring leaving group protonation (Section 1.4.2).[97]

The effect of buffer concentration on Hx excision by WT and mutant AlkA was also studied. Participation of small acidic species in an enzymatic reaction was observed previously with human carbonic anhydrase III, for which imidazole increases the rate of water release.[149]

Direct interactions between AlkA and the nucleobase at the transition state could be detected by examining the K_d of AlkA, a free nucleobase, and a transition state-mimicking oligonucleotide, pyrrolidine-DNA. If AlkA interacts with the nucleobase at the transition state, the apparent K_d of pyrrolidine-DNA will decrease in the presence of the nucleobase. Such a bipartite inhibitor of uracil DNA glycosylase (UDG) was formed by uracil and 1-aza-DNA, with the K_d of the ternary complex being 4000-fold lower than for 1-aza-DNA alone. [150]

Additional evidence for purine protonation by AlkA was obtained from the solvent deuterium kinetic isotope effects (SDKIEs) at different pL values (pL = pH or pD, depending on the isotope) and buffer conditions. The SDKIE is the change in rate when the reaction is performed in D_2O and reflects the extent of proton transfer at the transition state of the rate-determining step. [87,151]

Chapter 2. Materials and Methods

2.1 Materials

All radiolabelled glucoses were obtained from American Radiolabeled Chemicals, Inc. [γ-^{33}P]-labelled adenosine 5'-triphosphate (ATP) was obtained from Perkin-Elmer Inc. *S. cerevisiae* hexokinase (HK), rabbit muscle pyruvate kinase (PK), rabbit muscle myokinase (MK), *Leuconostoc mesenteroides* glucose-6-phosphate dehydrogenase (G6PDH), *S. cerevisiae* 6-phosphogluconic dehydrogenase (6PGDH), spinach phosphoriboisomerase (PRI), *Aspergillus niger* adenylic acid deaminase (ADA) were obtained from Sigma-Aldrich. Human apurinic/apyrimidinic endonuclease 1 (hAPE1) was from New England Biolabs, Inc. T4 polynucleotide kinase and Moloney murine leukemia virus reverse transcriptase (MMLV-RT) were obtained from Life Technologies Corp. Ecoscint A was from National Diagnostics. Protease-inhibitor cocktail for His-tagged proteins was obtained from Sigma-Aldrich or BioShop Canada. All other materials were reagent-grade. *Lactobacillus leichmannii* ribonucleoside triphosphate reductase (RTR), *E. coli* phosphoribosylpyrophosphate synthetase (PRPPase), *S. cerevisiae* adenine phosphoribosyltransferase (APRT) were prepared as previously described.[152]

2.2 Purification of WT and mutant AlkA

The Y222F, R22M, R244M, Y273F, and W272F mutations were inserted into pET24a-His$_6$AlkA (a gift from Dr. Patrick O' Brien, University of Michigan) according to the Agilent QuikChange mutagenesis protocol. Plasmids containing the mutant and WT AlkA constructs were amplified using the QIAprep miniprep kit and sequenced to confirm their identities.

BL21*(DE3) *E. coli* cells were transformed with pET24a-His$_6$AlkA by heat shock and grown in 2 × 1 L LB with 50 μg/mL kanamycin at 37 °C until OD$_{600}$ ~ 1. Expression of AlkA was induced with 1 mM IPTG and the cultures were incubated at 16 °C to 18 °C overnight. Cells were harvested by centrifugation at 5000 × *g*. The cell paste was resuspended in lysis buffer containing 50 mM tris(hydroxymethyl)aminomethane hydrochloride (Tris-HCl), pH 7.5, 150 mM NaCl, and 20 mM imidazole, and protease-inhibitor cocktail for His-tagged proteins (i.e., without EDTA). Cell lysis was performed using an EmulsiFlex-C5 homogenizer (Avestin Inc.). The lysate was centrifuged at 20000 × *g* for 30 min at 4 °C and the supernatant was syringe-filtered (0.45 μm filter). The filtered supernatant was applied to a Ni^{2+}–charged 1 mL HiTrap Chelating HP column (GE Healthcare). The column was washed with 20 column volumes of lysis buffer. The column was then washed with 20 column volumes of a wash buffer containing 50 mM Tris‑HCl, pH 7.5, 150 mM NaCl, and 80 mM imidazole. An elution buffer containing 50 mM Tris‑HCl, pH 7.5, 150 mM NaCl, and 500 mM imidazole was applied until A_{280} of the eluate reported no protein. AlkA was dialyzed into a storage buffer containing 20 mM sodium 4-(2-hydroxyethyl)-1-piperazineethanesulfonate (NaHEPES), 100 mM NaCl, 1 mM dithiothreitol (DTT), 0.2 mM ethylenediaminetetraacetic acid (EDTA), 50 mM L-arginine, and 50 mM L-glutamic acid, pH 7.5. The protein was quantified according to the method of Pace and Edelhoch.[153]

2.3 Oligonucleotides

ATI26, G19, C18, THF35, I25, and I24comp (Table 2.1) were synthesized by Integrated DNA Technologies, Inc. PYR35 was synthesized by MOBIX Lab (McMaster University) using a pyrrolidine-CE phosphoramidite from Glen Research Corp. All oligonucleotides were purified by polyacrylamide gel electrophoresis (PAGE) before use and quantified by A_{260}, with ε_{260} calculated by the nearest-neighbour method.[154].

ATI26, THF53, THF47, THF41, THF35, and PYR35 form hairpins. The inosine is bulged in ATI26 while the abasic sites in PYR35 and THF35 are internal (Figure 2.1). I25 and I24comp were annealed to form the 24-mer Hx-bulge duplex, IB25, under the same conditions as the assays they were used in (Figure 2.1).

Table 2.1. Oligonucleotides used in the studies described in Chapter 3, Chapter 4, and Chapter 5

The bolded letter indicates the scissile/binding site: I = hypoxanthine (Hx), P = pyrrolidine (Figure 1.11E), F = tetrahydrofuran (Figure 1.11B).

ATI26	5′ GAGGAAGTCCGTTTCGGAC**I**TTCCTC 3′
G19	5′ GAGGAAGTCCGTTTCGGAC 3′
C18	5′ GAGGAACGTCCGAAACGG 3′
THF53	5′ ACGAGGAACACC**F**AGTGGAAGTCAGTTTCTGACTTCCACTCGGTGTTCCTCGT 3′
THF47	5′ AGGAACACCG**F**GTGGAAGTCAGTTTCTGACTTCCACTCGGTGTTCCT 3′
THF41	5′ AACACCGA**F**TGGAAGTCAGTTTCTGACTTCCACTCGGTGTT 3′
PYR35	5′ AACACCGA**P**TGGAAGTTTTACTTCCACTCGGTGTT 3′
THF35	5′ AACACCGA**F**TGGAAGTTTTACTTCCACTCGGTGTT 3′
I25	5′ CGATAGCATCCT**I**CCTTCTCTCCAT 3′
I24comp	5′ ATGGAGAGAAGGAGGATGCTATCG 3′

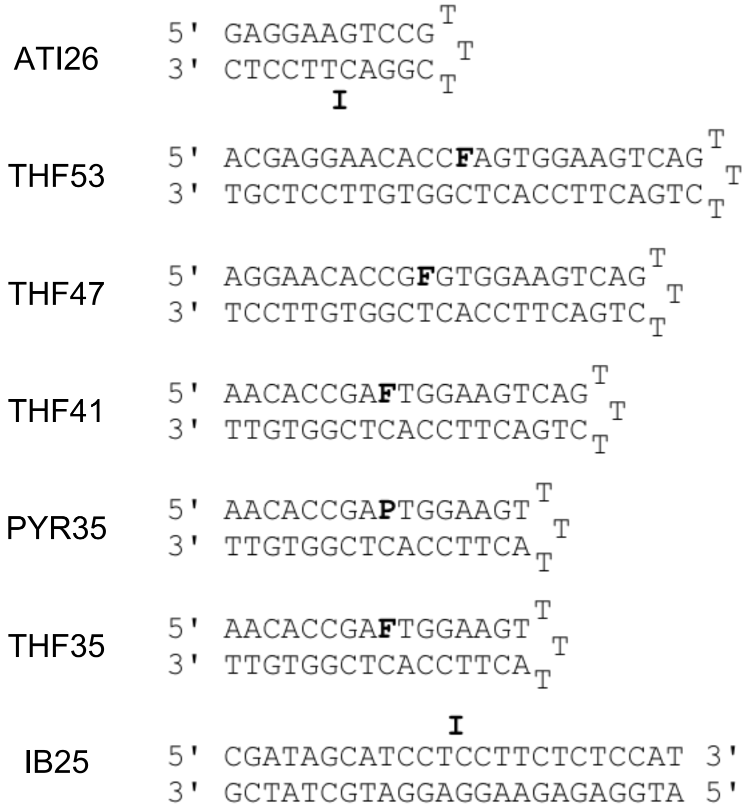

Figure 2.1. Secondary structures formed by oligonucleotides listed in Table 2.1
The bolded letter indicates the scissile/binding site: I = hypoxanthine (Hx), P = pyrrolidine (Figure 1.11E), F = tetrahydrofuran (Figure 1.11B). In IB25, the Hx-containing strand is I25 and its complement is I24comp.

2.4 5’-^{33}P Labelling

ATI26/I25 (1 μM) or PYR35/THF35 (0.005 μM) were 5’-labelled in a reaction containing 10 to 14 μCi of [γ-^{33}P]-labelled ATP, 70 mM Tris-HCl, pH 7.6, 10 mM $MgCl_2$, and 100 mM KCl, and 1 mM 2-mercaptoethanol, was reacted with 0.4 U/μL to 0.8 U/μL T4 polynucleotide kinase at 37 °C for 1 h. The reaction was quenched with 1 μL 0.5 M EDTA pH 8.0. The reaction was diluted 2-fold and extracted with chloroform. The aqueous phase containing the labelled strand was run through an illustra MicroSpin G-25 column (GE Healthcare).

2.5 Electrophoretic mobility shift assay (EMSA)

2.5.1 K$_d$ *determination*

[5’-^{33}P]PYR35 (125 pM) or [5’-^{33}P]THF35 DNA (200 pM) was incubated with 12 AlkA concentrations (0 to 5 μM for PYR35, 0 μM to 10 μM for THF35) in 25 mM potassium phosphate, pH 7.0 (also pH 6.0 and 8.0 for PYR35), 50 mM KCl, 0.5 mM EDTA, 0.5 mM DTT, 10% glycerol, and 0.5 mg/mL bovine serum albumin (BSA). Loading dye (0.25% bromophenol blue, 0.25% xylene cyanol, 30% glycerol in 1× TBE) was added only to the sample containing 0 nM AlkA (1 μL). Samples were incubated for 1 h at room temperature. Samples were loaded onto a 10% native polyacrylamide gel in 0.5× TBE at 4 °C as it was running at 250 V. The voltage was increased to 1100 V (50 V/cm). After both dyes entered the gel (2 to 3 min), the voltage was decreased to 250 V. The gel was dried onto blotting paper using a Hoefer gel dryer (GE Healthcare) and the dried gel was exposed to a storage-phosphor screen overnight. The screen was scanned on a phosphorimager. The resultant autoradiogram was imported into ImageJ (Wayne Rasband, National Institutes of Health) using the LOCI Bio-Formats importer (University of Wisconsin, Madison). The dissociation constants of AlkA complexes with PYR35 at pH 6 and 8 and THF53, THF47, THF41, and THF35 at pH 7 were calculated using equation 2.1, where f_{bound} is the fraction of DNA bound by AlkA, $[\text{DNA}]_0$ is the total DNA concentration, and the [E] is the enzyme concentration. For the THF ligands, f_{bound} is not normalized against the maximal f_{bound} value and is defined by equation 2.2, where A_{bound} is the intensity of the band corresponding to bound DNA and A_{free} is the intensity of the band corresponding to free DNA. For the PYR ligand at pH 6 and 8, f_{bound} is defined in terms of equation 2.1 and normalized against the maximal f_{bound} value (equation 2.3).

$$f_{\mathrm{bound}} = \frac{([\mathrm{E}]+[\mathrm{DNA}]_0+K_{\mathrm{d}})-\sqrt{([\mathrm{E}]+[\mathrm{DNA}]_0+K_{\mathrm{d}})^2-4[\mathrm{E}][\mathrm{DNA}]_0}}{2[\mathrm{DNA}]_0} \quad \textbf{(2.1)}$$

$$f_{\mathrm{bound}_{\mathrm{non-normalized}}} = \frac{\mathrm{A}_{\mathrm{bound}}}{\mathrm{A}_{\mathrm{bound}}+\mathrm{A}_{\mathrm{free}}} \quad \textbf{(2.2)}$$

$$f_{\mathrm{bound}_{\mathrm{normalized}}} = \frac{f_{\mathrm{bound}_{\mathrm{non-normalized}}}}{f_{\mathrm{bound}_{\mathrm{non-normalized}_{\mathrm{max}}}}} \quad \textbf{(2.3)}$$

The dissociation constant of AlkA complexes with PYR35 at pH 7 were fitted to the two-site model in equation 2.4, where f_{bound} is defined by equation 2.2, [E] is the enzyme concentration, $K_{\mathrm{d},1}$ and $K_{\mathrm{d},2}$ are the dissociation constants for each site, and C_1 and C_2 are the capacities of each site.

$$f_{\mathrm{bound}} = \left(\frac{[\mathrm{E}]C_1}{[\mathrm{E}]+K_{\mathrm{d},1}}\right)+\left(\frac{[\mathrm{E}]C_2}{[\mathrm{E}]+K_{\mathrm{d},2}}\right) \quad \textbf{(2.4)}$$

2.5.2 Detection of ternary complexes

[5’-^{33}P]PYR35 (125 pM) was incubated with 2.4 nM AlkA and up to 2 mM adenine, nicotinamide, or Hx (up to 2 mM) in 25 mM potassium phosphate, pH 7.0, 50 mM KCl, 0.5 mM EDTA, 0.5 mM DTT, 10% glycerol, and 0.5 mg/mL

BSA. Samples were incubated for 4 h at room temperature. Loading dye was not added to any of the samples at the end of the incubation period. Samples were loaded onto a 10% native polyacrylamide gel in 0.5× TBE at 4 °C as it was running at 250 V. The voltage was increased to 1100 V (50 V/cm). After 2 min, the voltage was decreased to 250 V. The gel was analyzed as described in Section 2.5.1.

2.6 Glycosylase assay

2.6.1 Hypoxanthine excision from ATI26

All reaction mixtures contained AlkA, ATI26 (unlabelled and 5’-^{33}P-labelled), 50 mM KCl, 1 mM dithiothreitol (DTT), and 0.5 mg/mL BSA. Reactions at pH 6.0 were performed in 50 mM potassium acetate. Reactions at pH 7.0 were performed in 50 mM potassium phosphate. Reactions performed with human apurinic/apyrimidinic endonuclease (hAPE1) were performed with 1 U/μL hAPE1 and 1 mM $MgCl_2$. Reactions performed without hAPE1 contained 1 mM EDTA. Aliquots (5 μL) were taken periodically, quenched with 1 μL 2 M KOH, heated at 95 °C for at least 5 min, mixed with 5 μL of 2 × denaturing loading dye, and run on a 20% denaturing polyacrylamide gel (7 M urea, 1 × TBE). The gel was exposed to a storage-phosphor screen (GE Healthcare) overnight and the screen was scanned on a phosphorimager. The product fraction f_{product} and the substrate fraction $f_{\text{substrate}}$ were calculated with equations 2.5 and 2.6, where

$A_{product}$ is the intensity of the product band and $A_{substrate}$ is the intensity of the substrate band in the autoradiogram, and [product] was calculated from $f_{product}$ using equation 2.7.

$$f_{product} = \frac{A_{product}}{A_{product} + A_{substrate}} \tag{2.5}$$

$$f_{substrate} = \frac{A_{substrate}}{A_{product} + A_{substrate}} \tag{2.6}$$

$$[\text{product}] = f_{product}[S]_0 \tag{2.7}$$

2.6.2 Hypoxanthine excision from IB25

Reactions containing AlkA and IB25 were performed in 75 mM buffer, 0.1 mg/mL BSA, and 1 mM DTT at 37 °C. Reactions contained at least 15000 cpm/µL [5'-^{33}P]IB25, with the remaining IB25 unlabelled. All reactions were adjusted to $I = 0.250$ using KCl. The final ionic strength of the reaction mixture (buffer and KCl) was calculated using the Debye-Hückel equation (equation 2.8), where $pK_{a,T}$ is the pK_a of the buffer at temperature T, pK_a is the pK_a of the buffer at $T = 298$ K, ξ_a is the charge of the conjugate acid/base, A is a constant ≈ 0.5, and I is the ionic strength.[155]

$$pK_{a,T} = pK_a + (2\xi_a - 1)\left[\frac{A\sqrt{I}}{1+\sqrt{1}} - 0.1I\right] \tag{2.8}$$

Aliquots (5 μL) were taken periodically, quenched with 2.5 μL 0.6 M KOH, and heated at 70 °C for 10 min. Samples were mixed with 10 μL formamide loading buffer (1 mg/mL xylene cyanol, 1 mg/mL bromophenol blue, and 10 mM EDTA pH 8.0 in formamide) and run on a 30% denaturing polyacrylamide gel (7 M urea, 1× TBE). Gels were exposed to a storage-phosphor screen overnight and the screen was scanned on a phosphorimager. Data analysis was performed as described in Section 2.6.1.

2.7 pH-rate profiles

Potassium cacodylate was used as the buffer for reactions at pH 4.5 to 6, while potassium acetate was used at pH 5.5 and 6, while potassium phosphate was used at pH 6, 7, and 8. All reactions were performed with 0.1 μM WT AlkA except those at pH 7 and 8, which were performed at 0.5 μM WT AlkA.

For each pH, [IB25] was varied from 0.1 μM to 10 μM. The reactions were sampled and analyzed according to Section 2.6.2. The initial rates (calculated from the slope of the [product] vs. *t* line) were fitted to the Michaelis-Menten equation (equation 1.1).

The parameters k_{cat} and $k_{\mathrm{cat}}/K_{\mathrm{M}}$ at each pH were fit to equation 2.9, where x is the kinetic parameter, $limit_x$ refers to the upper limit of x, and pK_a is the ionization on the relevant species for that parameter.

$$x = \frac{\mathrm{limit}_x}{10^{\mathrm{pH}-\mathrm{p}K_\mathrm{a}} + 1} \qquad \textbf{(2.9)}$$

2.8 Effect of buffer concentration on rate of AlkA-catalyzed hypoxanthine excision

Reactions were performed and analyzed as described in Section 2.6.2 with 2 μM IB25. For pH 5 and 6, 0.1 μM AlkA was used; for pH 7 and 8, 0.5 μM AlkA was used. Reactions in potassium cacodylate (0 mM to 200 mM) were performed at pH 5 to 7. Reactions in potassium phosphate (0 to 90 mM) were performed at pH 7 and 8. Reactions in bis-tris propane (BTP) (0 to 200 mM) were performed at pH 7 in 25 mM potassium phosphate. Rates as a function of buffer concentration were fit to a linear equation except the rates in BTP/phosphate, which were fit to equation 2.10, where $v_0/[\mathrm{E}]_0$ is the observed rate at each [BTP], $v_0/[\mathrm{E}]_{0,\mathrm{max}}$ is the highest observed rate (i.e., at [BTP] = 0 mM), and K_i is the inhibition constant.

$$\frac{v_0}{[\mathrm{E}]_0} = \frac{\left(\frac{v_0}{[\mathrm{E}]_0}\right)_{\mathrm{max}}}{1 + \frac{[\mathrm{BTP}]}{K_\mathrm{i}}} \qquad \textbf{(2.10)}$$

2.9 SDKIE measurement

DTT was dissolved in D_2O to a final concentration of 1 M. KCl was dissolved in D_2O to a final concentration of 2 M. BSA was dissolved in D_2O and lyophilized repeatedly. The lyophilized BSA was finally dissolved in D_2O to a final concentration of 5 mg/mL. DTT, KCl, and BSA were prepared in H_2O by dissolving them directly in H_2O to the same final concentrations as the D_2O solutions.

KH_2PO_4 and K_2HPO_4 were dissolved separately in D_2O and lyophilized repeatedly. The lyophilized KH_2PO_4 and K_2HPO_4 were dissolved separately in D_2O each to a final concentration of 1 M. KH_2PO_4 and K_2HPO_4 were mixed to produce 0.5 M potassium phosphate buffers at pD 6 and pD 7. pD was verified using a pH electrode (pD = pH + 0.4). Potassium phosphate buffers at pH 6 and pH 7 in H_2O were prepared by dissolving KH_2PO_4 to a final concentration of 0.5 M and by adjusting the solution pH with KOH.

Mixtures of I25/I24comp and [5'-^{33}P]I25/I24comp were lyophilized. The mixtures were resuspended in potassium phosphate buffer in D_2O and H_2O (10 mM potassium phosphate at pL 6, 10 mM potassium phosphate at pL 7, and 75 mM potassium phosphate at pL 7, $I = 0.250$ using KCl). The strands were annealed to form IB25 by heating at 95 °C and slow cooling to room temperature.

Using Amicon Ultra-0.5 mL 10 K MWCO centrifugal concentrators, AlkA was exchanged into potassium phosphate buffer in D_2O and H_2O (10 mM potassium phosphate at pL 6, 10 mM potassium phosphate at pL 7, and 75 mM potassium phosphate at pL 7, $I = 0.250$ using KCl). The protein was quantified according to the method of Pace and Edelhoch.[153]

Reaction mixtures were prepared at 10 mM potassium phosphate at pL 6, 10 mM potassium phosphate at pL 7, and 75 mM potassium phosphate at pL 7. Each mixture contained 0.1 mg/mL BSA, 1 mM DTT, and KCl so that $I = 0.250$ (see Section 2.6.2). Reactions at pL 6 and pL 7 were performed with 0.1 μM

AlkA and 0.5 μM AlkA, respectively. [IB25] in each reaction was 0.2, 2, and 10 μM, with each containing at least 15000 cpm/μL [5'-^{33}P]IB25. Reactions were incubated at 37 °C, sampled, and analyzed according to the procedure in Section 2.6.2.

2.10 Synthesis and purification of radiolabelled 2'-deoxyadenosine 5'-triphosphate (dATP)

Radiolabelled adenosine 5'-triphosphate (ATP) was synthesized at 37 °C with radiolabelled glucose (25 μCi of [^{3}H]glucose, 10 μCi of [^{14}C]glucose) (Table 2.2), 3.2 mM adenine, 1 mM DTT, 50 mM glycylglycine, pH 7.8, 55 mM potassium phosphate, pH 7.8, 10 mM $MgCl_2$, 0.1 mM ATP, 20 mM phosphoenolpyruvate (PEP), 5 mM nicotinamide adenine dinucleotide phosphate ($NADP^+$), 20 U/mL HK, 104 U/mL PK, 38.75 U/mL MK, 23.15 U/mL G6PDH, 1 U/mL 6PGDH, 5 U/mL PRI, 0.46 U/mL APRT, and 1.5 U/mL PRPPase. Reaction samples were analyzed by HPLC-UV (λ = 260 nm) using a Supelcosil LC-18-T (25 cm × 4.6 mm, 5 μm) column and isocratic elution in 55% A, 45% B at 1 mL/min, where A = 30% methanol, 100 mM potassium phosphate pH 7.2, 4 mM tetrabutylammonium sulfate (TBAS) and B = 100 mM potassium phosphate pH 6.0, 4 mM TBAS. Radioactivity in the eluate was measured by scintillation counting. ATP was reduced to 2'-deoxyadenosine 5'-triphosphate (dATP) by adding 1.4 mg/mL RTR, 20 μM coenzyme B_{12}, and 25 mM DTT to the reaction mixture, degassing the reaction mixture was degassed under vacuum, purging with $N_{2(g)}$, and incubating in the dark at 37 °C for at least 2 h. The mixture was passed through an Amicon Ultra 10K nominal molecular-weight cutoff centrifugal filter (EMD Millipore). dATP was purified from the filtrate by HPLC-UV (λ = 260 nm) using a Waters Delta-Pak C18 column (30 cm × 3.9 mm, 15 μm) and gradient elution, from 99% A to 84% A over 1 h at 1 mL/min, where A = 50 mM triethylammonium acetate pH 6.0 and B = methanol.

Table 2.2. Radiolabelled dATP produced from each radiolabelled starting material

Starting material	dATP
D-[2-^{3}H]glucose	[1'-^{3}H]dATP
D-[2-^{14}C]glucose	[1'-^{14}C]dATP
D-[6-$^3H_2$]glucose	[5'-$^3H_2$]dATP
D-[6-^{14}C]glucose	[5'-^{14}C]dATP
D-[6-^{14}C]glucose, [7-^{15}N]adenine	[7-^{15}N, 5'-^{14}C]dATP

2.11 Synthesis and purification of radiolabelled 2'-deoxyinosine 5'-triphosphate (dITP)

Lyophilized radiolabelled dATP was reacted with 7.5 U/mL ADA in 10 mM sodium citrate, pH 6.0 and 10 mM $NaWO_4$ at 37 °C for 30 min. 2'-Deoxyinosine 5'-triphosphate (dITP) was purified in the same way as dATP (see Section 2.10).

2.12 Synthesis and purification of radiolabelled ATI26

Radiolabelled ATI26 was synthesized from equimolar amounts of radiolabelled dITP (Table 2.3), G19, and C18 using 25 U/mL MMLV-RT in 40 mM Tris‑HCl, pH 8.0, 75 mM KCl, 3 mM $MgCl_2$, and 1 mM DTT (Figure 2.2).

The reaction was incubated for 6 h at 37 °C, then spiked with 10 U of MMLV-RT, 1 mM DTT, 250 μM 2'-deoxycytidine 5'-triphosphate (dCTP), 250 μM 2'-deoxythymidine 5'-triphosphate (dTTP), and 250 μM dITP. The spiked reaction mixture was incubated at 37 °C for at least 2 h. ATI26 was PAGE-purified and quantified by A_{260}, with $\varepsilon_{260} = 211654\ M^{-1}cm^{-1}$ (calculated by nearest-neighbour method).[154]

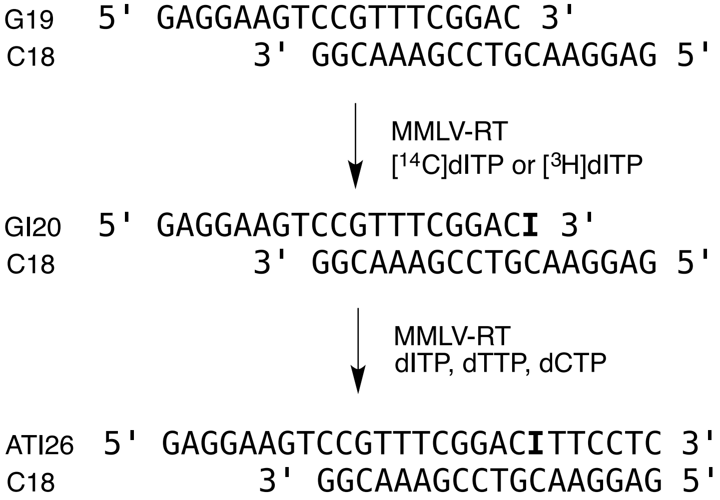

Figure 2.2. Schematic of incorporation of radiolabelled dITP into ATI26
G19 is the primer and C18 is the template.

Table 2.3. Radiolabelled ATI26 isotopologues produced from each radiolabelled dITP isotopologue

Radiolabelled dITP	Radiolabelled ATI26
[1'-^{3}H]dITP	[1'-^{3}H]ATI26
[5'-^{14}C]dITP	[5'-^{14}C]ATI26
[5'-$^{3}H_2$]dITP	[5'-$^{3}H_2$]ATI26
[1'-^{14}C]dITP	[1'-^{14}C]ATI26

2.13 Synthesis and purification of radiolabelled 2’-deoxyinosine 5’-monophosphate (dIMP)

Radiolabelled 2’-deoxyadenosine 5’-monophosphate (dAMP) was produced from radiolabelled dATP (Table 2.4) with 200 U/mL HK and 200 U/mL MK in 50 mM potassium phosphate, pH 7.6, 10 mM $MgCl_2$, 2 mM adenosine 5’-monophosphate (AMP), and 6.25 mM glucose at 37 °C for 2 h. dAMP was purified in the same way as dATP (see Section 2.10). dIMP was produced from dAMP and purified according to the procedure in Section 2.11.

Table 2.4. Radiolabelled dIMPs produced from radiolabelled dATPs

Radiolabelled dATP	Radiolabelled dIMP
[1’-^{3}H]dATP	[1’-^{3}H]dIMP
[5’-^{14}C]dATP	[5’-^{14}C]dIMP
[5’-$^3H_2$]dATP	[5’-$^3H_2$]dIMP
[1’-^{14}C]dATP	[1’-^{14}C]dIMP
[4’-^{3}H]dATP	[4’-^{3}H]dIMP
[7-^{15}N, 5’-^{14}C]dATP	[7-^{15}N, 5’-^{14}C]dIMP

2.14 Measurement of KIEs for the AlkA-catalyzed excision of hypoxanthine from ATI26

2.14.1 Method 1

2.14.1.1 Reaction conditions

In a reaction containing 50 mM potassium acetate, pH 6.0, 50 mM KCl, 1 mM DTT, 1 mM $MgCl_2$, 0.5 mg/mL BSA, and 0.3 U/mL hAPE1, two ATI26 isotopologues (≥ 12000 cpm for each isotopologue, Table 2.5) were mixed with an equimolar amount of WT AlkA. At t = 0 h, 1/3 of the reaction volume was removed and quenched immediately with KOH to a final concentration of 140 mM (0% reaction sample). The reaction was allowed to proceed in the remaining volume (2/3 of the initial volume) for 5 h at 37 °C (50% reaction sample), after which the reaction was also quenched with KOH (see above).

Table 2.5. Isotopologue pairs for competitive AlkA KIE measurements

KIE	ATI26 isotopologues
1’-^{3}H	[1’-^{3}H]ATI26, [5’-^{14}C]ATI26
5’-$^3H_2$	[5’-$^3H_2$]ATI26, [5’-^{14}C]ATI26
1’-^{14}C	[1’-^{14}C]ATI26, [5’-$^3H_2$]ATI26

2.14.1.2 Separation and analysis

Both the 50% and 0% samples were neutralized with HCl and diluted to 500 μL with mobile phase A (see below). Substrate and product were separated by fast protein liquid chromatography (FPLC) in the 0% and 50% reaction samples using a Mono-Q 5/50 GL column (GE Healthcare) and stepwise elution (Table 2.6). Mobile phase A = 10 mM NaOH, mobile phase B = 10 mM NaOH and 1.5 M NaCl, and the flow rate = 1.5 mL/min.

Table 2.6. Method 1 stepwise gradient

Time (min)	%B	[NaCl] (M)
0 - 1.3	0	0
1.3 – 11.3	20	0.3
11.3 – 21.3	70	1.05

The product, eluting at 300 mM NaCl, and the residual substrate, eluting at 1.05 M NaCl, were collected in pre-weighed scintillation vials. The liquid mass of each vial’s contents was split equally across two scintillation vials (1.6 g in each vial), 200 μL of 1 M potassium phosphate, pH 6.0 was added to each vial to neutralize the samples, and 21 g Bio-Safe II was added to all vials. A [^{14}C]glucose standard and blank sample were prepared at each [NaCl] identically to the other samples.

Samples were analyzed by dual-window scintillation counting. Windows (a measure of β-particle energy) were selected such that window 1 contained all the ^{3}H counts (and some 14C counts), while window 2 contained only ^{14}C. Counts per minute (CPM) in windows 1 and 2 were blank-corrected and converted to ^{3}H and ^{14}C CPM using equations 2.11 and 2.12.

$$\mathrm{CPM}_{^3\mathrm{H}} = \mathrm{CPM}_{\mathrm{window\,1}} - \mathrm{CPM}_{\mathrm{window\,2}}\left(\frac{\mathrm{CPM}_{\mathrm{window\,1}}}{\mathrm{CPM}_{\mathrm{window\,2}}}\right)^{^{14}\mathrm{C\,standard}} \qquad \textbf{(2.11)}$$

$$\mathrm{CPM}_{^{14}\mathrm{C}} = \mathrm{CPM}_{\mathrm{window\,2}} + \mathrm{CPM}_{\mathrm{window\,2}}\left(\frac{\mathrm{CPM}_{\mathrm{window\,1}}}{\mathrm{CPM}_{\mathrm{window\,2}}}\right)^{^{14}\mathrm{C\,standard}} \qquad \textbf{(2.12)}$$

KIEs were calculated using equation 2.13:

$$\frac{k}{k'} = \frac{\ln\left(\dfrac{\frac{A}{A'}}{\frac{A_0}{A_0'}}\right)}{\ln\left(1 - f\left(\dfrac{1+\frac{A_0}{A_0'}}{1+\frac{A}{A'}}\right)\right)} \qquad \textbf{(2.13)}$$

$$f = \frac{X + X'}{A + X + A' + X'} \qquad \textbf{(2.14)}$$

In the preceding equations, A = CPM of the light substrate (or product) isotopologue in the 50% reaction sample, A' = CPM of the heavy substrate (or product) isotopologue in the 50% reaction sample, A_0 = CPM of light substrate isotopologue in the 0% reaction sample, A_0' = CPM of the heavy substrate isotopologue in the 0% reaction sample, f = fractional extent of reaction (calculated from equation 2.14, where X = CPM of the light product isotopologue in the 50% reaction sample and X' = CPM of the heavy product isotopologue in the 50% reaction sample), and $\frac{k}{k'}$= KIE. Counting of each sample continued until the cumulative average of the KIE had stabilized.

2.14.2 Method 2

2.14.2.1 Reaction conditions

Reactions were performed as described in Section 2.14.1.1.

2.14.2.2 Separation and analysis

Both the 50% and 0% samples were neutralized with HCl and diluted to 500 µL with mobile phase A (see below). Substrate and product were separated by fast protein liquid chromatography (FPLC) from the 0% and 50% reaction samples using a Mono-Q 5/50 GL column (GE Healthcare) and stepwise elution (Table 2.7). Mobile phase A = 50 mM $MgCl_2$ and 8% acetonitrile, mobile phase B = 50 mM $MgCl_2$, 8% acetonitrile, and 1.5 M NaCl, and the flow rate = 1.5 mL/min.

The product, eluting at 150 mM NaCl, and the substrate, eluting at 330 mM NaCl, were collected in pre-weighed scintillation vials. The liquid mass of each vial’s contents was brought to 6 g with the appropriate mobile phase and split equally across two scintillation vials. Ecoscint A (20 g) was added to all vials. A [^{14}C]glucose standard and blank sample was prepared at each [NaCl] identically to the other samples. The liquid scintillation counts were analyzed as in Section 2.14.1.2.

Table 2.7. Method 2 stepwise gradient

Time (min)	%B	[NaCl] (M)
0 – 3	10	0.15
3 – 8	15	0.225
8 – 13	22	0.33
13 – 18	100	1.5

2.14.3 Method 3

2.14.3.1 Reaction conditions

Reactions were performed as described in Section 2.14.1.1.

2.14.3.2 Separation and analysis

Both the 50% and 0% samples were neutralized with HCl and diluted to 500 μL with mobile phase A (see below). Substrate and product were separated by fast protein liquid chromatography (FPLC) from the 0% and 50% reaction samples using a Mono-Q 5/50 GL column (GE Healthcare) and stepwise elution (Table 2.8). Mobile phase A = 50 mM $MgCl_2$ and 8% acetonitrile, mobile phase B = 50 mM $MgCl_2$, 8% acetonitrile, and 1.5 M NaCl, and the flow rate = 1.5 mL/min.

The product, eluting at 150 mM NaCl, the major form of the residual substrate, eluting at 600 mM NaCl, and the minor form of the residual substrate, eluting at 1.5 M NaCl, were collected in pre-weighed scintillation vials. The liquid mass of each vial's contents was brought to 6 g with the appropriate mobile phase, and split equally across two scintillation vials. Ecoscint A was added to all vials: 20 g to vials containing 150 mM and 600 mM NaCl, 23 g to vials containing 1.5 M NaCl. A [^{14}C]glucose standard and blank sample was prepared at each [NaCl] identically to the other samples. The liquid scintillation counts were analyzed as in Section 2.14.1.2.

Table 2.8. Method 3 stepwise gradient

Time (min)	%B	[NaCl] (M)
0 – 3	10	0.15
3 – 8	15	0.225
8 – 13	40	0.6
13 – 18	100	1.5

2.14.4 Method 4

2.14.4.1 Reaction conditions

The pair of ATI26 isotopologues for a given KIE measurement was mixed, purified by FPLC using Method 3 (see Section 2.14.3), and ethanol-precipitated. The purified substrates were then reacted with WT AlkA according to the conditions in Section 2.14.1.1.

2.14.4.2 Separation and analysis

Substrate and product were separated by fast protein liquid chromatography (FPLC) from the 0% and 50% reaction samples using a Mono-Q

5/50 GL column (GE Healthcare) and stepwise elution (Table 2.9). Mobile phase A = 50 mM $MgCl_2$ and 150 mM NaCl, mobile phase B = 50 mM $MgCl_2$ and 800 mM NaCl, and the flow rate = 1.5 mL/min.

The product, eluting at 150 mM NaCl, and the substrate, eluting at 800 mM NaCl, were collected in pre-weighed scintillation vials. The liquid mass of each vial's contents was brought to 6 g with the appropriate mobile phase and split equally across two scintillation vials. A [^{14}C]glucose standard and blank sample was prepared at each [NaCl] identically to the other samples. Ecoscint A (22 g) was added to all vials. The liquid scintillation counts were analyzed as in Section 2.14.1.2.

Table 2.9. Method 4 stepwise gradient

Time (min)	%B	[NaCl] (M)
0 – 6	0	0.15
6 – 14.4	100	0.8

2.15 Measurement of KIEs for the acid-catalyzed hydrolysis of 2'-deoxyinosine 5'-monophosphate (dIMP)

The pair of dIMP isotopologues for a given KIE measurement was mixed (Table 2.10), HPLC-purified (see Section 0), lyophilized, and redissolved in 0.1 M HCl and unlabelled dIMP (final [dIMP] = 1.25 mM) in a 300 µL total volume. The reaction was incubated at 30 °C for 90 min; 200 µL (2/3 of the initial volume) was removed and added to 1300 µL elution buffer (100 mM potassium phosphate, pH 6.0, 100 mM ribose, 10% ethanol) (50% reaction sample). The remaining 100 μL (1/3 of the initial volume) were incubated for > 22 h and quenched with 1400 μL elution buffer (100% reaction).

Table 2.10. Isotopologue pairs for competitive dIMP KIE measurements

KIE	dIMP isotopologues
1’-^{3}H	[1’-^{3}H]dIMP, [5’-^{14}C]dIMP
5’-^{3}H$_2$	[5’-^{3}H$_2$]dIMP, [5’-^{14}C]dIMP
1’-^{14}C	[1’-^{14}C]dIMP, [5’-^{3}H$_2$]dIMP
4’-^{3}H	[4’-^{3}H]dIMP, [5’-^{14}C]dIMP
7-^{15}N	[7-^{15}N, 5’-^{14}C]dIMP, [5’-^{3}H$_2$]dIMP

To determine the extent of reaction *f*, 100 μL of the 50% reaction sample were analyzed by HPLC-UV (λ = 260 nm) using a Supelcosil LC-18-T (25 cm × 4.6 mm, 5 μm) column with an isocratic method: 60% A, 40% B, where A = is 100 mM potassium phosphate, pH 7.2, 4 mM TBAS, and 20% methanol and B = 100 mM potassium phosphate, pH 6.0 and 4 mM TBAS.

To separate the product and substrate in the 50% and 100% reaction samples, six charcoal columns were prepared by applying 525 μL 190 mg/mL acid-washed Norit A activated charcoal suspension in elution buffer to QIAprep columns. The columns were washed by applying 500 μL elution buffer to each column and centrifuging them at 625 × *g* for 1 min. 500 μL of the 50% and 100% reaction samples were applied to each column and the columns were centrifuged at 625 × *g* for 1 min; the eluate was collected in pre-weighed scintillation vials. Each column was washed with 5 × 500 μL elution buffer, which was collected in the pre-weighed vials. The liquid masses in each vial were brought to 3.25 g with elution buffer. A [^{14}C]glucose standard and blank sample was also prepared in 3.25 g elution buffer. Ecoscint A (22 g) was added to each vial. The liquid scintillation counts were analyzed as in Section 2.14.1.2.

Chapter 3. Leaving-Group Activation

3.1 Introduction

The pH dependence of AlkA catalysis suggests that it protonates neutral purine substrates to promote leaving group departure. Whether it directly protonates the purine or does so indirectly is not known, but it is known that the rate of neutral-purine excision decreases with increasing pH.[118,156] The rate enhancements (k_{st}/k_{non}) for neutral and cationic *N*-alkylpurines in DNA are approximately the same, even though k_{non} for *N*-alkylpurines is $\approx 10^4$-fold greater than that for neutral purines. Therefore, there must be enzyme-induced compensation for the lower intrinsic reactivity of neutral-purine C−N bonds, potentially via leaving-group activation by protonation.

In order to identify the presumed general-acid catalyst in AlkA's active site that protonates neutral purines, potential proton-donating or hydrogen-bonding active-site residues were mutated and the kinetics of Hx excision from IB25 were measured. The candidate residues for AlkA were selected based on the X-ray crystal structure of an AlkA•1-aza-DNA complex (Figure 1.17).[111] The mutated residues were R22, R244, Y222, W272, and Y273. Replacing these residues with alanine could significantly alter the protein structure around these large aromatic residues; therefore, the mutations were made minimally disruptive. For example, in the R244M mutation, the non-polar

Met sidechain replaced the non-polar portion of the Arg sidechain but lack the ionizable and hydrogen-bonding guanidinium functionality.

The Hx excision rates from IB25 in D_2O and H_2O were studied as a function of buffer concentration. A linear relationship between buffer concentration and rate would indicate rate-limiting hydron (^1H or ^2H) transfer and the involvement of the buffer in the enzymatic Hx excision reaction. Confirmation of rate-limiting hydron transfer would be obtained from the SDKIE, the ratio of the rates in H_2O and D_2O.[87]

The participation of small acidic species in enzymatic reactions has been observed with human carbonic anhydrase (HCA) II and III, which catalyze HCO_3^- formation from H_2O, CO_2, and Zn^{2+}-bound OH^-. HCA is regenerated once the Zn^{2+}-bound OH^- is protonated to form water.[149] HCA II exhibited increased turnover rates in increasing concentrations of imidazole and 1-methylimidazole.[157] In HCA III, imidazolium ion was implicated in Zn^{2+}-bound OH^- protonation by the fact that the rate of water release depended on the imidazole buffer concentration, was independent of pH in the absence of imidazole, and was pH-dependent in 150 mM imidazole.[149] A single pK_a of 7.2 – the pK_a of imidazole – appeared in the latter pH profile. [149]

Buffers can restore activity to enzyme mutants that lack a critical ionizable residue. In *E. coli* aspartate aminotransferase (AAT), the ε-NH_2 group of residue K258 is part of the internal aldimine with pyridoxal 5’-phosphate (PLP) and mediates the 1,3-prototropic shift between the C_α of aspartate and $C_{4'}$ of PLP (Figure 3.1).[158] The K258A mutant is inactive, but exogenous primary amines re-activate it.[159] There was a strong correlation between the rate and the amines' molecular volume, providing evidence that the exogenous amine is indeed involved in the chemistry, as physical exclusion of a large amine would preclude its involvement in the reaction.[159] A similar observation was made with yeast triose phosphate isomerase (TIM), a glycolytic enzyme that catalyzes the interconversion of glyceraldehyde-3-phosphate (GAP) and dihydroxyacetone phosphate (DHAP).[160] The cationic K12 side chain stabilizes the anionic enediolate-like transition state, and addition of primary amines causes partial restoration of GAP conversion activity to the K12G mutant in a mostly pK_a-independent manner, while tertiary amines do not restore activity.[160]

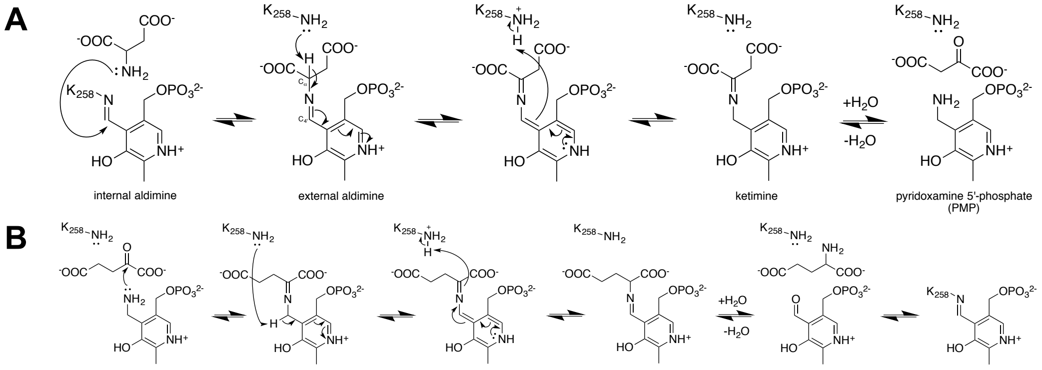

Figure 3.1. Mechanism of aspartate aminotransferase
The amino group is transferred from aspartate to α-ketoglutarate via pyridoxal 5’-phosphate (PLP), producing oxaloacetate and glutamate. K258 forms the internal aldimine with PLP. A) In the first half-reaction, aspartate displaces K258 to form an external aldimine. K258 deprotonates C_α of aspartate and protonates C4’ of PLP to form a ketimine, which is then hydrolyzed to produce pyridoxamine 5’-phosphate (PMP). B) In the second half-reaction, PMP forms a ketimine with α-ketoglutarate. K258 deprotonates C4’ of PMP and protonates C_2 of α-ketoglutarate to form an aldimine, which is then hydrolyzed to form glutamate and PLP. K258 reacts with PLP to regenerate the internal aldimine. Adapted from refs [158,159,161].

If the nucleobase moiety of AlkA’s transition state is partially protonated by a general acid-catalytic residue, then a single ligand that captures the nucleobase and the oxacarbenium ion-like features of the transition state should bind to AlkA with higher affinity than either of those functionalities separately. Alternatively, AlkA could bind a free purine along with a transition state-mimicking oligonucleotide. The translational and rotational freedom of the two untethered pieces would allow them to adopt conformations and positions that match the transition state, and the apparent dissociation constant for the oligonucleotide would decrease. Inhibition of ricin-catalyzed A removal from 28S ribosomal RNA was 10-fold greater with both free adenine and RNA containing 1-aza-1,2-dideoxy-4a-carba-D-*erythro*-pentofuranose (1-aza-RNA) than with

1-aza-RNA alone or an RNA with 8-aza-9-deazaadenine linked to 1-aza via a methylene bridge (Figure 3.2).[162] In the presence of free uracil, the apparent affinity of *E. coli* uracil DNA glycosylase toward 1-aza-DNA increases 4000-fold (K_d of 500 pM vs. 2 μM).[150] Given these precedents, the cooperative binding of a free nucleobase and DNA containing a pyrrolidine residue (pyr-DNA) by AlkA was studied to determine if base-specific interactions exist at the transition state.

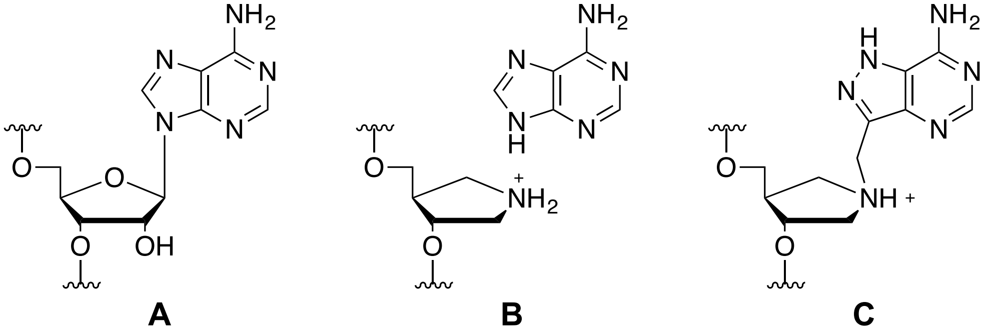

Figure 3.2. Ricin ligands
Structures and inhibition data from ref [162]. A) adenosine B) adenine and 1-aza, K_i = 12 nM C) *N*-(8-aza-9-deazaadenyl)methyl-1'-aza-1',2'-dideoxy-4'a-carba-D-*erythro*-pentofuranose, K_i = 94 nM (14-mer) or 163 nM (10-mer)

3.2 Results

3.2.1.1 pH vs. k_{cat} *and pH vs.* k_{cat}/K_M *profiles*

Rates were measured for Hx excision from IB25, a 24-mer DNA duplex with a bulged inosine residue in the longer 25-mer strand as the scissile site (Figure 2.1). The pH vs. k_{cat} and pH vs. k_{cat}/K_M profiles reported here for Hx excision from IB25 range from pH 4.5 to 8 (Figure 3.3). The rates were maximal at pH 4.5 and rates at pH < 4.5 could not be established due to enzyme denaturation. At pH 8, the initial rates were still linear over 2 h, but the enzyme has been slowed considerably. At pH 9, no rate could be detected. The reliability of the profiles was enhanced by the use of multiple buffers at pHs near the inflection point. The pH vs. k_{cat} and pH vs. k_{cat}/K_M profiles were each fit to a single-ionization model and yielded pK_as of 5.7 ± 0.1 and 5.1 ± 0.2, respectively. Given that the pH profiles for k_{cat} and k_{cat}/K_M reflect slightly different initial states (E•S and E + S, respectively), the fitted pK_a values likely represent the same ionizable residue.

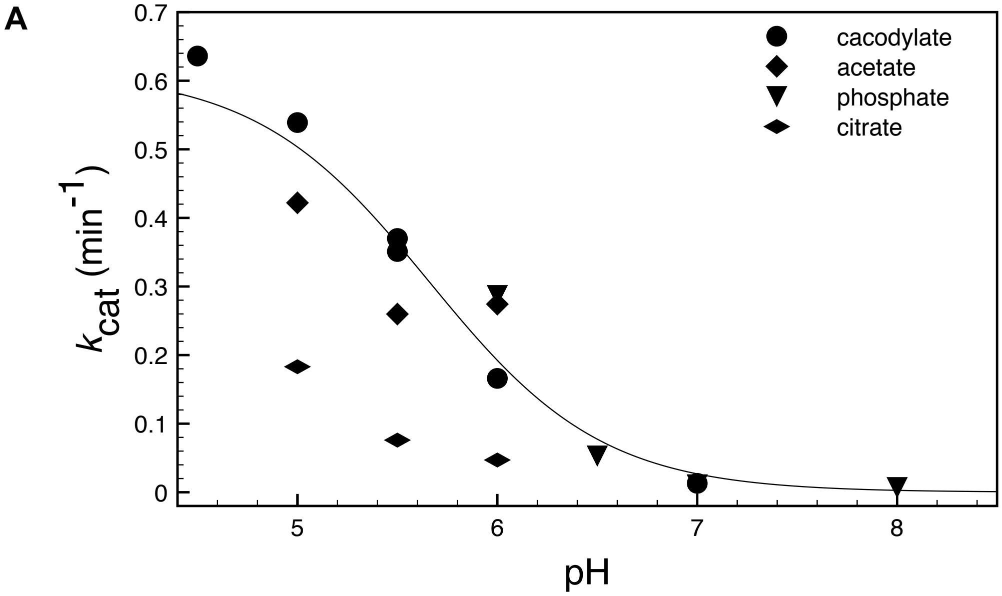

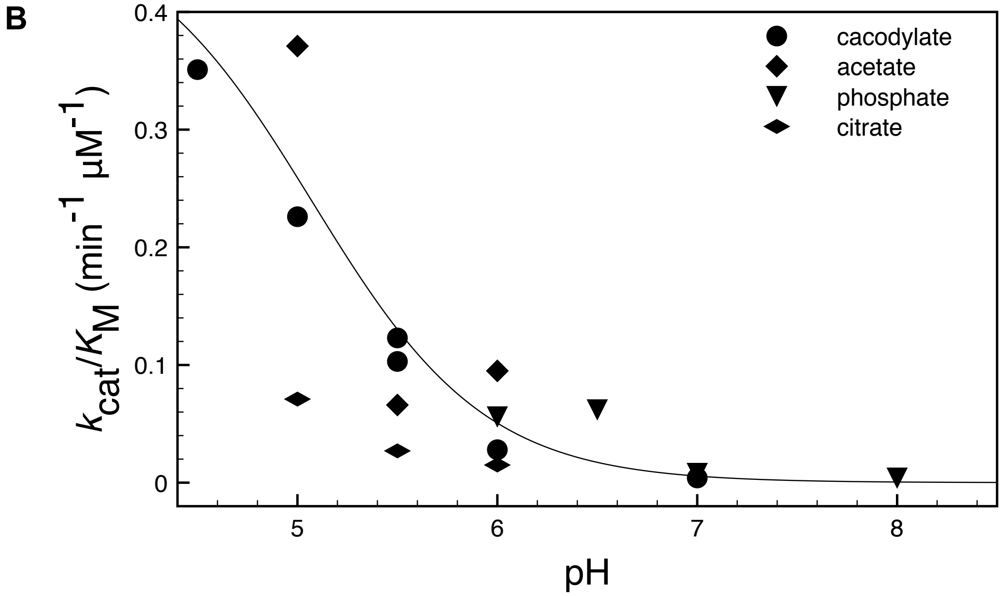

Figure 3.3. pH vs. rate profiles for WT AlkA

A) pH vs. k_{cat} B) pH vs. k_{cat}/K_M. Data were fitted to equation 2.9 (solid lines). For A, pK_a = 5.7 ± 0.1; for B, pK_a = 5.1 ± 0.2; the uncertainty is the standard error on the fit. Rates measured in citrate were consistently lower than in cacodylate, acetate, and phosphate and were not included in the fit.

3.2.1.2 K_d for WT AlkA•pyr-DNA complex

The pH dependence of pyr-DNA complexes was also investigated using EMSA studies of ternary AlkA•nucleobase•pyr-DNA complexes. The K_d of an AlkA•25-mer pyr-DNA complex was reported to be 16 pM, near the lower limit of detection.[137] This meant any increases in affinity, such as those caused by forming a ternary complex, would be difficult to measure. Shorter DNA oligomers were tested to find out how short they needed to be to bring the pyr-DNA K_d values into an easier-to-measure range. Initial tests were performed using a THF-containing DNA because of its easier availability; the THF site would be replaced by pyrrolidine, which is bound to AlkA 2800-fold more tightly, once an oligomer of correct length was found.[111,163] A series of stem-loop THF-DNA ligands with various stem lengths were tested (see Section 2.3).

No complexes were observed under previously reported conditions, but were observed after lowering the electrophoretic dead time, eliminating loading dye, using phosphate buffer, lowering the lower salt concentration, and including BSA in the reaction samples.[163] Under the new conditions, AlkA's affinities toward these ligands were measured (Figure 3.4, Table 3.1).

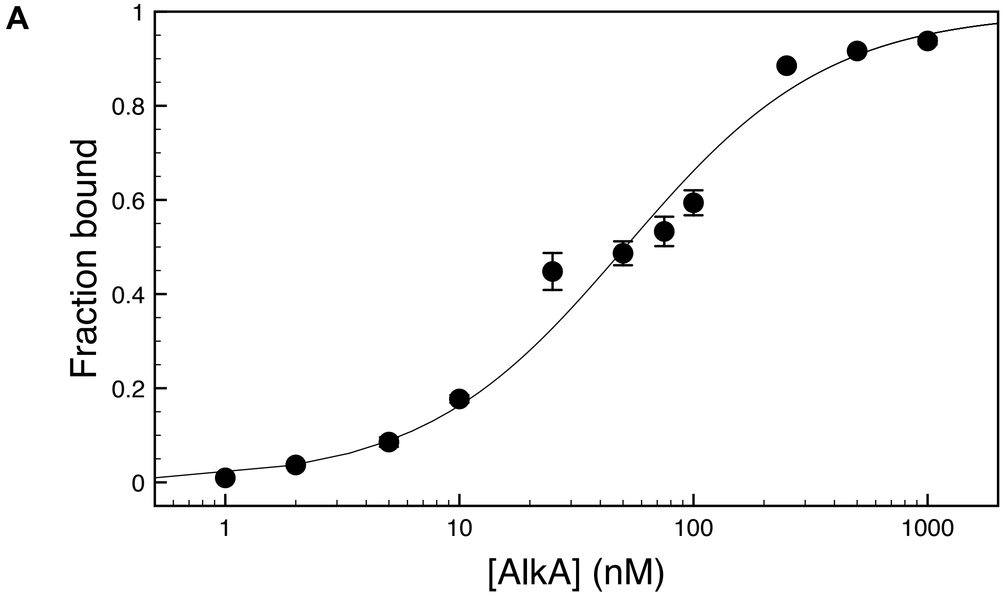

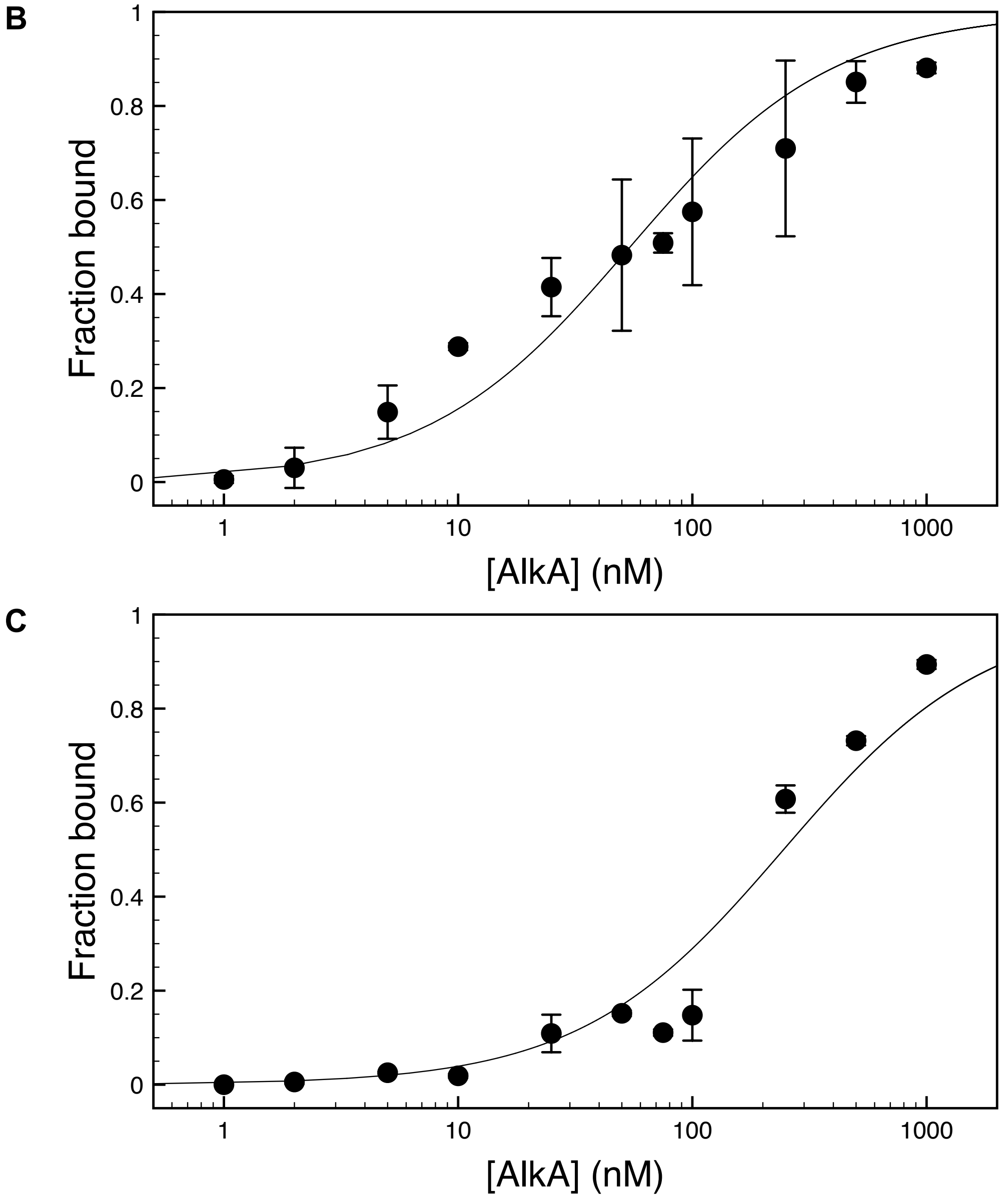
B
Fraction bound
1
0.8
0.6
0.4
0.2
0
1
10
100
1000
[AlkA] (nM)
C
Fraction bound
1
0.8
0.6
0.4
0.2
0
1
10
100
1000
[AlkA] (nM)

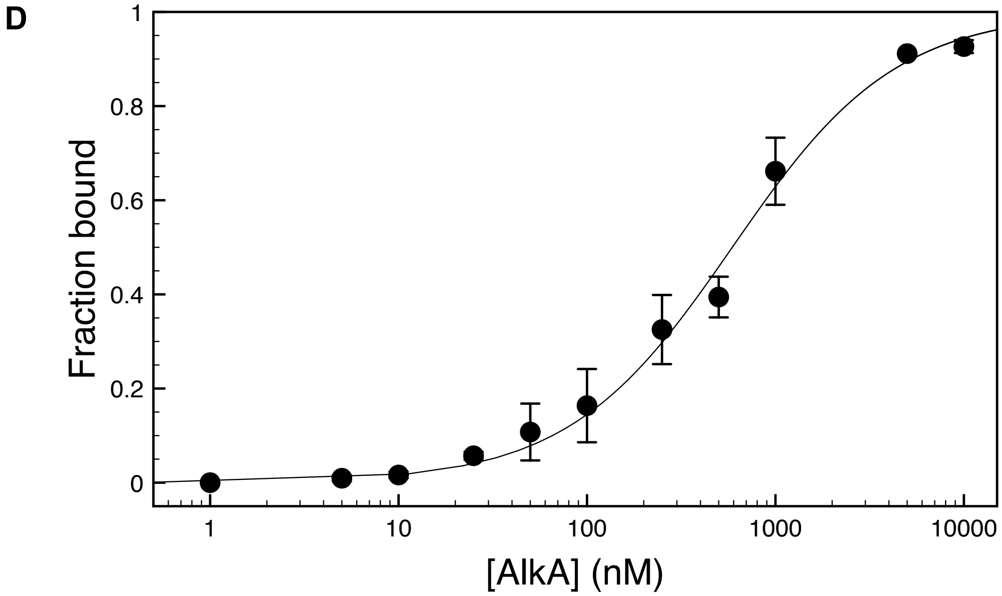

Figure 3.4. Binding isotherms of AlkA binding to THF-containing DNAs
A) THF53 (25 bp stem) B) THF47 (22 bp stem) C) THF41 (19 bp stem) D) THF35 (16 bp stem). Data were fit to equation 2.1 (solid lines). The K_ds are listed in Table 3.1. DNA sequences are found in Section 2.3.

Table 3.1. K_ds derived from binding isotherms of AlkA binding to THF-containing DNAs
Values were obtained from fits of Figure 3.4 data to equation 2.1. The number in parentheses indicates the number of replicates from which the average was calculated. The uncertainty is the standard deviation. DNA sequences are found in Section 2.3.

Ligand	K_d (nM)
THF53 (25 bp stem)	51 ± 11 (2)
THF47 (22 bp stem)	54 ± 14 (2)
THF41 (19 bp stem)	245 ± 8 (2)
THF35 (16 bp stem)	590 ± 177 (2)

These changes to the assay method did not appreciably affect the K_d values, as the AlkA•THF53 K_d value of (51 ± 11 nM) was within experimental error of a previously reported 25-mer THF-DNA oligomer (45 nM).[111]

The K_d of AlkA•THF35 was 590 nM, so it was predicted that AlkA would bind to the same 35-mer sequence with pyrrolidine in place of THF, i.e., PYR35, with $K_d \approx 1$ nM. AlkA binding to PYR35 was measured at pH 7 in triplicate and yielded a biphasic binding isotherm (Figure 3.5A). The data were fitted to a two-site model (equation 2.4) and $K_d = 1.7 \pm 0.5$ nM for AlkA binding to the high-affinity site on PYR35 was obtained (average of 3 replicates, with the standard deviation as the uncertainty); fitting only the high-affinity phase to a one-site model (equation 2.1) resulted in a similar K_d, 2.6 ± 0.3 nM.

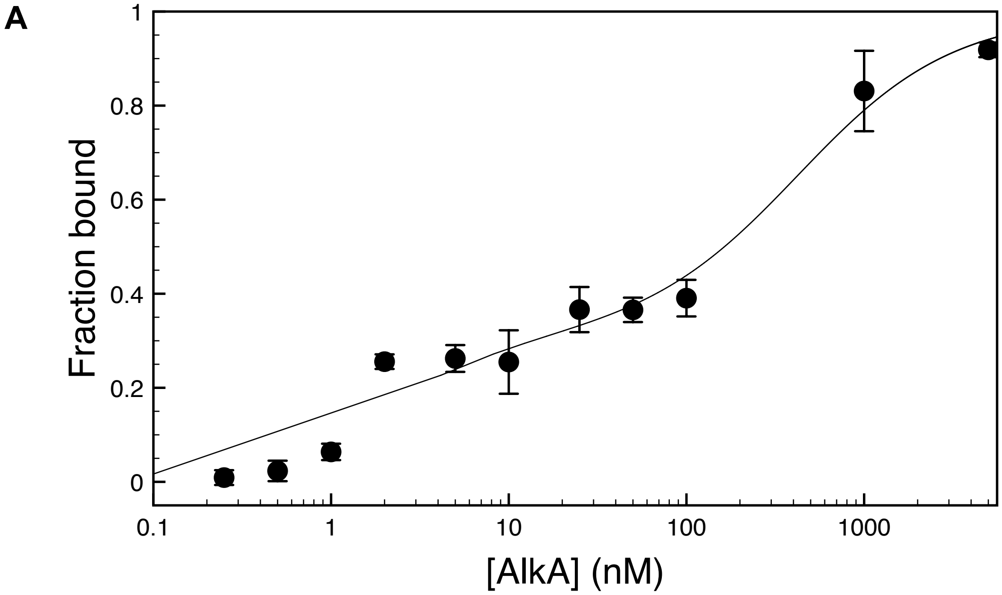

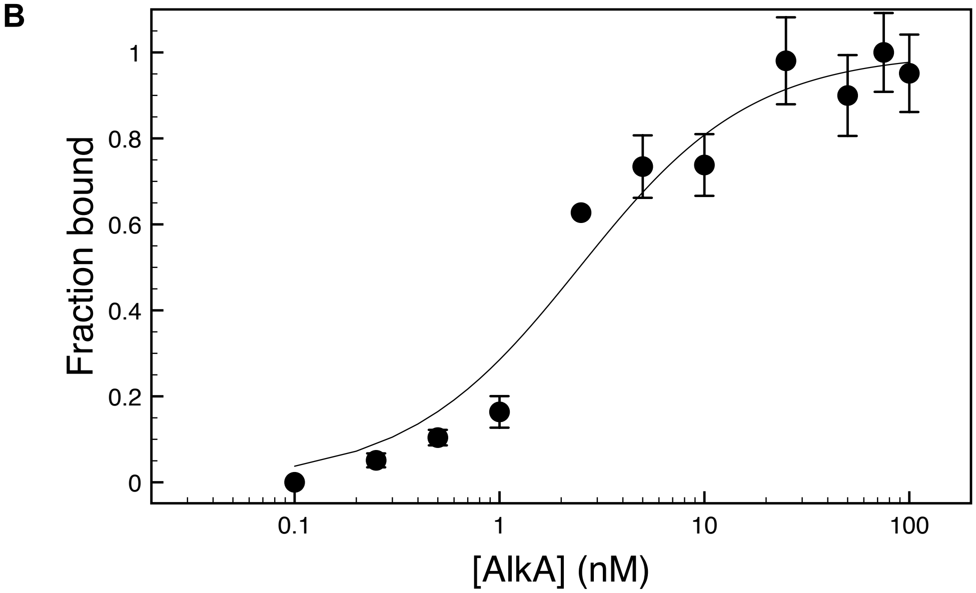

Figure 3.5. Binding isotherm of AlkA•PYR35 complexes at pH 7

Error bars indicate the standard deviation on the fraction bound at each [AlkA]. A) Both high-affinity and low-affinity phases ([AlkA] = 0 to 5000 nM). Data were fit to the two-site model in equation 2.4 (solid lines). B) High-affinity phase only ([AlkA] = 0 to 100 nM). Data were fit to the one-site model in equation 2.1 (solid lines). The PYR35 sequence is found in Section 2.3.

AlkA binding to PYR35 was then measured at pH 6 and 8 and biphasic binding isotherms were observed again. For both pHs, the K_d values derived from fitting each entire isotherm to the two-site model in equation 2.4 or fitting only the high-affinity phase to the one-site model in equation 2.1 were equal within experimental error (Table 3.2).

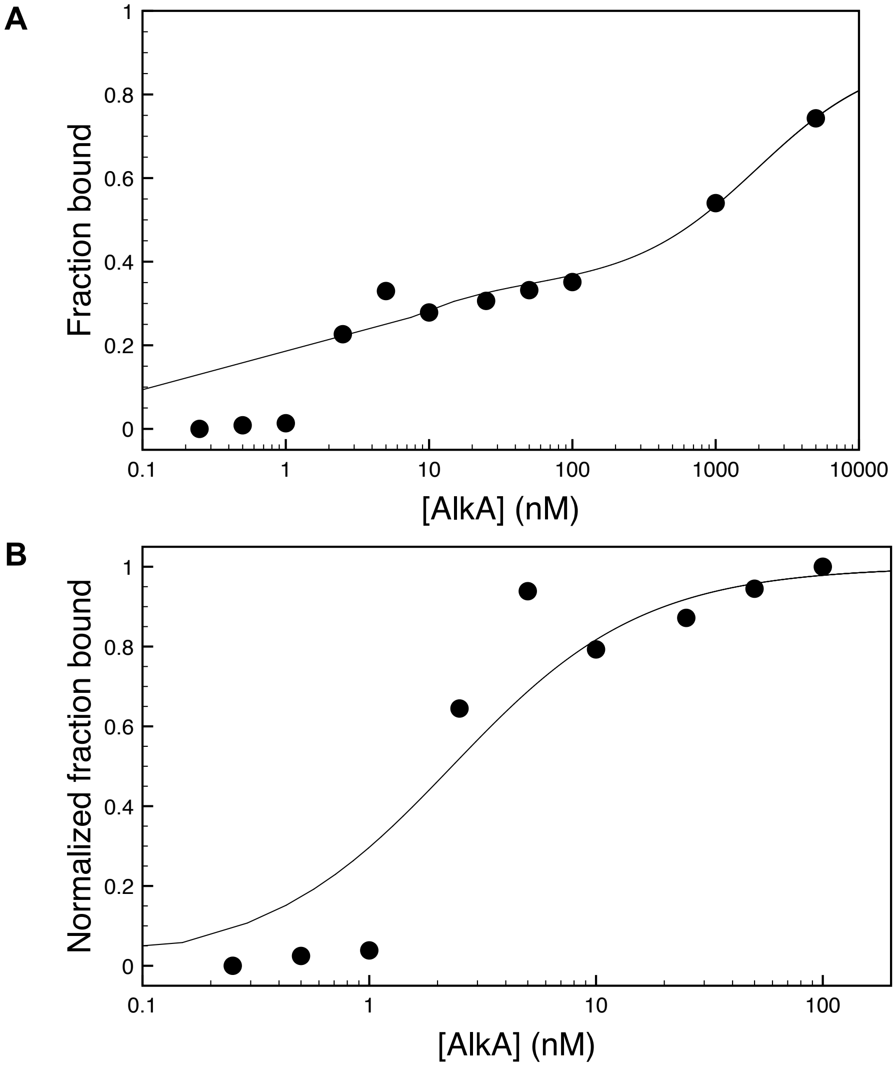

Figure 3.6. Binding isotherm of AlkA•PYR35 complexes at pH 6
A) Both high-affinity and low-affinity phases ([AlkA] = 0 to 5000 nM). Data were fit to the two-site model in equation 2.4 (solid lines). B) High-affinity phase only ([AlkA] = 0 to 100 nM). Data were fit to the one-site model in equation 2.1 (solid lines). The PYR35 sequence is found in Section 2.3.

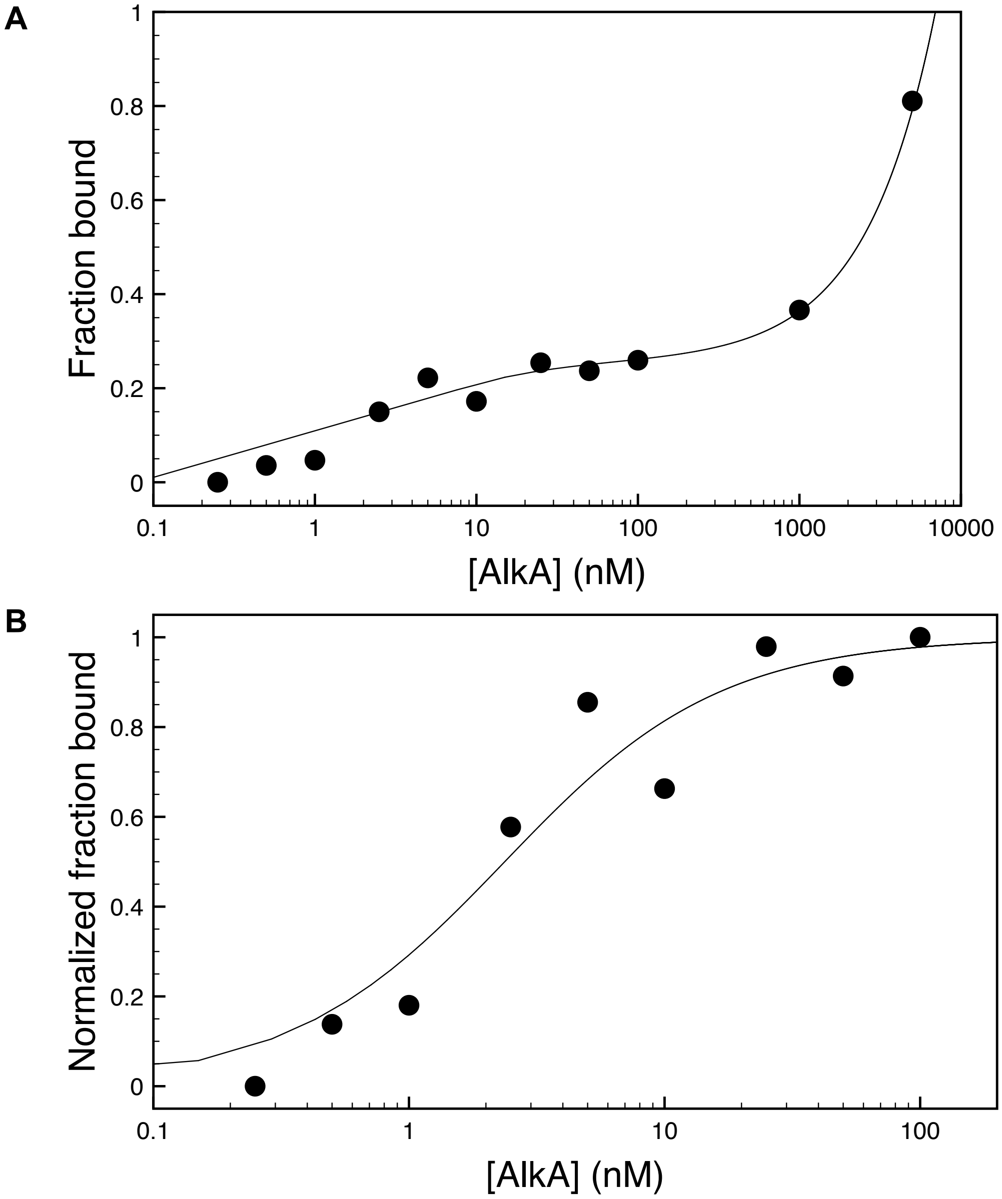

Figure 3.7. Binding isotherms of AlkA•PYR35 complexes at pH 8

A) Both high-affinity and low-affinity phases ([AlkA] = 0 to 5000 nM). Data were fit to the two-site model in equation 2.4 (solid lines). B) High-affinity phase only ([AlkA] = 0 to 100 nM). Data were fit to the one-site model in equation 2.1 (solid lines). The PYR35 sequence is found in Section 2.3.

Table 3.2. AlkA•PYR35 K_d values

The binding isotherms are shown in Figure 3.5, Figure 3.6, and Figure 3.7. For pH 6 and 8, the uncertainties are the standard errors on the fits. For pH 7, the uncertainty is the standard deviation (3 replicates).

pH	Model	K_d (nM)
6	One-site	2.2 ± 0.7
6	Two-site	3 ± 1
7	One-site	2.6 ± 0.3
7	Two-site	1.7 ± 0.5
8	One-site	2.2 ± 0.5
8	Two-site	2.4 ± 0.8

3.2.2 Mutants

Five active site mutants were prepared: W272F, R22M, Y222F, Y273F, and R244M. The steady-state kinetic parameters for Hx excision from IB25 were measured for each mutant in phosphate buffer at pH 7 (Table 3.3).

Table 3.3. Steady-state parameters for hypoxanthine (Hx) excision from IB25 by WT and mutant AlkAs

All reactions were performed in 75 mM phosphate at pH 7. T = 37 °C, I = 0.25. The uncertainty is the standard error on the fit.

	k_{cat} ($\times 10^{-3}$ min^{-1})	*x*-fold decrease relative to WT	k_{cat}/K_M ($\times 10^{-3}$ min^{-1} µM^{-1})	*x*-fold decrease relative to WT
WT	22 ± 3		21 ± 4	
R244M	6.2 ± 0.4	3.8	4.6 ± 0.5	4.6
Y222F	6.5 ± 0.7	3.4	5 ± 1	4.2
W272F	6.9 ± 0.5	3.2	3.8 ± 0.5	5.5
Y273F	7.3 ± 0.4	3.0	5.2 ± 0.4	4.0
R22M	13 ± 2	1.7	12 ± 3	1.8

The concern with any mutation is that changes in rate could be attributed not only to the loss of the functional group under investigation but to changes in active-site architecture or secondary structure. The fact that no steady-state kinetic parameter changed by > 4-fold showed that there was no gross disruption of the protein structure.

3.2.3 Effect of buffer concentration on reaction rate

The rate of Hx excision from IB25 by WT AlkA was measured as a function of buffer concentration at pHs 5 to 8, and rates of excision by R244M, Y222F, W272F, and Y273F were measured as a function of phosphate concentration at pH 7 (Figure 3.8, Table 3.4).

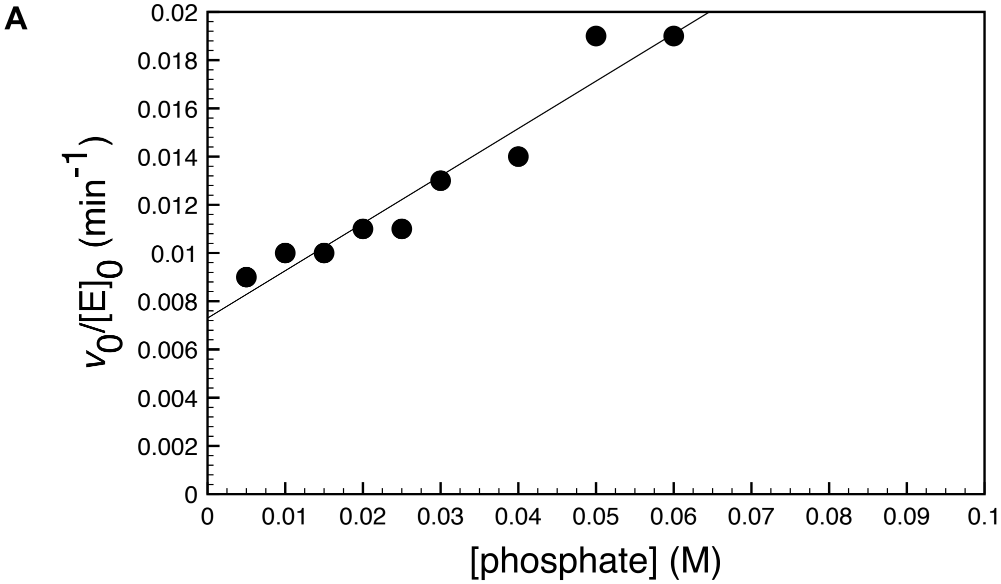

B

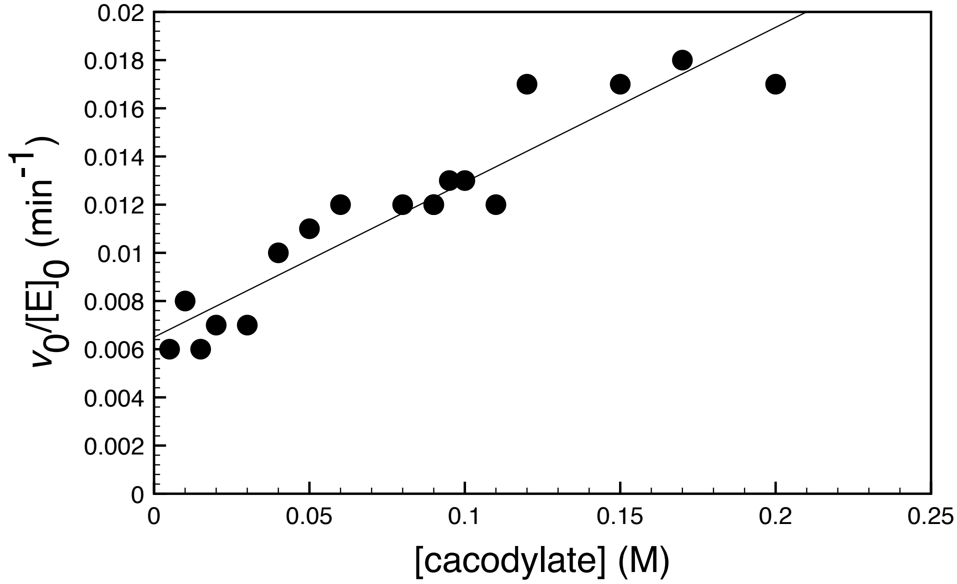
$v_0/[E]_0$ (min^{-1})
0
0.002
0.004
0.006
0.008
0.01
0.012
0.014
0.016
0.018
0.02
0
0.05
0.1
0.15
0.2
0.25
[cacodylate] (M)

C

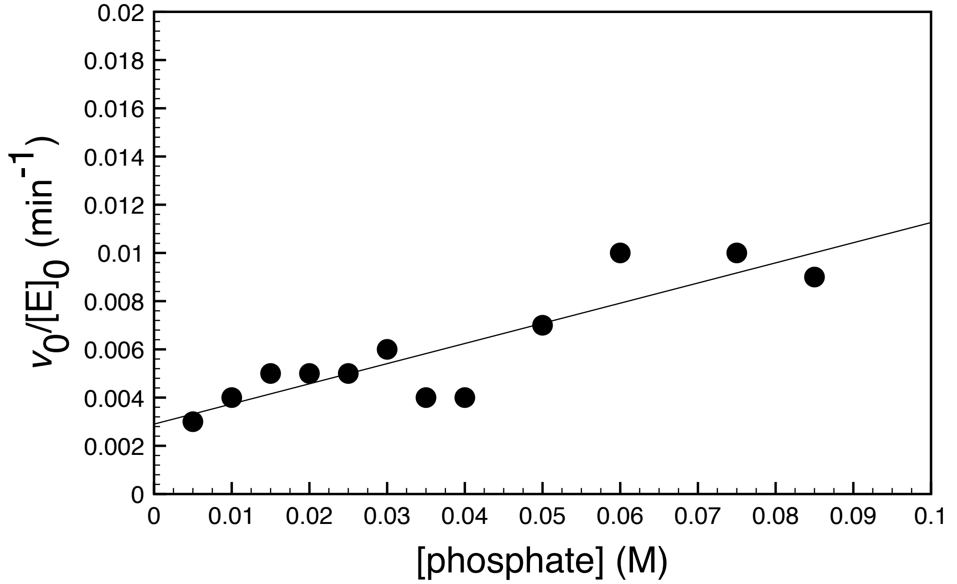
$v_0/[E]_0$ (min^{-1})
0
0.002
0.004
0.006
0.008
0.01
0.012
0.014
0.016
0.018
0.02
0
0.01
0.02
0.03
0.04
0.05
0.06
0.07
0.08
0.09
0.1
[phosphate] (M)

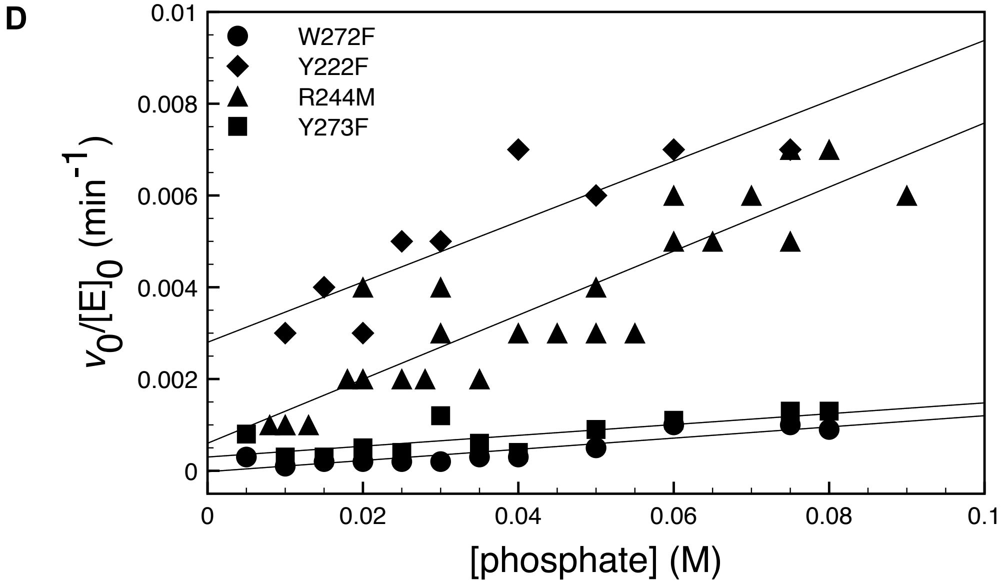

Figure 3.8. $v_0/[E]_0$ vs. [buffer] for hypoxanthine (Hx) excision from IB25 by WT and mutant AlkAs

[IB25] = 2 μM, T = 37 °C, I = 0.25. A) WT: phosphate, pH 7 B) WT: cacodylate, pH 7 C) WT: phosphate, pH 8 D) R244M, W272F, Y273F, and Y222F: phosphate, pH 7. Results of the linear fits are in Table 3.4.

Table 3.4. Regression parameters from linear fits of $v_0/[E]_0$ vs. [buffer] from pH 5 to 8 for hypoxanthine (Hx) excision from IB25 by WT and mutant AlkAs

[IB25] = 2 μM, T = 37 °C, I = 0.25. m = slope, R^2 = correlation coefficient. The uncertainties on m are the standard errors on the fits. These data are presented in Figure 3.8.

Enzyme	pH	Buffer	m	R^2
WT	5	cacodylate	0.2 ± 0.2	0.06
WT	6	cacodylate	-0.03 ± 0.05	0.04
WT	6.5	phosphate	0.09 ± 0.1	0.07
WT	7	cacodylate	0.064 ± 0.006	0.89
WT	7	phosphate	0.20 ± 0.01	0.96
WT	8	phosphate	0.08 ± 0.01	0.76
R244M	7	phosphate	0.070 ± 0.007	0.81
Y222F	7	phosphate	0.07 ± 0.01	0.77
Y273F	7	phosphate	0.012 ± 0.003	0.56
W272F	7	phosphate	0.012 ± 0.002	0.81

Below pH 7, there is no correlation between the WT excision rate and the buffer concentration (Table 3.4). At pH 7 and 8, however, the excision rate by

WT and mutant AlkAs increased with increasing concentrations of phosphate and cacodylate concentrations. Y222F, R244M, W272F, and Y273F were all less sensitive than WT to changes in the buffer concentration.

The apparent 2-fold-greater sensitivity toward phosphate relative to cacodylate exhibited by WT AlkA at pH 7 essentially disappeared when the excision rate was plotted against the true conjugate-acid ([HA]) concentration (i.e., $[HA] = [H_2PO_4^-]$ or $[(CH_3)_2AsO_2H]$), which constitutes ~15% of the total phosphate and ~7% of the total cacodylate (Figure 3.9 and Table 3.5). The same treatment of the rates at pH 8, where only ~1.5% of the total phosphate is $H_2PO_4^-$, showed that the sensitivity toward buffer at pH 8 was ≈5-fold greater than at pH 7 (Figure 3.9 and Table 3.5).

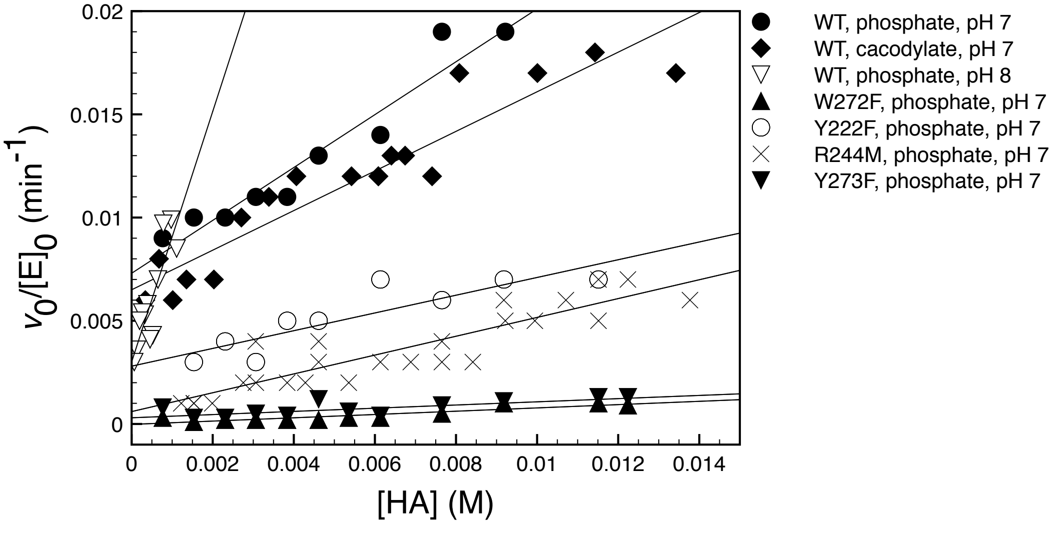

Figure 3.9. $v_0/[E]_0$ vs. [HA] for WT and mutant AlkAs
$[HA] = [H_2PO_4^-]$ or $[(CH_3)_2AsO_2H)]$, [IB25] = 2 μM, *T* = 37 °C, *I* = 0.25. Results of the linear fits are in Table 3.5.

Table 3.5. Regression parameters from linear fits of v_0/[E]$_0$ vs. [HA] at pH 7 and 8 for WT and mutant AlkAs

[DNA] = 2 μM, T = 37 °C, I = 0.25. m = slope, R^2 = correlation coefficient. The uncertainties on m are the standard errors on the fits. These data are presented in Figure 3.9.

Enzyme	pH	Buffer	*m*	R^2
WT	7	cacodylate	0.96 ± 0.09	0.89
WT	7	phosphate	1.28 ± 0.09	0.96
WT	8	phosphate	6 ± 1	0.76
R244M	7	phosphate	0.46 ± 0.05	0.81
Y222F	7	phosphate	0.42 ± 0.09	0.77
Y273F	7	phosphate	0.08 ± 0.02	0.56
W272F	7	phosphate	0.08 ± 0.01	0.81

Not all buffers were capable of promoting excision: increasing concentrations of bis-tris propane (BTP), a bulky, cationic buffer, reduced the excision rate in the presence of 25 mM phosphate (Figure 3.10). Citrate, a bulky, anionic buffer, had excision rates consistently lower than those measured in phosphate, cacodylate, or acetate, suggesting a possible inhibitor role (Figure 3.3).

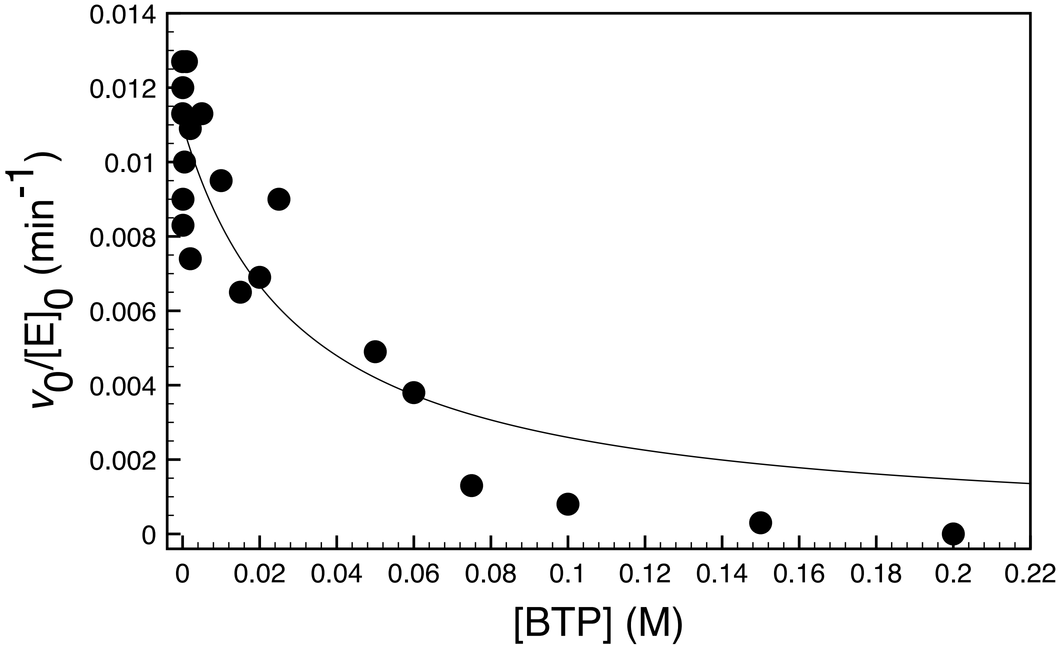

Figure 3.10. WT $v_0/[E]_0$ vs. [BTP] at pH 7
All reactions were performed in 25 mM phosphate; other conditions were as described in Figure 3.8. T = 37 °C, I = 0.25.

3.2.4 Solvent deuterium KIEs

One major explanation of the buffer concentration dependence of the reaction rate at pH ≥ 7 is rate-limiting proton transfer. Other effects, such as phosphate binding to AlkA and causing a conformational change that increases transition state stabilization are also possible. The solvent deuterium KIEs (SDKIEs) were measured to test whether rate-limiting hydron transfer was occurring. SDKIEs were measured at pL 6 and 7 (pL = pH or pD, depending on the solvent), at sub-saturating, intermediate, and saturating [DNA]; phosphate concentrations of 10 mM and 75 mM were used at pL 7, but only 10 mM at pL 6, given the lack of buffer concentration dependence (Table 3.6).

Table 3.6. SDKIEs on WT AlkA-catalyzed hypoxanthine (Hx) excision from IB25
T = 37 °C, I = 0.25. The uncertainty is the standard deviation on three independent replicates. P_i = phosphate.

	pL		
[IB25] (μM)	**6**	**7**	**7**
	10 mM P_i	**10 mM P_i**	**75 mM P_i**
0.2	0.44 ± 0.04	0.8 ± 0.1	0.6 ± 0.2
2	0.5 ± 0.2	0.7 ± 0.1	1.42 ± 0.06
10	0.55 ± 0.07	0.81 ± 0.05	1.7 ± 0.1

For IB25 in 75 mM phosphate buffer, pH 7, K_M = 1.0 μM, so the SDKIEs on k_{cat}/K_M and k_{cat} were found by measuring the SDKIEs at [IB25] = 0.2 μM and 10 μM, respectively. As [DNA] increases, the SDKIE is increasingly defined by the contribution of the chemical steps because at [DNA] << K_M, the SDKIE is on k_{cat}/K_M, which includes the substrate-binding step, while at [DNA] >> K_M, SDKIE reflects k_{cat}, which accounts for steps after substrate binding.

The inverse SDKIEs on k_{cat} at pL 6 and the higher reaction rates at pH 6 than at pH 7 (Figure 3.3) could reflect hydron transfer before the rate-determining step, presumably to the purine leaving group; a similar interpretation was made for *E. coli* MutY, for which an inverse SDKIE of 0.54 was reported under single-turnover conditions.[141] However, these SDKIEs may be inverse because at a given pL, SDKIEs also account for differences in pK_as of the relevant species in D_2O and H_2O. Generally, pK_as are higher in D_2O by ~0.5 compared with H_2O, so the observed pK_a of 5.7 from the k_{cat} vs. pH profile in H_2O would shift to approximately 6.2 in D_2O.[164] Consequently, the rate would increase in D_2O simply because the concentration of the deuterated ES complex ESD^+ would be greater than that of the protonated ES complex ESH^+, and the SDKIE would be inverse.

In 75 mM phosphate at pL 7, the observed SDKIE increased as [DNA] increased and became normal as the enzyme became saturated with substrate (Table 3.6). In 10 mM phosphate, however, the SDKIE was inverse at all DNA concentrations. Linearly extrapolating the SDKIE to 0 mM phosphate, the SDKIEs at [DNA] = 2 μM and [DNA] = 10 μM would be 0.63 and 0.67, respectively. Similarly, an extrapolated value of SDKIE = 1.8 was found for the fully buffer-catalyzed reaction at [IB25] = 2 μM and pL 7 (see Appendix 1). These normal SDKIEs are indicative of rate-limiting proton transfer during which phosphate acts as a general acid catalyst because $H_2PO_4^-$ is more acidic than $D_2PO_4^-$ (pK_a 7.2 vs. ~7.7). This is consistent with the observation that the rate increases as the phosphate concentration increases.

3.2.5 Ternary complexes

The binding of several nucleobases to the AlkA in the presence of the transition state mimic PYR35 was examined to search for evidence of AlkA•nucleobase interactions at the transition state. Adding high concentractions of adenine, Hx, or nicotinamide (a 5-formyluracil analogue) to AlkA and PYR35 at sub-K_d concentrations did not increase PYR35 binding (Figure 3.11).

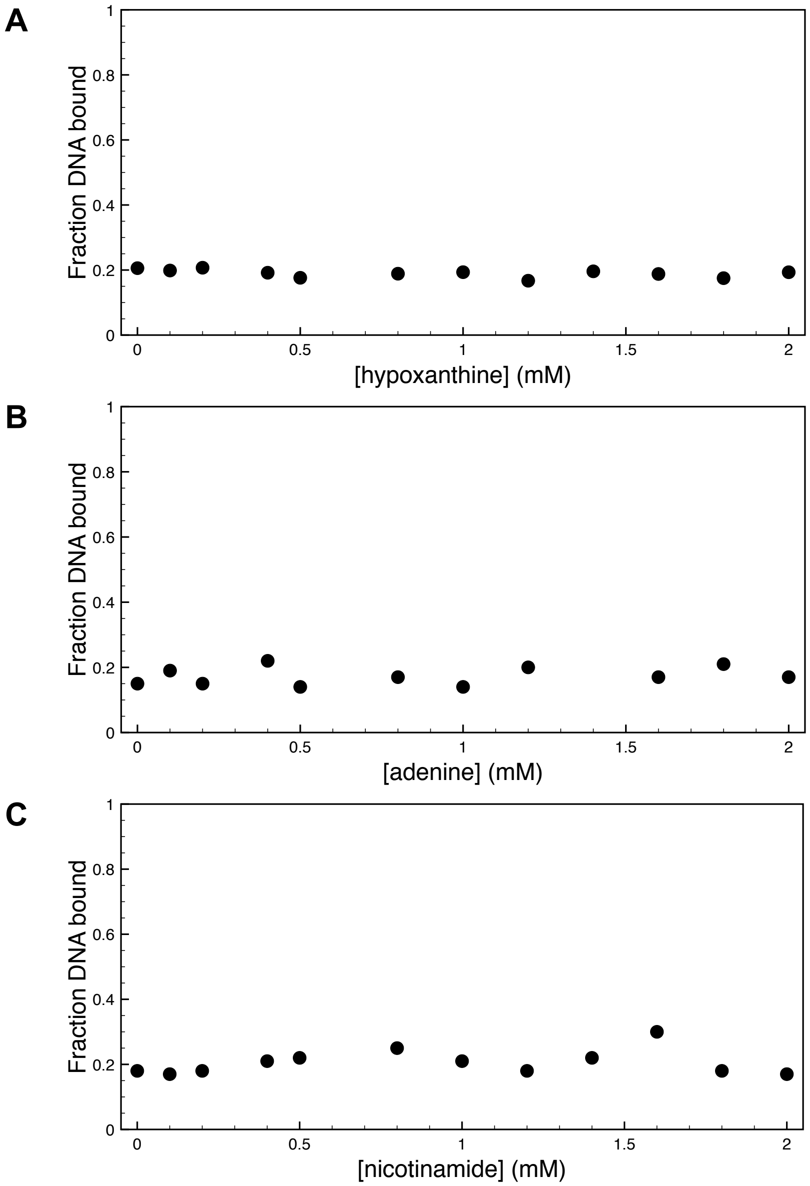

Figure 3.11. Titration of free nucleobases into solutions containing AlkA and PYR35

Varying concentrations of free nucleobases were added to 2.4 nM AlkA and 250 pM PYR35 (K_d = 2.2 nM) to probe for increased DNA binding due to ternary AlkA•nucleobase•PYR35 complex formation. A) hypoxanthine (Hx) B) adenine (A) C) nicotinamide

3.3 Discussion

3.3.1 pH profiles

The pH vs. k_{cat} and pH vs. $k_{\text{cat}}/K_{\text{M}}$ profiles for AlkA-catalyzed Hx excision from IB25 yielded fitted pK_{a} values 5.7 ± 0.1 and 5.1 ± 0.2, respectively. In contrast, the pH vs. k_{st} profile reported by O'Brien and Ellenberger reflects the ionization states in the enzyme-substrate (E•S) complex, so it fails to account for any perturbations to active-site residue pK_{a}s upon substrate binding.[118] The pH vs. $k_{\text{cat}}/K_{\text{M}}$ profile reflects the ionization states in the free enzyme and free substrate, so performing steady-state kinetics at several pHs to obtain both k_{cat} and $k_{\text{cat}}/K_{\text{M}}$ would provide useful information about ionizations in the free substrate and enzyme (E + S) and in the E•S complexes.[165] The reported pH vs. k_{st} profiles for guanine and εA excision were fit to a two-ionization model over a pH range of 6 to 9.[118] However, one of the reported ionizations arose from a single data point at pH 6, so it is not clear whether it is merely an artifact arising from a combination of normal experimental error and performing non-linear regression on limited data. It is also possible that G and εA excision have different pH dependencies.

The residue whose ionization is reflected in the pH vs. rate profiles for IB25 with AlkA must be protonated for maximal activity. Initially, the prime candidate would be D238; however, this is not consistent with D238's behaviour. The D238N mutant could not excise methylpurines from DMS-treated DNA, which would not require general-acid catalysis.[136] This suggests a role for D238 other than as a general-acid catalyst. There is strong experimental evidence that D238's δ-carboxylate group interacts with the developing positive charge on the oxacarbenium ion-like transition state. Specifically, AlkA binds pyr-DNA, which contains a positively charged residue, 2800-fold more tightly than THF-DNA, which contains a neutral residue.[111,136] The D238N mutation decreased pyr-DNA binding 50-fold.[136]

The observation of a close D238•••pyrrolidine contact in the AlkA•pyr-DNA crystal structure supports its role in stabilizing a positive charge (Figure 1.17).[111] In contrast to MutY, in which a single residue, E43, was proposed to both protonate N7 via a water relay and stabilize the oxacarbenium ion ring, D238 is located below the plane of the deoxyribosyl ring and is too far from N7 to protonate it.[111,141] In addition, if D238 were acting both as a general-acid catalyst to protonate the purine, with $pK_a = 5.7$, and then to stabilize the positive charge on the nascent oxacarbenium ion, then the K_d values of the AlkA•PYR35 complex should have decreased with increasing pH, which they did not (Table 3.2). The unperturbed pK_a value of an aspartate sidechain is 4.2, so it is possible for D238 to both stabilize the nascent oxacarbenium ion and bind to the pyrrolidine residue without having a measurable effect on the pH dependence of either activity or PYR35 binding.[166]

The unchanging K_d values for AlkA•PYR35 from pH 6 to 8 (Table 3.2) strongly suggests that whatever residue is responsible for the pH dependence of

AlkA's activity was not responsible for its binding to this transition state mimic. If it were, then K_d should have increased 100-fold between pH 6 and 8. To the extent that the pyrrolidine accurately mimics an oxacarbenium ion-like transition state, this implies that the pH dependence of activity was not due to changes in oxacarbenium ion stabilization, but instead reflected interactions with another part of the substrate molecule, namely the nucleobase.

3.3.2 AlkA mutants

Aside from D238, the AlkA active site is not rich in potential general-acid catalytic residues; only four out of the five residues selected for mutation possess an ionizable group, namely R22, Y222, Y273, and R244. The unperturbed sidechain pK_as of tyrosine's phenol group and arginine's guanidinium group are ~10.4 and ~12.5, respectively, in the free amino acid.[166] Tyrosine can act as a general acid, and despite its high pK_a, arginine may act as a general acid for some enzymes.[167] The fifth residue, W272, is not ionizable: tryptophan's indole nitrogen is not acidic ($pK_a = 16.20$), but it can still participate in hydrogen bonds.[168,169] Even if these residues do not donate a proton directly, they could be responsible for coordinating a water molecule for proton donation.

The effects of mutating these residues were minimal, with all effects being $\leq$ 4-fold on k_{cat} and $\leq$ 6-fold on $k_{cat}/K_{M.}$ This eliminates the mutated residues as being general-acid catalysts able to directly protonate the hypoxanthine ring.

However, it is still possible that AlkA can cause the scissile nucleobase to become protonated by changing its pK_a value to make it more basic, as described below.

3.3.3 Leaving-group protonation among N-*glycoside hydrolases*

Purine protonation has been observed in the KIE-derived transition states of reactions catalyzed by other *N*-glycoside hydrolases. An inverse 7-^{15}N KIE is the hallmark of N7 protonation at the transition state, and such values were obtained during the transition state analysis of ricin A-chain-catalyzed adenine excision from RNA and DNA, and *E. coli* MutY-catalyzed adenine excision from a G:A mismatch.[80,170] For *C. fasciculata* IU-NH, the 7-^{15}N KIE was not measured; however, the 9-^{15}N KIE, which reflects electron delocalization induced by N7 protonation in addition to the C1'-N9 bond order, indicated that N7 protonation had occurred.[171] Specifically, the experimental 9-^{15}N KIE of 1.026 was less than the expected value of 1.04, indicating either incomplete C1'-N9 bond cleavage or N7 protonation.[171] The 1'-^{3}H and 1'-^{14}C KIEs are inconsistent with incomplete C1'-N9 bond cleavage but are consistent with N7 protonation.[171] Similarly, the 9-^{15}N KIEs of the *N*-glycosylase reactions catalyzed by *Neisseria meningitides* and *E. coli* 5’-methylthioadenosine/*S*-adenosylhomocysteine nucleosidases (MTANs) supported N7 protonation.[172,173] The crystal structure of *E. coli* MTAN with transition state mimics showed an aspartate residue (D197) hydrogen-bonding with protonated N7, thus identifying the likely general-acid catalytic residue.[174]

While leaving-group protonation is a powerful catalytic strategy that appears to be employed by the majority of *N*-glycosylases, there are exceptions. Transition state analysis of MTA hydrolysis by *S. pneumoniae* and human MTANs showed that adenine was not protonated. The 9-^{15}N KIEs for *S. pneumoniae* and human MTANs were 1.037 and 1.039, respectively, indicative of an unprotonated (anionic) adenine leaving group.[95,96] During *E. coli* UDG-catalyzed uracil excision, uracil was also unprotonated at the transition state because the uracil anion was observed in the active site as part of the UDG•uracil•abasic-DNA product complex.[94,175]

3.3.4 Protonation with respect to the catalytic cycle

Because the pH vs. rate profiles for AlkA-catalyzed IB25 hydrolysis gave rise to only one ionization which cannot be assigned to the mutated residues, or D238, the ionization must reside on the substrate, or in the transition state complex E•S‡. There are no expected ionizations in DNA in that range, so the ionization responsible for the pH dependence most likely arises in the ES‡ complex. Presumably, the observed pK_a is from inosine protonation due to AlkA modulating its pK_a. There is precedent for this with *Trypanosoma vivax* IAG-NH, which was proposed to catalyze purine *N*-glycoside hydrolysis by lowering the purine pK_a so it could be protonated by solvent.[176] First, the thermodynamic favourability of N7 protonation on the purine's imidazole group is increased by an O•••H−C hydrogen bond between the deoxyribosyl O5' atom and H-C8 of the purine.[177] O•••H−C hydrogen bonds are generally much weaker than O•••H−O hydrogen bonds. The interaction energy *in vacuo* of an O•••H−O hydrogen bond between two water molecules is -18.8 kJ/mol, versus ≈8.4 kJ/mol for an O•••H−Cα hydrogen bond between water and an amino acid.[178] However, the *in vacuo* interaction energies of water with imidazole and imidazolium cation showed that protonation of imidazole raised the O•••H−C hydrogen bond interaction energy from -10.0 kJ/mol to -47.3 kJ/mol, which is comparable to the O•••H−N hydrogen bond interaction energy between imidazolium cation and water, -66.5 kJ/mol.[179] *In vacuo* interaction energies are much larger than they could be in solution, but these results demonstrated the similarity in hydrogen bonding energies by H−C and H−N in a protonated imidazole moiety. Experimental evidence for this came from the fact that removing the 5'-OH group caused a 6000-fold decrease in k_{cat}/K_M for IAG-NH-catalyzed hydrolysis of neutral nucleosides but only 50-fold for cationic nucleosides.[176] The 5'-OH group is accommodated by a pocket containing a Glu and an Asn residue, E184 and N173.[176] These residues appear to help position the 5'-OH group for the O5'•••H−C8 interaction because the double-alanine N173A/E184A mutant was only 10-fold less active toward 5'-deoxyguanosine than guanosine, while the wild-type enzyme was 6000-fold slower toward 5'-deoxyguanosine.[176] Similarly, the effect with cationic substrates was reduced from 50-fold to 2-fold in the double mutant.[176] In AlkA and other BER enzymes that flip the scissile base out of the DNA helix, the same O5'•••H−C8 interactions are unlikely to be possible, but the precedent of enzymes using stabilizing interactions to raise purines' pK_a values has been established.

The second proposed mechanism for IAG-NH to raise purine pK_a values is stacking interactions between an aromatic amino acid and a nucleobase to stabilize a positive charge on the purine, whether it was created from protonation or methylation. Small-molecule crystallization studies showed that co-crystallization of 9-ethyladenine with indole only yielded hydrogen bonds but no stacking interactions, while stacking interactions were observed in 1,9-dimethyladenine/indole-3-acetate crystals. [180,181] In *T. vivax* IAG-NH, W260 is proposed to raise the pK_a of the purine via aromatic stacking.[182] Its homologue *C. fasciculata* IU-NH has a histidine residue in the homologous position, which has been identified as its general-acid catalyst to protonate N7 in purine substrates.[182] Docking 3MeA into the AlkA•1-aza-DNA structure showed that W272 stacks with the nucleobase like W260 does in *T. vivax* IAG-NH (Figure 3.12).

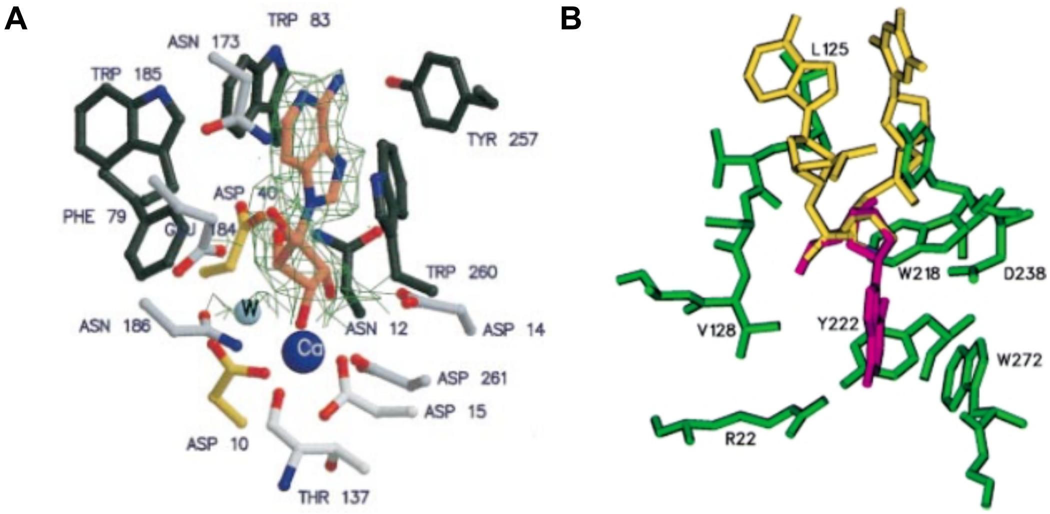

Figure 3.12. Structures of *T. vivax* IAG-NH and AlkA active sites
A) *T. vivax* IAG-NH. 3-Deaza-adenosine is shown in orange and blue. Tyr, Trp, and Phe residues are shown in olive green. Image obtained from ref [183]. B) AlkA. Docked 3MeA is shown in magenta and other residues in the oligonucleotide are shown in yellow. Amino acids are shown in green. Image obtained from ref [111].

Replacing W272 with phenylalanine reduces the sensitivity to buffer concentration. Presumably, this is a reflection of the fact that phenylalanine would be less effective than tryptophan at stacking with a purine, reducing the enzyme-induced purine pK_a shift. The combination of mutation and lack of buffer dependence made W272F AlkA 22-fold slower than WT in 75 mM phosphate at pH 7, corresponding to $\Delta\Delta G = 8$ kJ/mol for the mutation. Under these conditions, proton transfer is rate-limiting (as indicated by the SDKIEs), so if the increase in the activation free-energy is caused by making inosine protonation less favourable, the 8 kJ/mol $\Delta\Delta G$ corresponds to a 1.3-unit pK_a decrease caused by the mutation (see Appendix 2). Experimental confirmation of this pK_a change will need to be obtained.

In the active site model, the edges of the purine were flanked by Y222 and Y273.[111] The reduction in buffer sensitivity is modest in the Y222F mutant, but Y273F is as insensitive as W272F. Because Y273 does not stack with the purine and thus likely does not affect its pK_a, the Y273's phenolic hydroxyl group may be involved in coordination of a proton from hydronium ion or a buffer.

Protonation does not appear to be an obligate part of the catalytic cycle. That AlkA accepts purines with bulky alkyl adducts at N7 and N3 lends support to a solvent/buffer-dependent protonation mode, as a general-acid residue that is close enough to directly protonate the purine would sterically clash with alkyl adducts. As well, excision of modified pyrimidines can occur with rates comparable to methylpurines (e.g., 5-formyluracil) so specific interactions with the scissile base are not required for rapid excision.[123] This same pattern of behaviour is observed with some nucleoside hydrolases: purine-specific nucleoside hydrolases make specific contacts with the nucleobase, making *p*-nitrophenyl riboside a poor substrate despite its good leaving group. It is, however, a good substrate for the base-aspecific nucleoside hydrolases.[184]

3.3.5 Mechanistic implications of a solvent-exposed active site and the rate-buffer relationship

AlkA's solvent-exposed active site allows water to enter and attack C1'; however, without base protonation, the activation barrier for nucleophilic attack is higher. Diffusion of buffer species and hydronium into the active site allows them to donate their proton to the purine and increase the likelihood of successful nucleophilic attack.

The lack of buffer concentration dependence at pH 5 and 5.5 would be consistent with the enzyme-bound inosine with $pK_a \approx 5.7$; however, it was unexpected at pH 6 as ≈90% of the purine would not be protonated. Further, the concentration of the most likely proton donor in phosphate buffer, namely $H_2PO_4^-$ ($pK_a = 7.2$), is hardly different in 10 mM phosphate at pH 6, where there is 6.5 mM $H_2PO_4^-$, from 75 mM phosphate at pH 7, where there is 11 mM $H_2PO_4^-$.[155] Despite the small difference in $[H_2PO_4^-]$ between these conditions, rate-limiting proton transfer was only observable at pH 7. Thus, the proton-transfer rate cannot be determined solely by the concentration of the general-acid catalyst. The origin of the pH dependence on buffer catalysis – that is, the fact that it was observed at pH ≥ 7 but not pH ≤ 6 – is not clear. The K_d for the AlkA• $H_2PO_4^-$ complex could decrease dramatically below pH 7 such that AlkA was saturated with $H_2PO_4^-$ at concentrations < 10 mM, yielding no observable concentration dependence in the range tested, i.e., > 10 mM. However, it is also possible that a conformational change in AlkA or its ligands changed the active-site geometry such that buffer-catalyzed protonation of inosine was no longer possible. The buffer concentration dependence on its own does not answer this question, but the change in SDKIEs with pH (Table 3.6) implies a change in protonation mechanism in the pH range of 6 to 8.

The greatest significance of buffer catalysis is the mechanistic implications. Specifically, it shows that the active site of AlkA is solvent-accessible during catalysis, helping corroborate the mutational analysis results, which showed that the enzyme does not directly protonate the scissile nucleobase through its sidechains. The observation of buffer catalysis *in vitro* raises the question about its relevance *in vivo*. In *E. coli*, given a cytosolic pH of 7.6 and intracellular inorganic phosphate concentrations of ≈10 mM, phosphate alone is unlikely to have a significant effect on the rate of AlkA catalysis.[185-188] Other anionic metabolites, including organic phosphates and free amino acids, which account for more than half of the total metabolite concentration, could act as general-acid catalysts.[189] However, a moderate increase in reaction rate due to buffer catalysis is not likely to be physiologically significant.

3.3.6 Lack of ternary complexes

The lack of effect of any base tested on the binding of the AlkA•PYR35 complex was evidence that a ternary complex of AlkA•nucleobase•PYR35 is unlikely to be favourable, and that there is no synergistic binding of nucleobase and PYR35 to form a bipartite inhibitor of AlkA. This is in distinct contrast to ricin and UDG, where a nucleobase and transition state mimic together (adenine•1-aza-RNA and uracil•1-aza-DNA, respectively) formed much stronger inhibitors than either molecule alone.[150,162] The implication is that UDG and ricin form strong interactions with the nucleobase at the transition state of the reaction, while AlkA does not. AlkA-catalyzed release of 3MeA from MNU-treated calf thymus DNA was unimpeded by 5 mM 3MeA, so 3MeA does not bind to free AlkA or to its Michaelis complex long enough to interfere with excision.[156]

3.3.7 Unique properties of AlkA's active site that contribute to its behaviour

E. coli AlkA's closest homologues among BER enzymes in the HhH superfamily include *Schizosaccharomyces pombe* Mag1, *Bacillus subtilis* AlkA, *Bacillus halodurans* Mag, and *S. cerevisiae* MAG, with sequence identities of roughly 25% to 30%.[190-192] Among the five enzymes, the critical aspartate residue proposed to stabilize the oxacarbenium ion-like transition state – D238 in *E. coli* AlkA – and the tryptophan residue proposed here to lower the purine pK_a – W272 in *E. coli* AlkA – are conserved.[193,194] This residue may play the same role in *S. cerevisiae* MAG because it can excise Hx and G (the latter only from 2 kb DNA and not from oligonucleotides, however).[134,193,195]

E. coli AlkA's active site possesses the greatest hydrophobic character of the five enzymes. Y222 in *E. coli* AlkA is replaced by Met in the other four homologues[*].[193,194] Y273 in *E. coli* AlkA is replaced by Arg in *B. subtilis* AlkA

---

[*] Corresponding residues in *B. subtilis* AlkA and *B. halodurans* Mag were obtained from a Clustal Omega multiple sequence alignment with FASTA sequences from UniProt: *B. subtilis* AlkA, P37878; *E. coli* AlkA, P04395; *S. cerevisiae* MAG, P22134, *S. pombe* Mag1, Q92383; *B. halodurans* Mag, Q9KC25

and *S. cerevisiae* MAG and Lys in *S. pombe* Mag1 and *B. halodurans* Mag.[193] The hydrophobicity would facilitate AlkA binding of bulkier alkylpurines. The abilities of AlkA's other, less hydrophobic homologues to excise these lesions is not known.

There are three classes of alkylation-specific BER enzymes. The prototypical members are Class I – *E. coli* Tag1 (3MeA DNA glycosylase I), Class II – *E. coli* AlkA, and Class III – mammalian alkyladenine glycosylase (AAG). Unlike Tag1 and human AAG, AlkA does not specifically interact with nucleoside's functionalities, as shown here and illustrated by the AlkA•1-aza-DNA structure.[111] *E. coli* Tag1 can bind free 3MeA with $K_d = 68\ \mu M$, but not A. The phenolic hydroxyl group of a tyrosine residue and the carboxylate group of a glutamate residue appear to hydrogen-bond with N6 and N7 of 3MeA.[196] Also unlike AlkA, it also does not have a catalytic aspartate residue, which is consistent with its specificity for the already highly reactive 3MeA *N*-glycosidic bond.[196] While AlkA exhibits almost equal rate enhancements for most purines ($\sim 10^6$), human AAG's rate enhancement is greatest for Hx and more than 6000-fold lower for G and A.[115] This may be a consequence of AAG's specific contacts with the nucleobase. Purine stacking with two Tyr residues and a His residue and G/Hx O6-atom hydrogen-bonding with a main-chain amide would all be favourable, but G's exocyclic 2-amino group – absent in the more-efficiently-excised Hx – sterically clashes with an Asn side chain.[197]

Chapter 4. Towards the Transition State Analysis of the Acid-Catalyzed Hydrolysis of 2'-Deoxyinosine 5'-Monophosphate (dIMP)

4.1 Introduction

Determining the structures of enzymatic transition states can lead to the design of tight-binding transition state mimics as inhibitors.[148,174,198] However, the greatest insight into the mechanism – that is, the enzyme's catalytic strategies – comes from comparing its transition state with the corresponding nonenzymatic reaction. This can reveal how the enzyme manipulates the reaction pathway to achieve maximal transition state stabilization. For example, comparison of the transition states of protonating a methylene carbon in AroA- and acid-catalyzed hydrolysis of an enol ether showed that the enzymatic transition state was earlier than the non-enzymatic one; that is, the nascent C3-H^+ bond order was lower in the enzymatic transition state (Figure 4.1).[199,200] This demonstrated how, by powerfully stabilizing the positive charge formed during carbon protonation, the enzyme changed the transition state structure and achieved maximal transition state stabilization.[199,200]

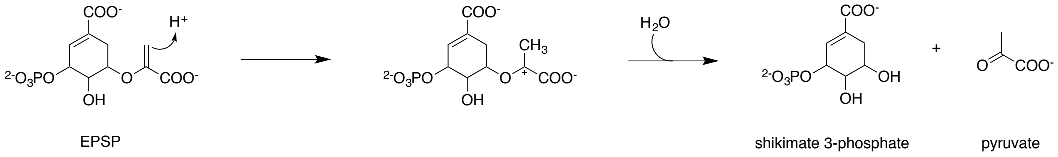

Figure 4.1. Hydrolysis of the enol ether enolpyruvylshikimate 3-phosphate (EPSP) Protonation of C3 forms an oxacarbenium ion, hydrolysis of which produces pyruvate and shikimate 3-phosphate.

N-Glycoside hydrolysis reactions are nucleophilic substitution reactions in which the C−N bond of a (deoxy)nucleoside is broken and replaced by a water nucleophile. In the vast majority of *N*-glycoside hydrolysis reactions, the transition state is highly dissociative; that is, C−N bond cleavage is far advanced over C−O bond formation, and the transition state is highly oxacarbenium ion-like.[76] Examples of both A_ND_N (S_N2, where leaving group departure and nucleophile approach occur in a concerted step) and D_N*A_N (S_N1, where a discrete oxacarbenium ion intermediate is formed) have been observed in experimentally determined transition state structures. One example was the solvolytic (non-catalyzed) hydrolysis of nicotinamide adenine dinucleotide (NAD^+), which follows an A_ND_N mechanism in which the C1’ bond order to the leaving group is 0.02 and the bond order to the nucleophile is much smaller, at 0.005.[82] NAD^+ hydrolysis by pertussis toxin also follows an A_ND_N mechanism, but is earlier than the solvolytic transition state.[77,79] The C1’−N bond order is 0.05, but there is almost no bonding to the nucleophile.[77,79] NAD^+ hydrolysis by cholera toxin A1 polypeptide (CTA) and diphtheria toxin follow more concerted A_ND_N mechanisms, with almost equal bond orders to the nucleophile and the leaving group (0.02 - 0.03).[77,78] All of the NAD^+ hydrolysis transition states exhibit significant oxacarbenium-ion character, but comparison of the non-enzymatic and enzymatic transition states show that enzymatic stabilization suppresses development of more advanced oxacarbenium-ion character.[77,78] *E. coli* MutY-catalyzed A excision follows a $D_N*A_N^‡$ mechanism like the non-enzymatic acid-catalyzed dAMP hydrolysis reaction. In both cases, C1’-N9 bond cleavage is reversible, yielding a discrete oxacarbenium-ion intermediate.[141] The reaction only becomes irreversible when C1’ undergoes nucleophilic attack by water to form the deoxyribosyl product.[141]

The aforementioned transition states were all determined from KIEs. In a competitive KIE measurement, a reaction mixture containing two reactant isotopologues is prepared. As the reaction progresses, the reactant becomes enriched in the slower-reacting isotope and the product becomes enriched in the faster-reacting isotope. The isotope ratios are measured at ≈50% extent of reaction and either 0% (in the reactant) or 100% (product). The samples at 0% and 100% establish the initial isotope ratio, and therefore, by comparison with the partial reaction, which isotopes are being enriched or depleted by the reaction.

If the KIE is measured using radiolabelled isotopologues, liquid scintillation counting can be used to quantify each radioisotope in the residual reactant or product in the 50% reaction, and in the 0% or 100% reaction samples. Radioactive samples are mixed in a scintillation fluid that contains an organic solvent and a fluor. The fluor detects radioactive decay via the transfer of kinetic energy from β-particles to solvent molecules, and then to the fluor.[201] The excited fluor molecule then releases a photon, which is detected by a photomultiplier tube. The β-particles' kinetic energy determines how many solvent molecules, and thence fluor molecules, become excited. The scintillation counter detects both the rate of radioactive decay events, reported as “counts per minute” (CPM), and the β-particles' energies, as reflected in the number of photons detected per decay event.[201] The scintillation counter is programmed to divide the energies into “windows”, with “window 1” containing decays from lower-energy β-particles, and “window 2” containing higher-energy decays. In the experiments described here, window 1 contained all the ^{3}H counts, plus some ^{14}C counts, while window 2 contained only ^{14}C counts. There is overlap in the energy distribution of ^{3}H and ^{14}C counts. A ^{14}C-containing standard is used to determine the proportion of ^{14}C counts that occur in each window, and combined with equations 2.11 and 2.12, this is used to determine the ^{3}H:^{14}C isotope ratio in any mixture (Figure 4.2).

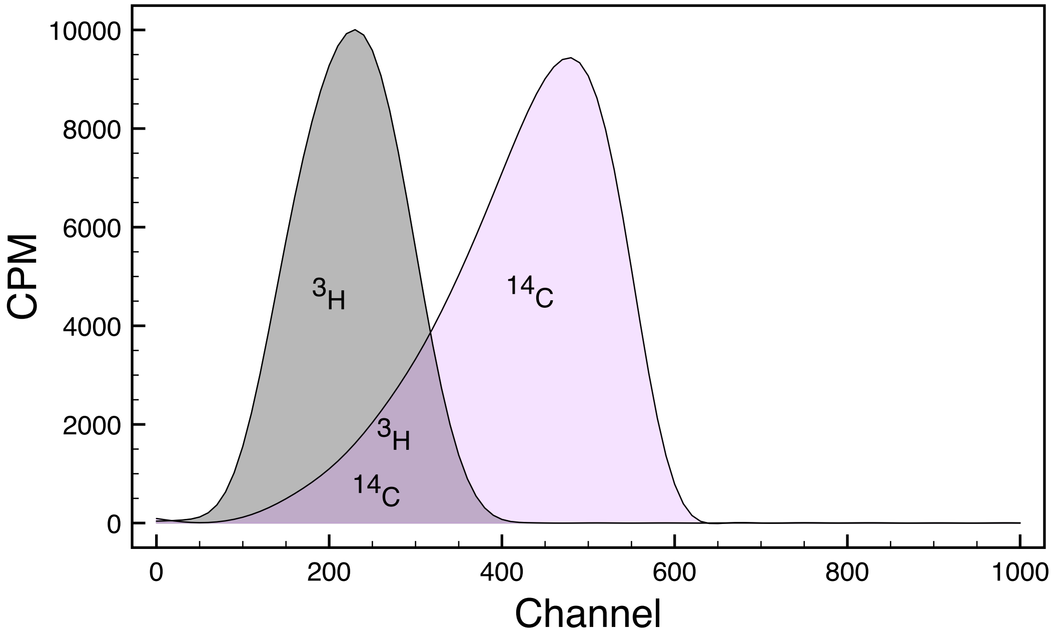

Figure 4.2. Energy spectrum of ^{3}H and ^{14}C
The energy scale is divided into 1000 "channels". Each window spans a specified number of channels.

In measuring KIEs by scintillation counting, only one isotope of interest is radioactive. For example, a ^{3}H KIE is the ratio of reaction rates for ^{3}H and ^{1}H at a given position. Since ^{1}H is not radioactive, it is necessary to label the reactant molecule with a radioisotope, ^{14}C, at a remote site where the label will not affect the reaction rate. Thus, the isotope ratio of interest, which is ^{1}H:^{3}H in this case, is followed experimentally by measuring the ^{14}C:^{3}H ratio, with ^{14}C acting as a reporter on ^{1}H at the site of interest. In cases where both the heavy and light isotopes of interest are non-radioactive, then a doubly-labelled reactant is synthesized. For example, to measure a ^{15}N KIE, the ^{15}N isotopologue possesses a ^{14}C reporter label and the ^{14}N isotopologue possesses a ^{3}H reporter label.

The translation of experimental KIEs into a transition state structure involves using quantum chemical calculations on candidate reactant and transition state structures.[76] Vibrational frequencies are calculated for the optimized reactant and transition state structures, and KIEs are calculated from these frequencies.[76] Alternatively, reactant and transition state models can be generated by empirical modeling methods, and vibrational frequencies are calculated for those structures using a simple harmonic-oscillator model, with KIEs finally calculated from those frequencies.[139] The transition state model whose calculated KIEs most closely matches the experimental KIEs is taken as the experimental transition state.

Calculated KIEs for transition state models can differ by less than 0.01, so experimental KIE values must be precise enough to distinguish between these models.[141,170,199,200] The measure of precision on experimental values is the 95% confidence interval, which specifies a range of values with 95% probability that the true value ("the population mean") will be found within it.

Described herein is the work toward precise measurement of KIEs on acid-catalyzed dIMP hydrolysis, the cognate nonenzymatic counterpart to AlkA-catalyzed Hx excision (Figure 4.3).

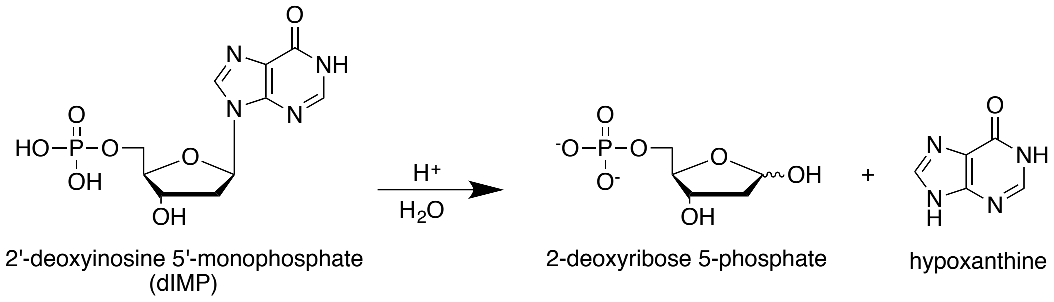

Figure 4.3. Acid-catalyzed 2’-deoxyinosine 5’-monophosphate (dIMP) hydrolysis

4.2 Results

4.2.1 Practical concerns

Unlike the KIE measurements for acid-catalyzed dAMP hydrolysis, KIE measurement for acid-catalyzed dIMP hydrolysis (and AlkA-catalyzed Hx excision) had to be performed using a biodegradable scintillation fluid. Because β-particle emission is detected indirectly through photon emission by the fluor, sample components – the scintillation fluid, water, and salts – can affect both the number of counts and the β-particle's apparent energy. Thus, biodegradable scintillation fluids were evaluated by measuring the reproducibility of the ratio of counts detected in window 1 versus window 2: $R_{windows} = CPM_{window\ 1}/CPM_{window\ 2}$. The scintillation fluids tested were Bio-Safe II, Ecoscint A, Ecoscint XR, and Ultima Gold (Table 4.1).

Ecoscint A was selected for KIE measurements in part because of the low standard deviation on the $R_{windows}$ ratio and because it produced the lowest $R_{windows}$ ratio. A low $R_{windows}$ value for a ^{14}C standard indicates that most of the ^{14}C counts are present in window 2 and not in window 1, where the ^{3}H counts are found. Ecoscint A also exhibits low quenching, as indicated by the H#. Quenching is any process that prevents a radioactive decay event from being detected or that lowers the number of photons detected. It can occur when the kinetic energy from the β-particle is dissipated as it is transferred to species other than the fluor, resulting in a reduction in the number of photons released per β-decay event.[202] It can also occur when coloured compounds in the sample absorb the photons released from the fluor.[202] Quenching is quantified by irradiating the experimental sample with γ-rays from ^{137}Cs, which causes electron scattering in the sample.[202] Kinetic energy is transferred from the scattered electrons to the fluor, which causes photon release, or to other molecules, which lowers the number of released photons. To calculate the H#, the number of photons from the sample is compared to the number of photons from an unquenched standard subject to the same γ-irradiation.[202]

Table 4.1. Counting of a ^{14}C standard

All samples contained 50 mM $MgCl_2$, 330 mM NaCl, and 8% (v/v) acetonitrile except the one prepared in Ultima Gold, which did not contain acetonitrile.

Fluid	H#	$R_{windows}$[a]	Std. dev.[a]	CoV[a]	95% CI[a]
Bio-Safe II	104	1.331	0.009	0.007	0.005
Ecoscint A	71	0.805	0.007	0.008	0.003
Ecoscint XR	103	1.30	0.01	0.01	0.006
Ultima Gold	78	1.264	0.009	0.007	0.006

[a] $R_{windows} = CPM_{window\ 1}/CPM_{window\ 2}$, std. dev. = standard deviation, CoV = coefficient of variation, 95% CI = 95% confidence interval

Competitive KIEs are measured by having both isotopologues present in the reaction mixture and tracking the change in isotope ratios during the reaction. This method of measuring KIEs is more precise than noncompetitive KIE measurements, where the reaction rates of each isotopologue are measured in separate reactions.

Quantifying the isotope ratios in the reactants and/or products involves taking aliquots of the partial reaction mixture and separating the reactants from products. Given the similarity of dAMP and dIMP, the same separation method used in the dAMP hydrolysis transition state analysis was also used here.[170] Reaction aliquots are applied to an activated charcoal resin that irreversibly retains dIMP and Hx, but not 2-deoxyribose 5-phosphate. Thus, isotope ratios were measured in the 2-deoxyribose 5-phosphate product in the partial reaction and in the 100% reaction (to determine the original isotope ratio).

The separation method was tested to ensure that 2-deoxyribose 5-phosphate was not retained. A dIMP hydrolysis reaction was taken to completion, and one half of the mixture was subject to separation while the other half was added directly to scintillation fluid. If 2-deoxyribose 5-phosphate were fully eluted, these two samples would have equal isotope ratios. The $^{14}C/^{3}H$ ratio was measured in these samples. It was 0.993 ± 0.006 (95% CI) in the sample eluted from the charcoal column and 0.988 ± 0.007 (95% CI) in the unchromatographed sample.

4.2.2 KIE measurements

4.2.2.1 [1'-^{3}H]dIMP KIE

By analogy to acid-catalyzed dAMP hydrolysis, it was expected that the transition state for acid-catalyzed dIMP hydrolysis would also be oxacarbenium ion-like.[170] In this case, the 1'-^{3}H KIE would be large, > 10%. Therefore, the 1'-^{3}H KIE can be diagnostic; an unusually small KIE would indicate problems with the separation of the reactants from the products (retention of 2-deoxyribose 5-phosphate or elution of dIMP). The 1'-^{3}H KIE was measured and found to be 1.25 ± 0.02 (Table 4.2). This is in the range of previously observed 1'-^{3}H KIEs, but the 95% CI was much wider than desired. Normally, 95% CI values of 0.002 to 0.005 are needed in transition state analysis to distinguish between competing transition state models.

Table 4.2. [1'-^{3}H]dIMP KIEs
The isotope of interest was 1'-^{3}H, with 5'-^{14}C as the reporter label.

Replicate	KIE[b]
1	1.263 (29)
2[a]	1.271 (22)
3[a]	1.241 (22)
4	1.246 (28)
5	1.217 (15)
6	1.229 (15)
Average	1.25
95% CI	0.02

[a] Measurements were performed on the same day.
[b] Numbers in parentheses indicate the number of counting cycles.

4.2.2.2 [4’-^{3}H]- and [5’-$^3H_2$]dIMP KIEs

The reporter labels for non-radioactive isotopologues can be 5’-^{14}C to report on ^{1}H in ^{3}H KIE measurements, and 5’-$^3H_2$ or 4’-^{3}H to report on ^{12}C in ^{14}C KIE measurements. The 5’-^{14}C KIE is assumed to be unity, but the 5’-$^3H_2$ and 4’-^{3}H KIEs are known to be non-unity in many reactions.[96,203-206] Thus, the 5’-$^3H_2$, and 4’-^{3}H KIEs must be measured, and for reactions in which they are reporter labels, the observed KIE must corrected using equation 4.1 (using the 5’-$^3H_2$ KIE in this example).

$$\mathrm{KIE} = \mathrm{KIE}_{\mathrm{observed}} \times \mathrm{KIE}_{5'-{}^3\mathrm{H}_2} \qquad \textbf{(4.1)}$$

The 4’-^{3}H KIE was measured in triplicate (Table 4.3).

Table 4.3. [4’-^{3}H]dIMP KIEs
The isotope of interest was 4’-^{3}H, with 5’-^{14}C as the reporter label.

Replicate	**KIE^a**
1	0.936 (45)
2	0.936 (63)
3	0.957 (45)
Average	0.94
95% CI	0.01

^{a} Numbers in parentheses indicate the number of counting cycles.

The 4’-^{3}H KIE value, 0.94 ± 0.01, is large and inverse. The variability on the KIE was too large for transition state modelling. The 5’-$^3H_2$ KIE was then measured instead but still exhibited unacceptably high variability (Table 4.4).

Table 4.4. [5’-$^{3}H_2$]dIMP KIEs

The isotope of interest was 5’-$^{3}H_2$, with 5’-^{14}C as the reporter label.

Replicate	KIE[c]
1[a]	0.992 (31)
2[a]	0.990 (30)
3	1.028 (10)
4	0.995 (10)
5[b]	0.974 (10)
6[b]	0.981 (10)
Average	0.99
95% CI	0.02

[a,b] Measurements were performed on the same day.

[c] Numbers in parentheses indicate the number of counting cycles.

4.2.2.3 [1’-^{14}C]- and [7-^{15}N]dIMP KIEs

The [1’-^{14}C]- and [7-^{15}N]dIMP KIEs were measured and corrected for the 5’-$^{3}H_2$ KIE using equation 4.1 (Table 4.5, Table 4.6).

Table 4.5. [1’-^{14}C]dIMP KIEs

The isotope of interest was 1’-^{14}C, with 5’-$^{3}H_2$ as the reporter label.

Replicate	Observed KIE[a]	Corrected KIE
1	1.009 (24)	1.001
2	1.006 (24)	0.999
3	1.001 (41)	0.993
4	0.999 (41)	0.992
Average	1.004	1.00
95% CI	0.004	0.02[b]

[a] Numbers in parentheses indicate the number of counting cycles.

[b] Interval accounts for uncertainties on both the uncorrected 1’-^{14}C KIE and the 5’-$^{3}H_2$ KIE correction factor.

Table 4.6. [7-^{15}N]dIMP KIEs

The isotope of interest was 7'-^{15}N, with 5'-^{14}C as the remote label. That is, the isotopologues were [7'-^{15}N, 5'-^{14}C]dIMP and [5'-^{3}H$_2$]dIMP.

Replicate	Uncorrected KIE	Corrected KIE
1[a]	0.965	0.958
2[a]	0.981	0.974
3	1.054	1.047
Average	1.00	0.993
95% CI	0.05	0.05[b]

[a] Measurements were performed on the same day.

[b] Interval accounts for uncertainties on both the uncorrected 7-^{15}N KIE and the 5'-^{3}H$_2$ KIE correction factor.

4.3 Discussion

4.3.1 [1'-^{3}H]dIMP KIE

The hypothesis that the transition state of acid-catalyzed dIMP hydrolysis is oxacarbenium ion-like was confirmed by the large, normal 1'-^{3}H KIE of 1.25. A large, normal KIE of 1.253 was observed for the acid-catalyzed hydrolysis of dAMP.[170] In an oxacarbenium ion-like transition state, which appears in D_N*A_N or dissociative A_ND_N mechanisms, steric crowding around C1' decreases because of the reduced total bond order at C1'. Consequently, the 1' hydron's out-of-plane bending motions increase, increasing the 1'-^{3}H KIE. There is also a simultaneous decrease in C1'−H1' bond stretching, which lowers the 1'-^{3}H KIE, but the out-of-plane bending mode is dominant (Table 4.7). [173,203]

The 95% CI is higher than desired, but 1'-^{3}H KIEs with large uncertainties have been reported (Table 4.7). There is generally a poor match between the intrinsic KIEs and the calculated KIEs from transition state models because solvent molecules or active-site residues can dampen 1'-^{3}H vibrations.[138]

Table 4.7. 1'-^{3}H KIEs for various *N*-glycoside breakdown reactions
The reactions were nucleophilic substitution reactions on *N*-glycosides, with water as the nucleophile (i.e., hydrolysis), phosphate (i.e., phosphorolysis) or phosphate analogues. The calculated KIEs were produced from the transition state assigned to each reaction.

Enzyme	*N*-glycoside, nucleophile	Intrinsic KIE	Calculated KIE	Ref.
Plasmodium falciparum OPRT[a]	OMP[b], phosphonoacetate	1.261 ± 0.014	1.335	207
human OPRT[a]	OMP[b], phosphonoacetate	1.199 ± 0.015	1.330	207
Streptococcus pneumoniae MTAN[c]	MTA[d], water	1.235 ± 0.002	1.47	95
human MTAP[e]	MTA[d], arsenate,	1.360 ± 0.003	1.200	96
E. coli MTAN[c]	MTA[d], water	1.160 ± 0.004	1.38	173
E. coli MutY	adenosine in DNA, water	1.150 ± 0.002	1.400	141
Acid-catalyzed	dAMP, water	1.253 ± 0.002	1.28, 1.38	170
N. meningitides MTAN[c]	MTA[d], water	1.03 ± 0.01	1.05	172
human PNP[f]	inosine, arsenate	1.210 ± 0.003	1.276	208

[a] orotate phosphoribosyltransferase
[b] orotidine 5'-monophosphate
[c] 5'-methylthioadenosine/*S*-adenosylhomocysteine nucleosidase
[d] 5'-methylthioadenosine
[e] 5'-methylthioadenosine phosphorylase
[f] purine nucleoside phosphorylase

4.3.2 [4'-^{3}H]-, [5'-^{3}H$_2$]-, [1'-^{14}C]-, and [7-^{15}N]dIMP KIEs

The models generated for *Salmonella pneumoniae* 5'-methylthioadenosine nucleosidase (MTAN)-catalyzed MTA hydrolysis and the human orotate phosphoribosyltransferase (*Hs*OPRT)-catalyzed OMP reaction with phosphonacetate show hyperconjugation between the O4' lone pairs and the σ* orbital of the C4'-H4' bond and were oxacarbenium ion-like.[95,207] The 4'-^{3}H KIEs yielded by these models were 0.945 and 0.972, respectively.[95,207] Based on these data, dIMP transition state models could presumably be found with a 4'-^{3}H KIE as low as 0.94 (to match the average KIE observed here). The [4'-^{3}H]dIMP KIE here is large and would result in a large correction factor being applied to KIEs measured using 4'-^{3}H as the reporter label. Ideally, the correction factor would be close to unity, but a large value does not prevent a transition state structure from being obtained. For example, the transition state structure of the *Hs*OPRT OMP/phosphonoacetate reaction was determined using ^{14}C and ^{15}N KIEs corrected using a large 4'-^{3}H KIE of 0.962 ± 0.002.[209]

The 5'-^{3}H$_2$ KIE was closer to unity and thus would result in a lower correction factor being applied to the 1'-^{14}C and 7-^{15}N KIEs, but it was inverse, and most *N*-glycoside breakdown reactions exhibit normal KIEs at this position, with the exception of *P. falciparum* OPRT, which was only slightly inverse – 0.993 ± 0.005.[207] More specifically, 5'-^{3}H$_2$ KIEs measured for non-enzymatic reactions were normal; the 5'-^{3}H$_2$ KIE for the acid-catalyzed dAMP hydrolysis, the reaction most similar to the reaction under study here, was 1.012 and the 5'-$^{3}H_2$ KIE for non-enzymatic NAD^+ hydrolysis was 1.000. [82,170]

The experimental errors on the 5'-$^{3}H_2$ and 4'-^{3}H KIEs were large enough that when they were used to correct the 1'-^{14}C KIE, the 95% CI for the 1'-^{14}C KIE was too large to be useful for transition state analysis. The possible range of 1'-^{14}C KIEs would be 0.98 to 1.02. At the lower limit, this is lower than any previously observed 1'-^{14}C KIE. The 1'-^{14}C KIE for ricin-catalyzed adenosine hydrolysis was also inverse, 0.993 ± 0.004.[80] This was evidence for a discrete oxacarbenium ion intermediate being formed (a D_N*A_N mechanism). Inverse ^{13}C KIEs were also observed at the central carbon atom of a nucleophilic substitution reaction for methanolysis of *p*-substituted 1-phenyl-1-bromoethanes.[80,210] So, an inverse KIE would be evidence for a discrete oxacarbenium ion intermediate being formed in a D_N*A_N mechanism. At the upper limit of 1.02 for the [1'-^{14}C]dIMP KIE, this would be consistent with a D_N*A_N or highly dissociative A_ND_N mechanism. Thus, while the experimental [1'-^{14}C]dIMP KIE supported an oxacarbenium ion-like transition state, the confidence interval was too large to allow detailed transition state analysis.

The 7-^{15}N KIEs are ambiguous, not because of the 5'-$^{3}H_2$ KIE correction factor, but because the confidence interval was so large that the number was uninterpretable. The average 7-^{15}N KIE is slightly inverse at 0.993; and inverse KIEs were observed for ricin A-chain-catalyzed adenine hydrolysis from

RNA/DNA, acid-catalyzed dAMP hydrolysis, and *E. coli* MutY-catalyzed adenine excision, with values of 0.981 to 0.992.[80,141,170] The 7-^{15}N KIE is inverse when N7 is protonated and inversely proportional to the extent of N7 protonation.[76] Again, the individual measurements here span from inverse to normal, so the poor precision precludes any definitive interpretation about N7 protonation at the transition state.

The main line of inquiry into measurement variability was periodically testing for inconsistent retention of 2-deoxyribose 5-phosphate and/or elution of dIMP during the chromatography step. This was done by comparing the ^{14}C/^{3}H ratios in unseparated reaction samples with 100% reaction samples subject to chromatography. When this was performed during the measurement of the fourth 1'-^{3}H KIE replicate, the average ^{14}C/^{3}H ratios across the samples were equal. This was performed again with the first 4'-^{3}H KIE replicate but with unseparated portions of the 0%, 50%, and 100% reactions. Again, the average ^{14}C/^{3}H ratio for the four samples were within error of each other. These results and the results of the separate experiment performed before KIE measurements were taken (see Section 4.2.1) showed that there were no chromatographic effects on the isotope ratios. Furthermore, specifically controlling for the quality of the resin slurry by using the same batch across multiple measurements did not improve the inter-experiment reproducibility. Performing replicate measurements on the same day did not have a consistent effect on the reproducibility, but measurements performed on different days were not necessarily different from each other either. Therefore, the variability persisted despite keeping experimental variables constant and despite efforts to identify the source of the variability.

Chapter 5. Towards the Transition State Analysis of the AlkA-Catalyzed Excision of Hypoxanthine

5.1 Introduction

DNA/RNA base-excision enzymes like *E. coli* MutY, *E. coli* UDG, and ricin A-chain have been the subject of transition state analyses using KIEs, and the overall approach of these studies was followed in order to elucidate the transition state structure of AlkA-catalyzed base excision. Specifically, competitive KIE measurements were carried out with oligonucleotide substrates containing a radiolabelled (deoxy)nucleoside.[80,141,211] Early efforts in AlkA transition state analysis resulted in the design of a 26-mer Hx-bulge hairpin substrate, ATI26.[212] ATI26 has a number of features that make it suitable for KIE measurement. First, ATI26 is double-stranded; bases from double-stranded DNA are excised more quickly than from single-stranded DNA.[118] Second, by being self-complementary, it ensures that all of the radiolabelled inosine in solution occupies an identical double-stranded context of equivalent reactivity to AlkA. Third, the bulged scissile inosine base is preferentially excised by AlkA over the surrounding normal bases.[118,212] Fourth, radiolabelled inosine can be enzymatically synthesized and incorporated into the oligonucleotide.

Besides the substrate, the same overall procedure and concerns apply to AlkA KIE measurement as they do for dIMP hydrolysis KIE measurement (see Sections 4.1 and 4.2.1). Specifically, KIE measurement requires that the residual substrate and product be completely separated so that quantitative recovery of the radiolabels in each species is possible. This is not trivial for a BER enzyme, as the product of AlkA-catalyzed Hx excision from ATI26 is a DNA 26-mer containing an abasic site. Non-enzymatic nicking can occur at abasic sites and AlkA can potentially re-bind released abasic product (based on its affinity for the THF product analogue), causing inhibition as product accumulates.[136] The approach developed during MutY transition state analysis was also used here, namely that the abasic 26-mer was degraded *in situ* by human apurinic/apyrimidinic endonuclease I (hAPE1) to a radiolabelled 7-mer with a 3' abasic end and a 19-mer (Figure 5.1). The reaction was then quenched with 140 mM KOH, which causes β,δ-elimination of residual abasic 26-mer, β-elimination on the abasic 7-mer, and degradation of 4,5-dihydroxy-pent-2-enal 5-phosphate (DP5P) to 4-oxopent-2-enal. ATI26, G19, and 4-oxopent-2-enal can be separated by ion-exchange chromatography. This work describes development of ion-exchange separation methods for the measurement of KIEs on AlkA-catalyzed Hx excision from ATI26.

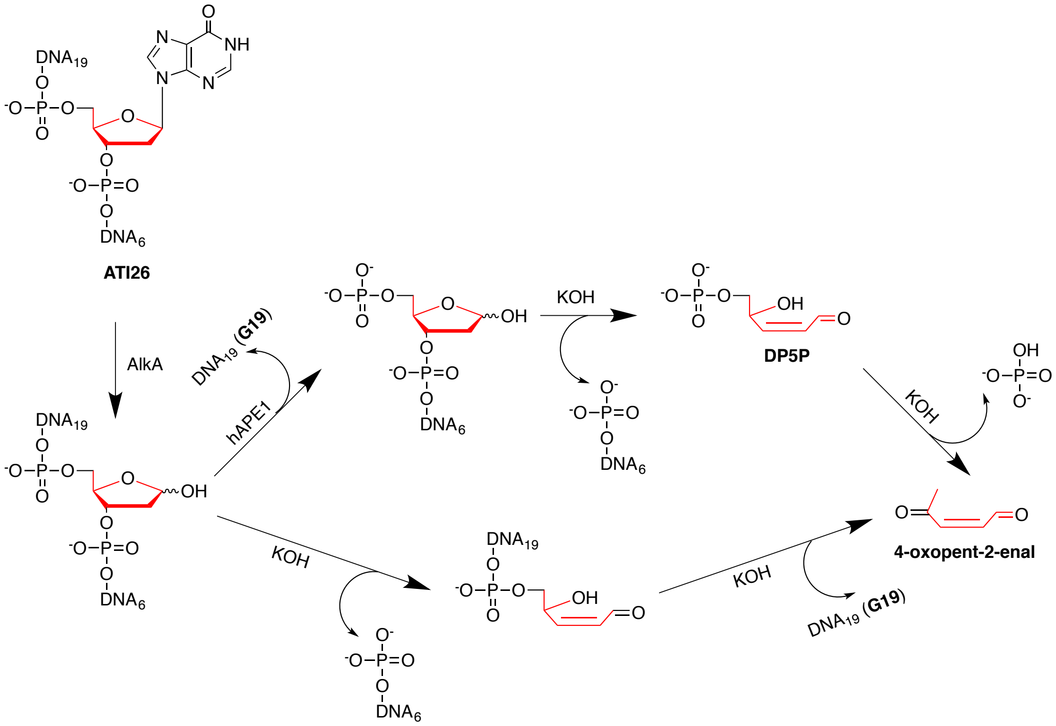

Figure 5.1. Schematic of the fate of the radiolabel after AlkA-catalyzed excision of hypoxanthine (Hx) from ATI26
The red bonds indicate the placement of the radiolabel (^{14}C or ^{3}H).
DP5P = 4,5-dihydroxy-pent-2-enal 5-phosphate

5.2 Results

5.2.1 ATI26 excision kinetics

To identify the time needed for the reaction to reach 50% completion, reactions with [5’-^{33}P]ATI26 were performed under the KIE-measurement reaction conditions. The extent of reaction reached a plateau between 60% and 80%, regardless of whether hAPE1 was present (Figure 5.2).

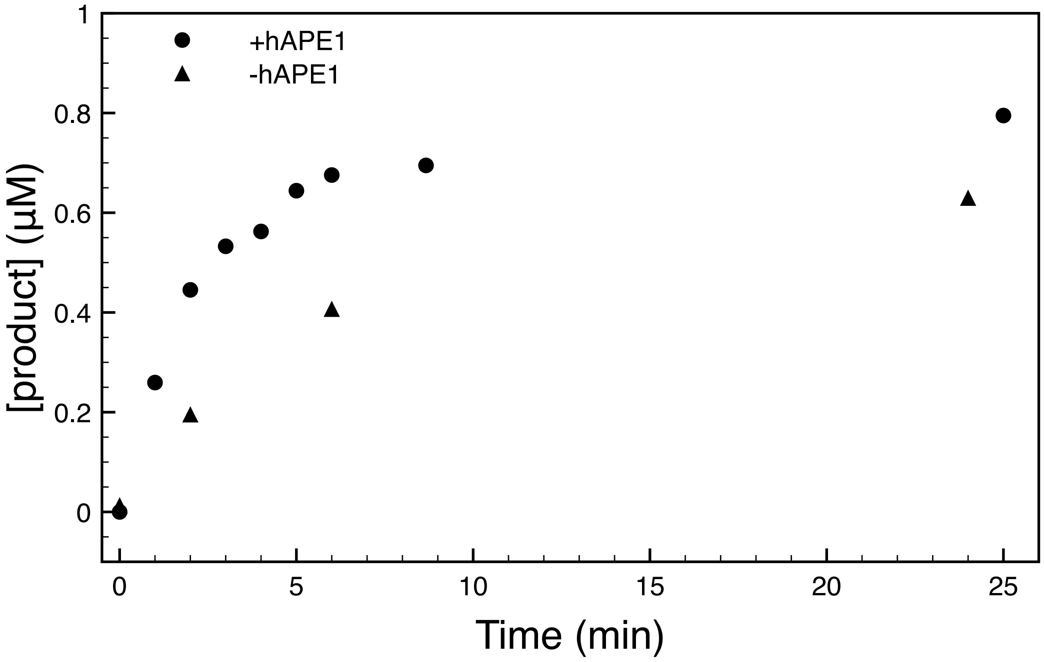

Figure 5.2. Product-formation time course with 1 μM AlkA and 1 μM ATI26 at pH 6
Product = G19 (see Figure 5.1 for G19-formation pathway). +hAPE1 = 0.3 U/μL hAPE1, 10 mM $MgCl_2$. –hAPE1 = 10 mM EDTA.

As long as the plateau was not caused by a non-reactive substrate subpopulation, the inability to reach 100% extent of reaction was not necessarily a roadblock to successful KIE measurement because a reaction could be sampled at 50% and either 0% or 100% extent of reaction.

5.2.2 Method development

The first method evaluated for separating ATI26 from the AlkA reaction products was a slight modification to the method used for MutY transition state analysis. For MutY, reaction mixtures were separated using anion ion-exchange chromatography; products (DP5P) were eluted at 0.66 M NaCl and substrate was eluted at 1.1 M NaCl, with 10 mM NaOH as a denaturant.[141] Here, DP5P was eluted at 0.3 M NaCl and the substrate was eluted at 1.05 M NaCl, with 10 mM NaOH as a denaturant (Figure 5.3) The 1'-^{3}H KIE calculated using isotope ratios in the residual substrate was 1.05 (Table 5.1).

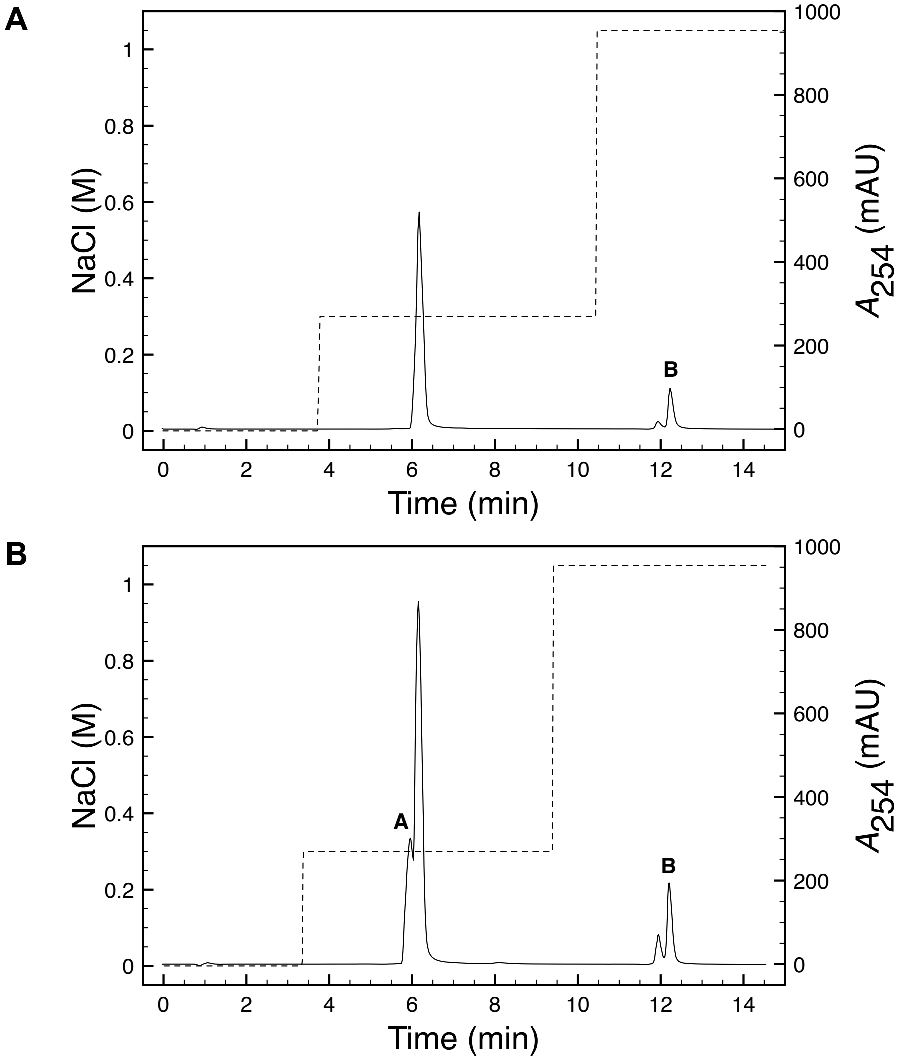

Figure 5.3. Ion-exchange chromatogram of reaction mixture containing AlkA, [5'-^{14}C]ATI26, and [1'-^{3}H]ATI26 (separation by method 1)
A = DP5P, B = ATI26. The dotted line indicates NaCl concentration. A) 0% reaction B) 50% reaction

Table 5.1. AlkA-catalyzed [1’-^{3}H]ATI26 KIEs

The isotope of interest was 1’-^{3}H, with 5’-^{14}C as the reporter label. All KIEs were calculated from substrate isotope ratios in the 0% and 50% reactions. For method 1, the KIE was calculated from the isotope ratios in peak B shown in Figure 5.3. For method 2, the KIEs were calculated from the isotope ratios in peak C only or from both peak C and peak D, shown in Figure 5.4. For method 3, the KIEs were calculated from the isotope ratios in peak C shown in Figure 5.5.

	KIE[a]			
Replicate	**1**	**2 (peak C)**	**3**	**2 (peak C and D)**
1	1.05 (37)	1.037 (51)	0.82 (34)	1.215 (21)
2		1.189 (26)		1.217 (32)
3		1.128 (30)		1.205 (52)
4		1.069 (21)		1.169 (25)
5		1.081 (5)		
Average		1.10		1.202
95% CI		0.05		0.008

[a] Number in parentheses indicates number of counting cycles.

The value of 1.05 was lower than expected for an enzyme for which evidence exists of an oxacarbenium ion-like transition state (Table 4.7). As well, the samples containing 1.05 M NaCl prepared in biodegradable Bio-Safe II scintillation fluid exhibited high quenching (see Section 4.2) and poor stability. That is, the samples did not remain clear and homogeneous during counting); this was not a problem when non-biodegradable fluids were used. Therefore, a new method was devised: the salt concentration needed to elute the substrate was lowered from 1.05 M to 0.33 M by including 50 mM $MgCl_2$ in the mobile phases, with 8% acetonitrile to replace NaOH as the denaturant, and Ecoscint A, an alternate biodegradable scintillation fluid with lower quenching and higher aqueous capacity than Bio-Safe II, was used. Resolution of all relevant species was still obtained. The 1’-^{3}H KIE obtained using this method was 1.10 ± 0.05 (Table 5.1, Figure 5.4).

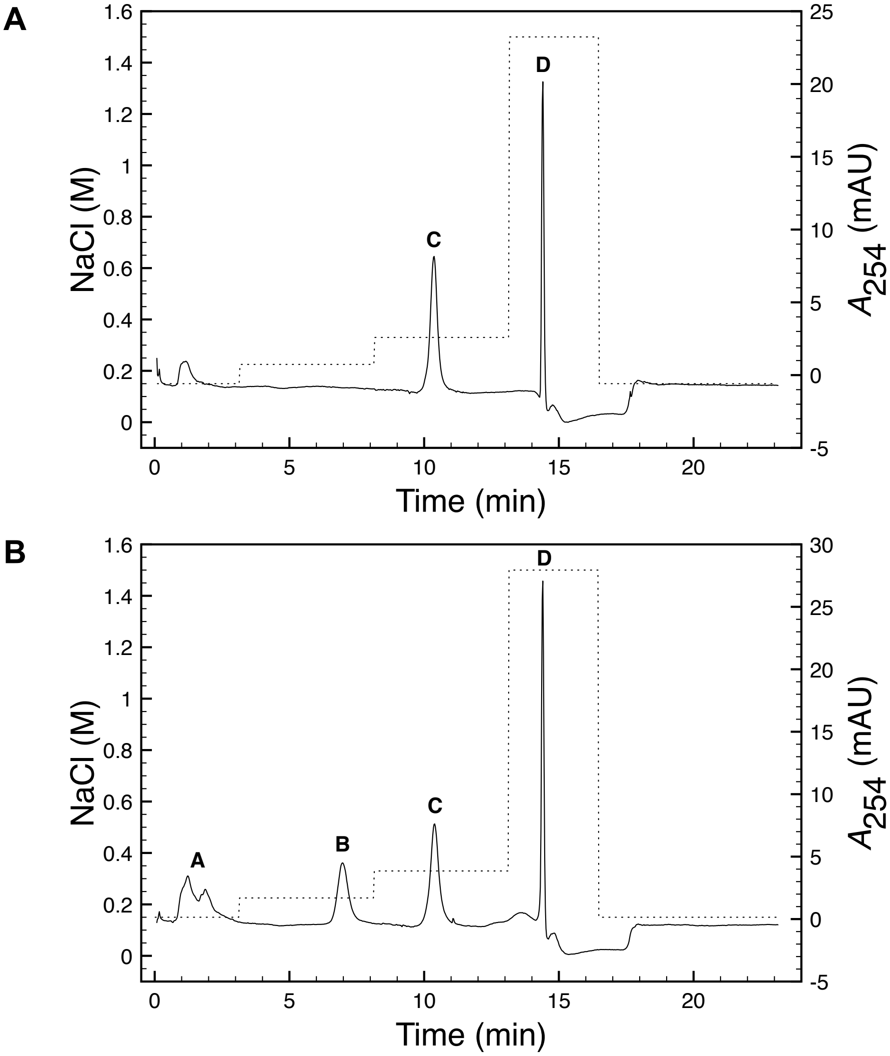

Figure 5.4. Ion-exchange chromatogram of reaction mixture containing AlkA, [5’-^{14}C]ATI26, and [1’-^{3}H]ATI26 (separation by method 2)
A = DP5P, B = G19, C = ATI26, D = unknown. The dotted line indicates NaCl concentration. A) 0% reaction B) 50% reaction

Method 2 contains a segment in which the column is flushed with high salt (1.5 M NaCl), and a peak of unknown identity (peak D, $t_R = 14 - 15$ min, Figure

5.4) contained approximately 10% of the total radioactivity. When [1'-^{3}H]ATI26 without enzyme or the other isotopologue was injected, a peak at t_R = 14 − 15 min (peak D) appeared; collecting this peak, ethanol-precipitating the eluate, and re-injecting the isolated material yielded both peaks at t_R = 10 – 11 min (peak C) and t_R = 14 − 15 min (peak C). The conversion of peak D to peak C showed that they are both forms of the substrate, so the two forms were eluted together at 0.6 M NaCl. With this adjusted method, the 1'-^{3}H KIE was 0.82 (Table 5.1, Figure 5.5). A large, inverse 1'-^{3}H KIE is inconsistent with an oxacarbenium ion-like transition state and not within a realistic range for secondary KIEs on *N*-glycoside breakdown reactions.[138]

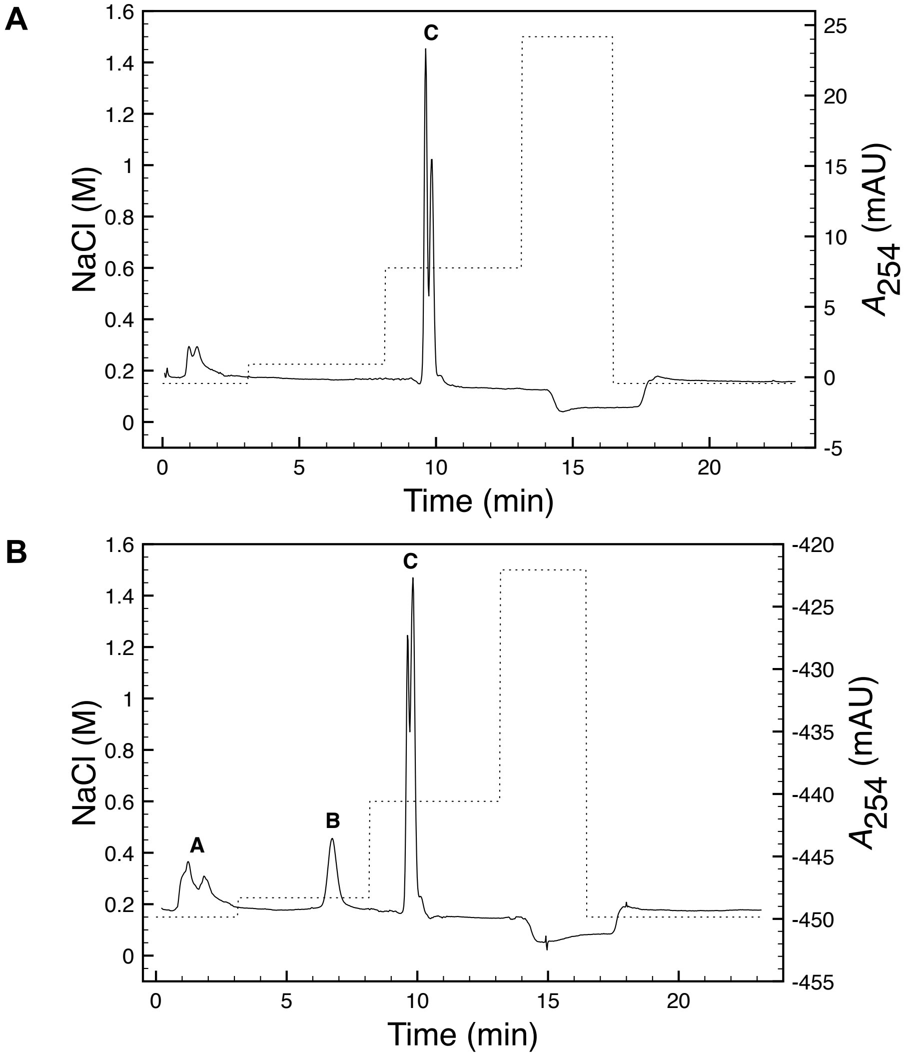

Figure 5.5. Ion-exchange chromatogram of reaction mixture containing AlkA, [5'-^{14}C]ATI26, and [1'-^{3}H]ATI26 (separation by method 3)
A = DP5P, B = G19, C = ATI26, D = unknown. The dotted line indicates NaCl concentration. A) 0% reaction B) 50% reaction

It was unclear at this point whether the two separate substrate peaks were a consequence of the separation method or that they represented two forms in solution of potentially unequal reactivity. Efforts were then directed toward isolating the main form. Injecting [1'-^{3}H]ATI26, collecting the ATI26 eluate (*t*$_R$ = 10 – 11 min, Figure 5.5), ethanol-precipitating the eluate, and re-injecting the isolated DNA only produced a single peak where ATI26 elutes (*t*$_R$ = 10 – 11 min, Figure 5.5) and another peak between 11 and 13 min that disappeared when acetonitrile was removed from the mobile phase. Thus, [1'-^{3}H]ATI26 and [5’-^{14}C]ATI26 were mixed, ion-exchange-purified together to isolate the single ATI26 form with *t*$_R$ = 10 – 11 min, and ethanol-precipitated before being used in a reaction. The minor form reappeared when the twice-purified substrates were incubated with AlkA. Because eluting both forms together yielded a large, inverse KIE, both forms were collected separately. Measured this way, 1’-^{3}H and 5’-$^3H_2$ KIEs were 1.202 ± 0.008 (Table 5.1) and 0.92 ± 0.03 (Table 5.2), respectively.

Table 5.2. AlkA-catalyzed [5’-$^3H_2$]ATI26 KIE using method 2 (both substrate forms collected)

The isotope of interest was 5’-$^3H_2$, with 5’-^{14}C as the reporter label. The KIE was calculated from the isotope ratios in peak C and D (Figure 5.5).

Replicate	**KIE**[a]
1	0.900 (15)
2	0.906 (15)
3	0.954 (8)
Average	0.92
95% CI	0.03

[a] The number in parentheses indicates the number of counting cycles.

The 1’-^{3}H KIE’s uncertainty and value were acceptable but the 5’-$^3H_2$ KIE uncertainty and value were not despite both KIEs having been measured the same way. Acetonitrile was later found to broaden the substrate peak, so it was removed from the mobile phases. The salt concentration was also increased to 800 mM to elute both forms together. The 1'-^{14}C KIE was measured using this method and calculated from the isotope ratios in peak B (Figure 5.6). The observed 1'-^{14}C KIE was 1.117 (17 counting cycles), and the corrected KIE (using equation 4.1 and the average 5’-$^{3}H_2$ KIE in Table 5.2) was 1.027.

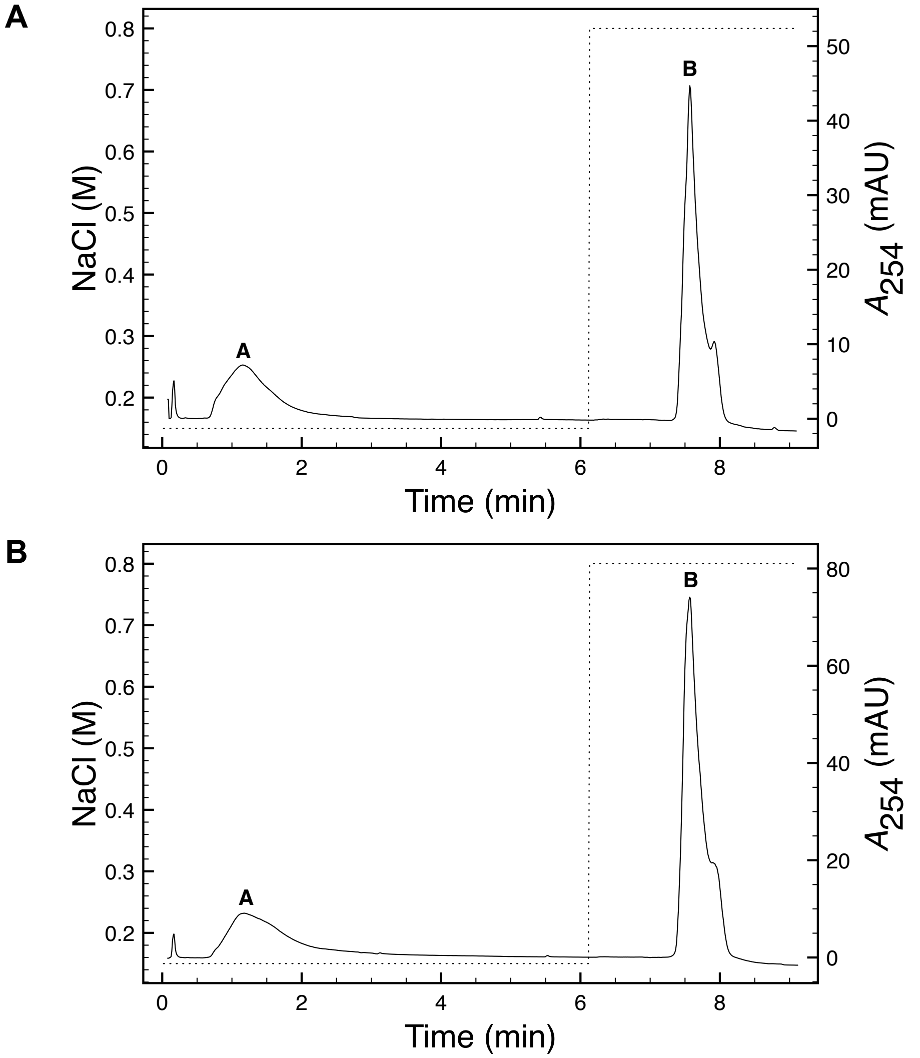

Figure 5.6. Ion-exchange chromatogram of reaction mixture containing AlkA, [5’-$^{3}H_2$]ATI26, and [1’-^{14}C]ATI26 (separation by method 4)
A = DP5P, B = ATI26. The dotted line indicates NaCl concentration. A) 0% reaction B) 50% reaction

5.2.3 ATI26 excision kinetics vs. IB25 excision kinetics

The two substrate forms revealed by the separation of AlkA reaction mixtures may have been related to the plateau in Figure 5.2. A large excess of enzyme may not eliminate the plateau if the two forms are unequally reactive. When a 100-fold excess of AlkA was used, the expected 19-mer product initially accumulated, but at 20 h, its concentration was decreasing (Figure 5.7). After the 20 h sample was taken, the protein was replaced with new protein (while keeping the final concentration constant), but this did not increase 19-mer formation; in fact, both the 19-mer and the substrate concentrations decreased while the concentration of low-molecular-weight (LMW) products (smaller than 19 nucleotides) continued to increase. ATI26 consumption was 50% complete by 2 h and 80% complete within 3 days, but by this point, the products did not arise from Hx excision only. However, Hx excision from IB25, the substrate used in the leaving-group activation studies, was complete within 60 min, despite a smaller enzyme excess (28-fold) and a higher reaction pH (pH 7). The initial velocity of Hx excision from IB25 was 20-fold faster than ATI26 (Table 5.3).

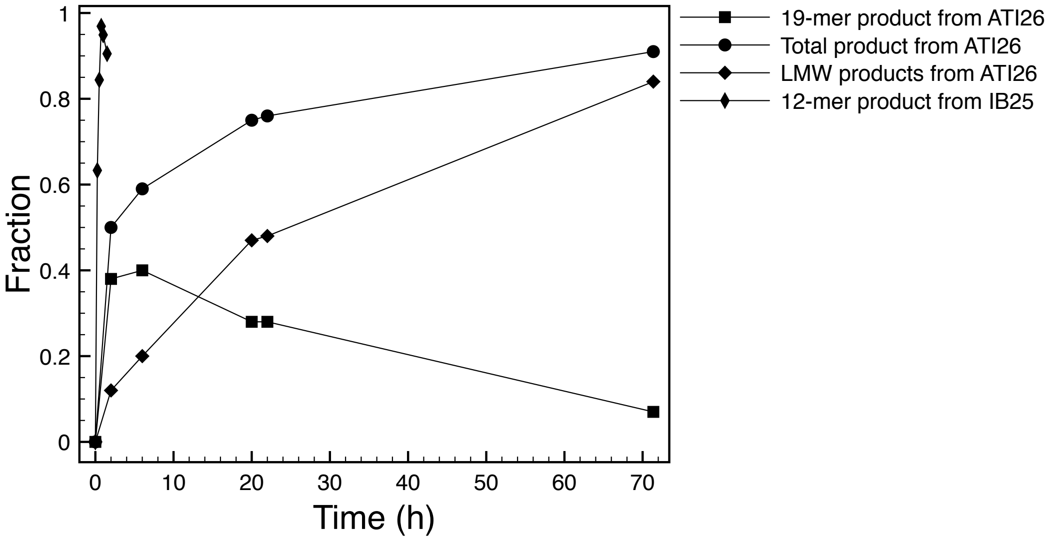

Figure 5.7. Product-formation time course with ATI26, IB25, and excess AlkA
The amount of each species was expressed as a fraction of the total radioactivity at each time point. Reactions either contained 10 µM AlkA with 0.1 µM ATI26 (100-fold enzyme excess) or 3.2 µM AlkA with 0.115 µM IB25 (28-fold excess). The IB25 reaction was performed at pH 7. The ATI26 reaction was performed at pH 6 and at 20 h, the reaction was heat-quenched and AlkA was re-added to maintain a concentration of 10 µM.

Table 5.3. Hypoxanthine (Hx) excision rates from ATI26 and IB25 at pH 7

Substrate	[substrate] (µM)	[AlkA] (µM)	Rate (min^{-1})
ATI26	0.45	0.1	1.6×10^{-4} min^{-1}
ATI26	0.45	0.5	2.0×10^{-4} min^{-1}
IB25	0.5	0.2	4.0×10^{-3} min^{-1}

5.3 Discussion

The large, inverse AlkA 1’-^{3}H KIEs were outside the range of any 1'-^{3}H KIE observed or calculated previously, and were rejected outright. They pointed to a greater problem in the measurement procedure, even if the procedure recovered all the radioactivity in the experiment. Conversely, realistic values consistent with existing evidence that are produced from methods in which there is only partial radioactivity recovery cannot be accepted either.

Despite the existence of two non-isolable substrate forms, the 1’-^{3}H KIE, 5’-$^3H_2$, and 1’-^{14}C KIEs were measured. Given what is known about the nature of 1’-^{3}H KIEs (see Section 4.3.1), the 1’-^{3}H KIE of 1.202 ± 0.008 was reasonable in its precision and magnitude. The 5’-$^3H_2$ KIE of 0.92 ± 0.03 was more inverse than observed previously. However, the expected KIE at this remote position are not well defined, and distortion of the DNA backbone upon binding to the enzyme is within the realm of possibility, as large binding KIEs have been observed in other *N*-glycoside reactions.[209,213] Applying the 5’-$^3H_2$ KIE to correct the observed 1'-^{14}C KIE of 1.117 gave a corrected 1'-^{14}C KIE of 1.033, which was consistent with an oxacarbenium ion-like transition state. With such a large uncertainty on the 5’-$^3H_2$ KIE, however, the corresponding range of uncertainty on the 1’-^{14}C KIE means that it cannot be used to distinguish between a D_N*A_N mechanism and an dissociative A_ND_N mechanism. The 5’-$^3H_2$ KIE for MutY-catalyzed A excision was also inverse, 0.968, and its calculated KIEs did not exceed 0.97.[141] This KIE was attributed to DNA-backbone distortions at the transition state. AlkA’s inverse KIE is consistent with the DNA backbone distortion observed in AlkA complexed with the transition state-mimicking 1-aza-DNA, but interpretation of a large, imprecise KIE is ill-advised.[111] Normal 5’-$^3H_2$ KIEs were observed in reactions involving nucleosides, as distinct from nucleic acid substrates, including those catalyzed by human thymidine phosphorylase, *P. falciparium* and human OPRTs, and *S. pneumoniae*, *N. meningitides*, and *E. coli* MTANs.[95,172,173,205,207] These normal KIEs were attributed to rotational restriction of the 5' end of the molecule at the transition state.

The existence of two forms of ATI26 complicated the measurement of KIEs. That ATI26 was eluting at two different times was established through re-injection of the late-eluting form (t_R = 14 – 15 min, Figure 5.4), which produced the early-eluting form (t_R = 10 – 11 min, Figure 5.4) again, and through isolation of the early-eluting form, which produced two forms again as part of a reaction mixture. The late-eluting form may be the dimer complex, which is distinct from the stem-loop monomer form (Figure Figure 5.8). For the purposes of the following discussion, the early- and late-eluting forms are assumed to be the monomer and dimer forms, respectively. High salt concentrations (e.g., 1 M NaCl) and 10 mM $MgCl_2$ shifted the equilibrium toward the dimer at 4 °C to > 40% of the total.[214] ATI26 was not exposed to high salt concentrations until the separation step, but 10 mM $MgCl_2$ was present in the reaction mixture and 50 mM $MgCl_2$ was present in the mobile phase. Any change to the monomer:dimer distribution during the separation step would have no bearing on the measured isotope effect as long as both species eluted together, but eluting them together did not consistently improve the precision and magnitude of the observed KIEs.

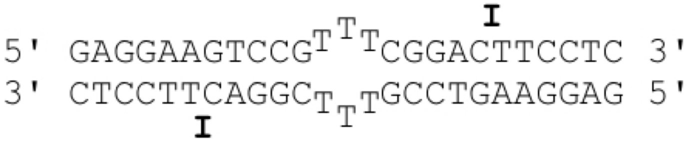

Figure 5.8. Secondary structure of ATI26 dimer

The monomer:dimer equilibrium could potentially be sensitive to isotopic labelling and to slightly different conditions between experiments. If AlkA prefers one form over the other, then the isotopologue that is present in the more reactive form will be consumed preferentially, leading to an apparent KIE that reflects the isotope effect on the monomer:dimer equilibrium, rather than the chemical steps of the reaction. During a KIE measurement using method 2 (Figure 5.4), the early:late peak area ratio changed from 1.4 to 0.8 as the reaction progressed from 0% to 50%. The ratio change could be caused by AlkA's preference toward the early-eluting form and, if the late-eluting form is the duplex, possibly an equilibrium shift of the duplex toward the hairpin as the hairpin is being consumed. If re-equilibration were occurring on a timescale comparable to excision, then the early:late peak-area ratio would remain constant, but this is not observed.

The early plateauing of the reaction shown in Figure 5.2 may provide evidence of a less reactive substrate subpopulation hinted at by the chromatographic appearance of two substrate forms. The plateau was not caused by enzyme denaturation, because replenishing the enzyme did not increase 19-mer formation. When sub-stoichiometric or equimolar amounts of AlkA and substrate were used, the reaction stopped once all the early-eluting form was consumed. Adding more AlkA may cause excision from the second form, but the increase in lower molecular weight products would suggest that base excision at other sites was faster than at the bulged I residue.

The reaction plateau and the existence of two forms appear to be specific to ATI26 because AlkA-catalyzed Hx excision reached completion with the double-stranded substrate IB25, and no low molecular weight products appeared with IB25. The difference between the two substrates, besides the fact that ATI26 is self-complementary and IB25 is not, is that in IB25, the scissile Hx is in the centre of a 24-nucleotide stretch, while in ATI26, the scissile Hx is in the centre of a 11-nucleotide stretch. AlkA's affinity toward THF35, a THF-containing hairpin with 16-nucleotide stems, is ~10-fold lower than THF53, a THF-containing hairpin with 25-nucleotide stems. With the shorter stem, non-specific binding predominates, because the K_d for THF35 is 544 nM, versus 450 nM for the undamaged oligonucleotide.[118] It is not surprising then that Hx is excised much more slowly from ATI26 than from IB25 and that adding more enzyme does not cause an increase in specific Hx excision from ATI26. However, Hx was excised from ATI56, a 56-mer variant of ATI26 with 25-nucleotide stems, at rates comparable to those for ATI26 [$(4.2 \pm 1.6) \times 10^{-3}$ min^{-1} vs. $(2.6 \pm 1.0) \times 10^{-3}$ min^{-1}].[212] Consistently higher rates were observed with IB25, so using a hairpin substrate based on IB25 in a KIE study has the potential to eliminate some of the issues that arose with ATI26.

Chapter 6. Conclusions and Future Work

AlkA is a BER enzyme with a uniquely broad specificity, which makes its mechanism an intriguing investigational target. The evidence presented here shows that AlkA interacts non-specifically with the purine moiety and, unlike some of its analogues and homologues, is incapable of binding a free base, regardless of whether DNA is present. AlkA-catalyzed Hx excision is pH-dependent, revealing a pK_a of ≈5.5, which was assigned to the substrate, not the enzyme. This assignment was based on the fact that mutation of candidate residues caused only ≤ 10-fold decreases in rate constants, and binding of a transition state-mimicking pyrrolidine-containing DNA, pyr-DNA, likely mediated by D238, was pH-independent. Buffers were capable of participating in *N*-glycoside hydrolysis, based on the buffer-concentration dependence at pH 7 and 8. SDKIEs confirmed that there is a proton-transfer event, which is rate-limiting at pH ≥ 7. Among the mutants, W272F showed the lowest sensitivity toward a buffer, which suggested that it may be involved in substrate pK_a modulation via aromatic stacking. Its effect on the observed pK_a can be examined by generating pH-rate profiles with the W272F mutant. As well, because intracellular glutamate and glutathione concentrations are high enough to potentially act as proton donors to AlkA, the biological relevance of buffer catalysis can be explored by performing buffer-concentration experiments with these amino acids.

For the transition state analysis of acid-catalyzed dIMP hydrolysis, several KIEs were measured, and, in general, the average 1’-^{3}H and 1’-^{14}C values were reasonable. However, the reproducibility of the measurements was poor despite the fact that the separation method was identical to that used for the transition state analysis of acid-catalyzed dAMP hydrolysis. After trying to control for all other factors that could affect the KIE measurements, the only remaining difference is that Ecoscint A, a biodegradable scintillation fluid, was used in place of Liquiscint, the non-biodegradable fluid used previously. In principle, Ecoscint A should be a better choice, having higher aqueous loading capacity and higher ^{3}H counting efficiency than Liquiscint. However, its higher ^{3}H counting efficiency and lower quenching allow a greater number of low-energy ^{3}H decay events to be detected, which leads to poorer resolution of ^{14}C and ^{3}H counts, possibly leading to higher variability in ^{3}H:^{14}C ratios. A KIE measurement with Liquiscint will be performed to confirm whether this is the cause of the variability.

The presence of two interconvertible substrate forms of ATI26 and slow, incomplete Hx excision relative to longer substrates would suggest that ATI26 is not the ideal substrate for a KIE study; any partitioning of the label by something other than isotopic discrimination by the enzyme will distort the observed KIE.

Because reproducible excision occurs with IB25, a hairpin substrate based on this sequence should be evaluated. If the scintillation fluid is established to contribute to the variability of the KIEs on acid-catalyzed dIMP hydrolysis, then Liquiscint could also be used for AlkA KIE measurements. A re-evaluation of the separation method used during *E. coli* MutY transition state analysis would then be required, since the method-development work presented here was performed because of the switch to a biodegradable scintillation fluid.

Chapter 7. References

(1) Mitchell, J. R.; Hoeijmakers, J. H.; Niedernhofer, L. J. Divide and conquer: nucleotide excision repair battles cancer and ageing. *Curr. Opin. Cell Biol.* **2003**, *15* (2), 232–240.

(2) Breen, A. P.; Murphy, J. A. Reactions of oxyl radicals with DNA. *Free Radical Biol. Med.* **1995**, *18* (6), 1033–1077.

(3) Baier, J.; Maisch, T.; Maier, M.; Engel, E.; Landthaler, M.; Bäumler, W. Singlet Oxygen Generation by UVA Light Exposure of Endogenous Photosensitizers. *Biophys. J.* **2006**, *91* (4), 1452–1459.

(4) Keyer, K.; Gort, A. S.; Imlay, J. A. Superoxide and the Production of Oxidative DNA Damage. *J. Bacteriol.* **1995**, *177* (23), 6782–6790.

(5) Davies, K. J. Oxidative stress: the paradox of aerobic life. *Biochem. Soc. Symp.* **1995**, *61*, 1–31.

(6) Halliwell, B.; Gutteridge, J. M. Oxygen toxicity, oxygen radicals, transition metals and disease. *Biochem. J.* **1984**, *219* (1), 1–14.

(7) Cadet, J.; Douki, T.; Ravanat, J.-L.; Di Mascio, P. Sensitized formation of oxidatively generated damage to cellular DNA by UVA radiation. *Photochem. Photobiol. Sci.* **2009**, *8* (7), 903–911.

(8) Delaney, M. O.; Wiederholt, C. J.; Greenberg, M. M. Fapy•dA Induces Nucleotide Misincorporation Translesionally by a DNA Polymerase. *Angew. Chem., Int. Ed. Engl.* **2002**, *41* (5), 771–773.

(9) Wiederholt, C. J.; Greenberg, M. M. Fapy·dG Instructs Klenow Exo$^-$ to Misincorporate Deoxyadenosine. *J. Am. Chem. Soc.* **2002**, *124* (25), 7278–7279.

(10) Lovell, M. A.; Markesbery, W. R. Oxidative DNA damage in mild cognitive impairment and late-stage Alzheimer's disease. *Nucleic Acids Res.* **2007**, *35* (22), 7497–7504.

(11) Wang, D.; Kreutzer, D. A.; Essigmann, J. M. Mutagenicity and repair of oxidative DNA damage: insights from studies using defined lesions. *Mutat. Res., Fundam. Mol. Mech. Mutagen.* **1998**, *400* (1-2), 99–115.

(12) Mehta, A.; Haber, J. E. Sources of DNA Double-Strand Breaks and Models of Recombinational DNA Repair. *Cold Spring Harbor Perspect. Biol.* **2014**, *6* (9), a016428–a016428.

(13) Cadet, J.; Sage, E.; Douki, T. Ultraviolet radiation-mediated damage to cellular DNA. *Mutat. Res., Fundam. Mol. Mech. Mutagen.* **2005**, *571* (1-2), 3–17.

(14) Chan, G. L.; Doetsch, P. W.; Haseltine, W. A. Cyclobutane Pyrimidine Dimers and (6-4) Photoproducts Block Polymerization by DNA

Polymerase I. *Biochemistry* **1985**, *24* (21), 5723–5728.

(15) Tzu-chien, V. W.; Smith, K. C. Postreplicational formation and repair of DNA double-strand breaks in UV-irradiated *Escherichia coli uvrB* cells. *Mutation Research/DNA Repair Reports* **1986**, *165* (1), 39–44.

(16) Budke, B.; Kuzminov, A. Hypoxanthine Incorporation Is Nonmutagenic in *Escherichia coli*. *J. Bacteriol.* **2006**, *188* (18), 6553–6560.

(17) Caulfield, J. L.; Wishnok, J. S.; Tannenbaum, S. R. Nitric oxide-induced deamination of cytosine and guanine in deoxynucleosides and oligonucleotides. *J. Biol. Chem.* **1998**, *273* (21), 12689–12695.

(18) Lindahl, T.; Nyberg, B. Heat-induced deamination of cytosine residues in deoxyribonucleic acid. *Biochemistry* **1974**, *13* (16), 3405–3410.

(19) Weiss, B. Evidence for Mutagenesis by Nitric Oxide during Nitrate Metabolism in Escherichia coli. *J. Bacteriol.* **2006**, *188* (3), 829–833.

(20) Beranek, D. T. Distribution of methyl and ethyl adducts following alkylation with monofunctional alkylating agents. *Mutat. Res., Fundam. Mol. Mech. Mutagen.* **1990**, *231* (1), 11–30.

(21) Abbott, P. J.; Saffhill, R. DNA synthesis with methylated poly(dC-dG) templates. Evidence for a competitive nature to miscoding by O^6-methylguanine. *Biochim. Biophys. Acta* **1979**, *562* (1), 51–61.

(22) Swann, P. F. Why do O^6-alkylguanine and O^4-alkylthymine miscode? The relationship between the structure of DNA containing O^6-alkylguanine and O^4-alkylthymine and the mutagenic properties of these bases. *Mutat. Res., Fundam. Mol. Mech. Mutagen.* **1990**, *233* (1-2), 81–94.

(23) Shrivastav, N.; Li, D.; Essigmann, J. M. Chemical biology of mutagenesis and DNA repair: cellular responses to DNA alkylation. *Carcinogenesis* **2010**, *31* (1), 59–70.

(24) Fujii, T.; Saito, T.; Nakasaka, T. Purines. XXXIV. 3-Methyladenosine and 3-Methyl-2'-deoxyadenosine. Their Synthesis, Glycosidic Hydrolysis, and Ring Fission. *Chem. Pharm. Bull.* **1989**, *37* (10), 2601–2609.

(25) Zoltewicz, J. A.; Clark, D. F.; Sharpless, T. W. Kinetics and Mechanism of the Acid-Catalyzed Hydrolysis of Some Purine Nucleosides. *J. Am. Chem. Soc.* **1970**, *92* (6), 1741–1750.

(26) Fronza, G.; Gold, B. The Biological Effects of N3-Methyladenine. *J. Cell. Biochem.* **2004**, *91* (2), 250–257.

(27) O'Connor, T. R.; Boiteux, S.; Laval, J. Ring-opened 7-methylguanine residues in DNA are a block to *in vitro* DNA synthesis. *Nucleic Acids Res.* **1988**, *16* (13), 5879–5894.

(28) Saffhill, R.; Abbott, P. J. Formation of O2-methylthymine in poly(dA-dT) on methylation with N-methyl-N-nitrosourea and dimethyl

sulphate. Evidence that O2-methylthymine does not miscode during DNA synthesis. *Nucleic Acids Res.* **1978**, *5* (6), 1971–1978.
(29) Rydberg, B.; Lindahl, T. Nonenzymatic methylation of DNA by the intracellular methyl group donor S-adenosyl-L-methionine is a potentially mutagenic reaction. *EMBO J.* **1982**, *1* (2), 211–216.
(30) Posnick, L. M.; Samson, L. D. Influence of *S*-Adenosylmethionine Pool Size on Spontaneous Mutation, Dam Methylation, and Cell Growth of *Escherichia coli*. *J. Bacteriol.* **1999**, *181* (21), 6756–6762.
(31) Haque, M.; Nadalig, T.; Bringel, F. Fluorescence-Based Bacterial Bioreporter for Specific Detection of Methyl Halide Emissions in the Environment. *Appl. Environ. Microbiol.* **2013**, *79* (21), 6561–6567.
(32) Rippey, J. C. R.; Stallwood, M. I. Nine cases of accidental exposure to dimethyl sulphate - a potential chemical weapon. *Emergency Medicine Journal* **2005**, *22* (12), 878–879.
(33) García-Santos, M. D. P.; Calle, E.; Casado, J. Amino Acid Nitrosation Products as Alkylating Agents. *J. Am. Chem. Soc.* **2001**, *123* (31), 7506–7510.
(34) Calmels, S.; Ohshima, H.; Vincent, P.; Gounot, A. M.; Bartsch, H. Screening of microorganisms for nitrosation catalysis at pH 7 and kinetic studies on nitrosamine formation from secondary amines by *E. coli* strains. *Carcinogenesis* **1985**, *6* (6), 911–915.
(35) Taverna, P.; Sedgwick, B. Generation of an endogenous DNA-methylating agent by nitrosation in *Escherichia coli*. *J. Bacteriol.* **1996**, *178* (17), 5105–5111.
(36) Marnett, L. J. Lipid peroxidation-DNA damage by malondialdehyde. *Mutat. Res., Fundam. Mol. Mech. Mutagen.* **1999**, *424* (1-2), 83–95.
(37) Nair, J.; Barbin, A.; Velic, I.; Bartsch, H. Etheno DNA-base adducts from endogenous reactive species. *Mutat. Res., Fundam. Mol. Mech. Mutagen.* **1999**, *424* (1-2), 59–69.
(38) Dronkert, M.; Kanaar, R. Repair of DNA interstrand cross-links. *Mutat. Res., DNA Repair* **2001**, *486* (4), 217–247.
(39) Cheng, K. C.; Preston, B. D.; Cahill, D. S.; Dosanjh, M. K.; Singer, B.; Loeb, L. A. The vinyl chloride DNA derivative N^2,3-ethenoguanine produces G→A transitions in *Escherichia coli*. *Proc. Natl. Acad. Sci. U. S. A.* **1991**, *88* (22), 9974–9978.
(40) Barbin, A. Etheno-adduct-forming chemicals: from mutagenicity testing to tumor mutation spectra. *Mutat. Res., Rev. Mutat. Res.* **2000**, *462* (2-3), 55–69.
(41) Noll, D. M.; Mason, T. M.; Miller, P. S. Formation and Repair of Interstrand Cross-Links in DNA. *Chem. Rev.* **2006**, *106* (2), 277–301.
(42) Deans, A. J.; West, S. C. DNA interstrand crosslink repair and cancer.

2011, *11* (7), 1–14.

(43) Caulfield, J. L.; Wishnok, J. S.; Tannenbaum, S. R. Nitric Oxide-Induced Interstrand Cross-Links in DNA. *Chem. Res. Toxicol.* **2003**, *16* (5), 571–574.

(44) Wyman, C.; Ristic, D.; Kanaar, R. Homologous recombination-mediated double-strand break repair. *DNA Repair* **2004**, *3* (8-9), 827–833.

(45) Iwasaki, H.; Takahagi, M.; Shiba, T.; Nakata, A.; Shinagawa, H. *Escherichia coli* RuvC protein is an endonuclease that resolves the Holliday structure. *EMBO J.* **1991**, *10* (13), 4381–4389.

(46) Ananthaswamy, H. N.; Eisenstark, A. Repair of Hydrogen Peroxide-Induced Single-Strand Breaks in *Escherichia coli* Deoxyribonucleic Acid. *J. Bacteriol.* **1977**, *130* (1), 187–191.

(47) Lieber, M. R.; Ma, Y.; Pannicke, U.; Schwarz, K. Mechanism and regulation of human non-homologous DNA end-joining. *Nat. Rev. Mol. Cell Biol.* **2003**, *4* (9), 712–720.

(48) Brissett, N. C.; Doherty, A. J. Repairing DNA double-strand breaks by the prokaryotic non-homologous end-joining pathway. *Biochem. Soc. Trans.* **2009**, *37* (Pt 3), 539–545.

(49) van Houten, B. Nucleotide Excision Repair in *Escherichia coli. Microbiol. Rev.* **1990**, *54* (1), 18–51.

(50) Truglio, J. J.; Croteau, D. L.; Van Houten, B.; Kisker, C. Prokaryotic Nucleotide Excision Repair: The UvrABC System. *Chem. Rev.* **2006**, *106* (2), 233–252.

(51) Fuchs, R. P.; Fujii, S. Translesion DNA Synthesis and Mutagenesis in Prokaryotes. *Cold Spring Harbor Perspect. Biol.* **2013**, *5* (12), a012682–a012682.

(52) Berardini, M.; Mackay, W.; Loechler, E. L. Evidence for a Recombination-Independent Pathway for the Repair of DNA Interstrand Cross-Links Based on a Site-Specific Study with Nitrogen Mustard. *Biochemistry* **1997**, *36* (12), 3506–3513.

(53) Noll, D. M.; Webba da Silva, M.; Noronha, A. M.; Wilds, C. J.; Colvin, O. M.; Gamcsik, M. P.; Miller, P. S. Structure, Flexibility, and Repair of Two Different Orientations of the Same Alkyl Interstrand DNA Cross-Link. *Biochemistry* **2005**, *44* (18), 6764–6775.

(54) Grilley, M.; Griffith, J.; Modrich, P. Bidirectional Excision in Methyl-directed Mismatch Repair. *J. Biol. Chem.* **1993**, *268* (16), 11830–11837.

(55) Modrich, P. Mismatch Repair, Genetic Stability, and Cancer. *Science* **1994**, *266* (5193), 1959–1960.

(56) Fox, K. R.; Allinson, S. L.; Sahagun-Krause, H.; Brown, T. Recognition of GT mismatches by Vsr mismatch endonuclease. *Nucleic Acids Res.*

2000, *28* (13), 2535–2540.
(57) Tsutakawa, S. E.; Jingami, H.; Morikawa, K. Recognition of a TG Mismatch: The Crystal Structure of Very Short Patch Repair Endonuclease in Complex with a DNA Duplex. *Cell* **1999**, *99* (6), 615–623.
(58) Dzidic, S.; Radman, M. Genetic requirements for hyper-recombination by very short patch mismatch repair: Involvement of *Escherichia coli* DNA polymerase I. *Mol. Gen. Genet.* **1989**, *217* (2-3), 254–256.
(59) Robertson, A. B.; Matson, S. W. Reconstitution of the Very Short Patch Repair Pathway from *Escherichia coli*. *J. Biol. Chem.* **2012**, *287* (39), 32953–32966.
(60) Zell, R.; Fritz, H. J. DNA mismatch-repair in *Escherichia coli* counteracting the hydrolytic deamination of 5-methyl-cytosine residues. *EMBO J.* **1987**, *6* (6), 1809–1815.
(61) Lieb, M.; Allen, E.; Read, D. Very Short Patch Mismatch Repair in Phage Lambda: Repair Sites and Length of Repair Tracts. *Genetics* **1986**, *114* (4), 1041–1060.
(62) Jones, M.; Wagner, R.; Radman, M. Mismatch Repair and Recombination in *E. coli*. *Cell* **1987**, *50* (4), 621–626.
(63) Kahramanoglou, C.; Prieto, A. I.; Khedkar, S.; Haase, B.; Gupta, A.; Benes, V.; Fraser, G. M.; Luscombe, N. M.; Seshasayee, A. S. N. Genomics of DNA cytosine methylation in *Escherichia coli* reveals its role in stationary phase transcription. *Nat. Commun.* **2012**, *3*, 886–889.
(64) Takahashi, N.; Naito, Y.; Handa, N.; Kobayashi, I. A DNA Methyltransferase Can Protect the Genome from Postdisturbance Attack by a Restriction-Modification Gene Complex. *J. Bacteriol.* **2002**, *184* (22), 6100–6108.
(65) Myles, G. M.; Sancar, A. DNA Repair. *Chem. Res. Toxicol.* **1989**, *2* (4), 197–226.
(66) Taylor, A. F.; Weiss, B. Role of Exonuclease III in the Base Excision Repair of Uracil- Containing DNA. *J. Bacteriol.* **1982**, *151* (1), 351–357.
(67) Larson, K.; Sahm, J.; Shenkar, R.; Strauss, B. Methylation-induced blocks to in vitro DNA replication. *Mutat. Res., Fundam. Mol. Mech. Mutagen.* **1985**, *150* (1-2), 77–84.
(68) Ezaz-Nikpay, K.; Verdine, G. L. The effects of N7-methylguanine on duplex DNA structure. *Chem. Biol. (Oxford, U. K.)* **1994**, *1* (4), 235–240.
(69) Yu, S. L.; Lee, S. K.; Johnson, R. E.; Prakash, L.; Prakash, S. The Stalling of Transcription at Abasic Sites Is Highly Mutagenic. *Mol. Cell. Biol.* **2003**, *23* (1), 382–388.

(70) Ljungquist, S.; Lindahl, T.; Howard-Flanders, P. Methyl Methane Sulfonate-Sensitive Mutant of *Escherichia coli* Deficient in an Endonuclease Specific for Apurinic Sites in Deoxyribonucleic Acid. *J. Bacteriol.* **1976**, *126* (2), 646–653.

(71) Weiss, B.; Rogers, S. G.; Taylor, A. F. The endonuclease activity of exonuclease III and the repair of uracil-containing DNA in *Escherichia coli*. In *DNA Repair Mechanisms*; Fox, C. F., Friedberg, E. C., Hanawalt, P. C., Eds.; Academic Press New York, 1978; Vol. 9, pp 191–194.

(72) Franklin, W. A.; Lindahl, T. DNA deoxyribophosphodiesterase. *EMBO J.* **1988**, *7* (11), 3617–3622.

(73) Boiteux, S.; Gajewski, E.; Laval, J.; Dizdaroglu, M. Substrate Specificity of the *Escherichia coli* Fpg Protein (Formamidopyrimidine-DNA Glycosylase): Excision of Purine Lesions in DNA Produced by Ionizing Radiation or Photosensitization. *Biochemistry* **1992**, *31* (1), 106–110.

(74) Golan, G.; Zharkov, D. O.; Feinberg, H.; Fernandes, A. S.; Zaika, E. I.; Kycia, J. H.; Grollman, A. P.; Shoham, G. Structure of the uncomplexed DNA repair enzyme endonuclease VIII indicates significant interdomain flexibility. *Nucleic Acids Res.* **2005**, *33* (15), 5006–5016.

(75) Doetsch, P. W.; Cunningham, R. P. The enzymology of apurinic/apyrimidinic endonucleases. *Mutat. Res., Fundam. Mol. Mech. Mutagen.* **1990**, *236* (2-3), 173–201.

(76) Berti, P. J.; McCann, J. A. B. Toward a detailed understanding of base excision repair enzymes: transition state and mechanistic analyses of N-glycoside hydrolysis and N-glycoside transfer. *Chem. Rev.* **2006**, *106* (2), 506–555.

(77) Berti, P. J.; Blanke, S. R.; Schramm, V. L. Transition State Structure for the Hydrolysis of NAD$^+$ Catalyzed by Diphtheria Toxin. *J. Am. Chem. Soc.* **1997**, *119* (50), 12079–12088.

(78) Rising, K. A.; Schramm, V. L. Transition State Analysis of NAD$^+$ Hydrolysis by the Cholera Toxin Catalytic Subunit. *J. Am. Chem. Soc.* **1997**, *119* (1), 27–37.

(79) Scheuring, J.; Schramm, V. L. Kinetic Isotope Effect Characterization of the Transition State for Oxidized Nicotinamide Adenine Dinucleotide Hydrolysis by Pertussis Toxin. *Biochemistry* **1997**, *36* (15), 4526–4534.

(80) Chen, X.-Y.; Berti, P. J.; Schramm, V. L. Ricin A-Chain: Kinetic Isotope Effects and Transition State Structure with Stem-Loop RNA. *J. Am. Chem. Soc.* **2000**, *122* (8), 1609–1617.

(81) Ho, M.-C.; Sturm, M. B.; Almo, S. C.; Schramm, V. L. Transition state analogues in structures of ricin and saporin ribosome-inactivating

proteins. *Proc. Natl. Acad. Sci. U. S. A.* **2009**, *106* (48), 20276–20281.

(82) Berti, P. J.; Schramm, V. L. Transition State Structure of the Solvolytic Hydrolysis of NAD. *J. Am. Chem. Soc.* **1997**, *119* (50), 12069–12078.

(83) Mentch, F.; Parkin, D. W.; Schramm, V. L. Transition-State Structures for *N*-Glycoside Hydrolysis of AMP by Acid and by AMP Nucleosidase in the Presence and Absence of Allosteric Activator. *Biochemistry* **1987**, *26* (3), 921–930.

(84) Zoltewicz, J. A.; Clark, D. F.; Sharpless, T. W.; Grahe, G. Kinetics and mechanism of the acid-catalyzed hydrolysis of some purine nucleosides. *J. Am. Chem. Soc.* **1970**, *92* (6), 1741–1750.

(85) Garrett, E. R.; Mehta, P. J. Solvolysis of Adenine Nucleosides. I. Effects of Sugars and Adenine Substituents on Acid Solvolyses. *J. Am. Chem. Soc.* **1972**, *94* (24), 8542–8547.

(86) Hevesi, L.; Wolfson-Davidson, E.; Nagy, J. B.; Nagy, O. B.; Bruylants, A. Contribution to the Mechanism of the Acid-Catalyzed Hydrolysis of Purine Nucleosides. *J. Am. Chem. Soc.* **1972**, *94* (13), 4715–4720.

(87) Anslyn, E. V.; Dougherty, D. A. *Modern Physical Organic Chemistry*; University Science, 2005.

(88) Capon, B.; Connett, B. E. 832. The Mechanism of the Hydrolysis of *N*-Aryl-D-glucosylamines. *J. Chem. Soc.* **1965**, 4497–6.

(89) Zoltewicz, J. A.; Clark, D. F. Kinetics and Mechanism of the Hydrolysis of Guanosine and 7-Methylguanosine Nucleosides in Perchloric Acid. *J. Org. Chem.* **1972**, *37* (8), 1193–1197.

(90) Tsuboi, M.; Kyogoku, Y.; Shimanouchi, T. Infrared absorption spectra of protonated and deprotonated nucleosides. *Biochim. Biophys. Acta* **1962**, *55* (1-2), 1–12.

(91) Broomhead, J. M. The Structures of Pyrimidines and Purines. IV. The Crystal Structure of Guanine Hydrochloride and its Relation to that of Adenine Hydrochloride. *Acta Crystallogr.* **1951**, *4* (2), 92–100.

(92) Sigel, H.; Massoud, S. S.; Corfù, N. A. Comparison of the Extent of Macrochelate Formation in Complexes of Divalent Metal Ions with Guanosine (GMP^{2-}), Inosine (IMP^{2-}), and Adenosine 5'-Monophosphate (AMP^{2-}). The Crucial Role of N-7 Basicity in Metal Ion-Nucleic Base Recognition. *J. Am. Chem. Soc.* **1994**, *116* (7), 2958–2971.

(93) Kampf, G.; Kapinos, L. E.; Griesser, R.; Lippert, B.; Sigel, H. Comparison of the acid-base properties of purine derivatives in aqueous solution. Determination of intrinsic proton affinities of various basic sites. *J. Chem. Soc., Perkin Trans. 2* **2002**, *7*, 1320–1327.

(94) Werner, R. M.; Stivers, J. T. Kinetic Isotope Effect Studies of the Reaction Catalyzed by Uracil DNA Glycosylase: Evidence for an Oxocarbenium Ion-Uracil Anion Intermediate. *Biochemistry* **2000**.

(95) Singh, V.; Schramm, V. L. Transition-State Analysis of *S. pneumoniae* 5'-Methylthioadenosine Nucleosidase. *J. Am. Chem. Soc.* **2007**, *129* (10), 2783–2795.

(96) Singh, V.; Schramm, V. L. Transition-State Structure of Human 5′-Methylthioadenosine Phosphorylase. *J. Am. Chem. Soc.* **2006**, *128* (45), 14691–14696.

(97) Gopaul, D. N.; Meyer, S. L.; Degano, M.; Sacchettini, J. C.; Schramm, V. L. Inosine-Uridine Nucleoside Hydrolase from *Crithidia fasciculata*. Genetic Characterization, Crystallization, and Identification of Histidine 241 as a Catalytic Site Residue. *Biochemistry* **1996**, *35* (19), 5963–5970.

(98) Parkin, D. W.; Schramm, V. L. Binding Modes for Substrate and a Proposed Transition-State Analogue of Protozoan Nucleoside Hydrolase. *Biochemistry* **1995**.

(99) Landini, P.; Volkert, M. R. Regulatory Responses of the Adaptive Response to Alkylation Damage: a Simple Regulon with Complex Regulatory Features. *J. Bacteriol.* **2000**, *182* (23), 6543–6549.

(100) Koivisto, P.; Duncan, T.; Lindahl, T.; Sedgwick, B. Minimal Methylated Substrate and Extended Substrate Range of *Escherichia coli* AlkB Protein, a 1-Methyladenine-DNA Dioxygenase. *J. Biol. Chem.* **2003**, *278* (45), 44348–44354.

(101) Duncan, T.; Trewick, S. C.; Koivisto, P.; Bates, P. A.; Lindahl, T.; Sedgwick, B. Reversal of DNA alkylation damage by two human dioxygenases. *Proc. Natl. Acad. Sci. U. S. A.* **2002**, *99* (26), 16660–16665.

(102) Trewick, S. C.; Henshaw, T. F.; Hausinger, R. P.; Lindahl, T. Oxidative demethylation by *Escherichia coli* AlkB directly reverts DNA base damage. *Nature* **2002**.

(103) Rippa, V.; Amoresano, A.; Esposito, C.; Landini, P.; Volkert, M.; Duilio, A. Specific DNA Binding and Regulation of Its Own Expression by the AidB Protein in *Escherichia coli*. *J. Bacteriol.* **2010**, *192* (23), 6136–6142.

(104) Mulrooney, S. B.; Howard, M. J.; Hausinger, R. P. The *Escherichia coli* alkylation response protein AidB is a redox partner of flavodoxin and binds RNA and acyl carrier protein. *Arch. Biochem. Biophys.* **2011**, *513* (2), 81–86.

(105) Landini, P.; Hajec, L. I.; Volkert, M. R. Structure and Transcriptional Regulation of the *Escherichia coli* Adaptive Response Gene *aidB*. *J. Bacteriol.* **1994**, *176* (21), 6583–6589.

(106) Sedgwick, B. Repairing DNA-methylation damage. *Nat. Rev. Mol. Cell Biol.* **2004**, *5* (2), 148–157.

(107) Kondo, H.; Nakabeppu, Y.; Kataoka, H.; Kuhara, S.; Kawabata, S.; Sekiguchi, M. Structure and Expression of the *alkB* Gene of *Escherichia coli* Related to the Repair of Alkylated DNA. *J. Biol. Chem.* **1986**, *261* (33), 15772–15777.

(108) Nakabeppu, Y.; Sekiguchi, M. Regulatory mechanisms for induction of synthesis of repair enzymes in response to alkylating agents: Ada protein acts as a transcriptional regulator. *Proc. Natl. Acad. Sci. U. S. A.* **1986**, *83* (17), 6297–6301.

(109) Teo, I.; Sedgwick, B.; Kilpatrick, M. W.; McCarthy, T. V.; Lindahl, T. The Intracellular Signal for Induction of Resistance to Alkylating Agents in *E. coli*. *Cell* **1986**, *45* (2), 315–324.

(110) Saget, B. M.; Walker, G. C. The Ada protein acts as both a positive and a negative modulator of *Escherichia coli*'s response to methylating agents. *Proc. Natl. Acad. Sci. U. S. A.* **1994**, *91* (21), 9730–9734.

(111) Hollis, T.; Ichikawa, Y.; Ellenberger, T. DNA bending and a flip-out mechanism for base excision by the helix-hairpin-helix DNA glycosylase, *Escherichia coli* AlkA. *EMBO J.* **2000**, *19* (4), 758–766.

(112) Shao, X.; Grishin, N. V. Common fold in helix-hairpin-helix proteins. *Nucleic Acids Res.* **2000**, *28* (14), 2643–2650.

(113) Fersht, A. *Structure and Mechanism in Protein Science*; W. H. Freeman and Company: New York.

(114) Cornish-Bowden, A. *Fundamentals of Enzyme Kinetics*, 4 ed.; John Wiley & Sons, 2012.

(115) O'Brien, P. J.; Ellenberger, T. Dissecting the broad substrate specificity of human 3-methyladenine-DNA glycosylase. *J. Biol. Chem.* **2004**, *279* (11), 9750–9757.

(116) Cleland, W. W. Partition Analysis and the Concept of Net Rate Constants as Tools in Enzyme Kinetics. *Biochemistry* **1975**, *14* (14), 3220–3224.

(117) Schermerhorn, K. M.; Delaney, S. A Chemical and Kinetic Perspective on Base Excision Repair of DNA. *Acc. Chem. Res.* **2014**, *47* (4), 1238–1246.

(118) O'Brien, P. J.; Ellenberger, T. The *Escherichia coli* 3-Methyladenine DNA Glycosylase AlkA Has a Remarkably Versatile Active Site. *J. Biol. Chem.* **2004**, *279* (26), 26876–26884.

(119) Saparbaev, M.; Laval, J. Excision of hypoxanthine from DNA containing dIMP residues by the *Escherichia coli*, yeast, rat, and human alkylpurine DNA glycosylases. *Proc. Natl. Acad. Sci. U. S. A.* **1994**, *91* (13), 5873–5877.

(120) Laval, J. Two enzymes are required from strand incision in repair of alkylated DNA. *Nature* **1977**, *269* (5631), 829–832.

(121) Karran, P.; Hjelmgren, T.; Lindahl, T. Induction of a DNA glycosylase for *N*-methylated purines is part of the adaptive response to alkylating agents. *Nature* **1982**, *296* (5859), 770–773.

(122) Bjelland, S.; Bjørås, M.; Seeberg, E. Excision of 3-methylguanine from alkylated DNA by 3-methyladenine DNA glycosylase I of *Escherichia coli*. *Nucleic Acids Res.* **1993**, *21* (9), 2045–2049.

(123) Masaoka, A.; Terato, H.; Kobayashi, M.; Honsho, A.; Ohyama, Y.; Ide, H. Enzymatic Repair of 5-Formyluracil. *J. Biol. Chem.* **1999**, *274* (35), 25136–25143.

(124) Habraken, Y.; Carter, C. A.; Kirk, M. C.; Ludlum, D. B. Release of 7-Alkylguanines from *N*-(2-Chloroethyl)-*N'*-cyclohexyl-*N*-nitrosourea-modified DNA by 3-Methyladenine DNA Glycosylase II. *Cancer Res.* **1991**, *51* (2), 499–503.

(125) Matijasevic, Z.; Stering, A.; Niu, T.-Q.; Austin-Ritchie, P.; Ludlum, D. B. Release of sulfur mustard-modified DNA bases by *Escherichia coli* 3-methyladenine DNA glycosylase II. *Carcinogenesis* **1996**, *17* (10), 2249–2252.

(126) Habraken, Y.; Ludlum, D. B. Release of chloroethyl ethyl sulfide-modified DNA bases by bacterial 3-methyladenine-DNA glycosylases I and II. *Carcinogenesis* **1989**, *10* (3), 489–492.

(127) Saparbaev, M.; Kleibl, K.; Laval, J. *Escherichia coli*, *Saccharomyces cerevisiae*, rat and human 3-methyladenine DNA glycosylases repair 1,N^6-ethenoadenine when present in DNA. *Nucleic Acids Res.* **1995**, *23* (18), 3750–3755.

(128) Matijasevic, Z.; Sekiguchi, M.; Ludlum, D. B. Release of N^2,3-ethenoguanine from chloroacetaldehyde-treated DNA by *Escherichia coli* 3-methyladenine DNA glycosylase II. *Proc. Natl. Acad. Sci. U. S. A.* **1992**, *89* (19), 9331–9334.

(129) Guliaev, A. B.; Singer, B.; Hang, B. Chloroethylnitrosourea-derived ethano cytosine and adenine adducts are substrates for *Escherichia coli* glycosylases excising analogous etheno adducts. *DNA Repair* **2004**, *3* (10), 1311–1321.

(130) Habraken, Y.; Carter, C. A.; Sekiguchi, M.; Ludlum, D. B. Release of N^2,3-ethanoguanine from haloethylnitrosourea-treated DNA by *Escherichia coli* 3-methyladenine DNA glycosylase II. *Carcinogenesis* **1991**, *12* (10), 1971–1973.

(131) Terato, H.; Masaoka, A.; Asagoshi, K.; Honsho, A.; Ohyama, Y.; Suzuki, T.; Yamada, M.; Makino, K.; Yamamoto, K.; Ide, H. Novel repair activities of AlkA (3-methyladenine DNA glycosylase II) and endonuclease VIII for xanthine and oxanine, guanine lesions induced by nitric oxide and nitrous acid. *Nucleic Acids Res.* **2002**, *30* (22), 4975–

4984.

(132) McCarthy, T. V.; Karran, P.; Lindahl, T. Inducible repair of O-alkylated DNA pyrimidines in *Escherichia coli*. *EMBO J.* **1984**, *3* (3), 545–550.

(133) Privezentzev, C. V.; Saparbaev, M.; Sambandam, A.; Greenberg, M. M.; Laval, J. AlkA Protein Is the Third *Escherichia coli* DNA Repair Protein Excising a Ring Fragmentation Product of Thymine. *Biochemistry* **2000**, *39* (46), 14263–14268.

(134) Berdal, K. G.; Johansen, R. F.; Seeberg, E. Release of normal bases from intact DNA by a native DNA repair enzyme. *EMBO J.* **1998**, *17* (2), 363–367.

(135) Admiraal, S. J.; O'Brien, P. J. DNA-*N*-Glycosylases Process Novel *O*-Glycosidic Sites in DNA. *Biochemistry* **2013**, *52* (23), 4066–4074.

(136) Labahn, J.; Schärer, O. D.; Long, A.; Ezaz-Nikpay, K.; Verdine, G. L.; Ellenberger, T. E. Structural Basis for the Excision Repair of Alkylation-Damaged DNA. *Cell* **1996**, *86* (2), 321–329.

(137) Schärer, O. D.; Ortholand, J.-Y.; Ganesan, A.; Ezaz-Nikpay, K.; Verdine, G. L. Specific binding of the DNA repair enzyme AlkA to a pyrrolidine-based inhibitor. *J. Am. Chem. Soc.* **1995**, *117* (24), 6623–6624.

(138) Berti, P. J.; Tanaka, K. S. Transition State Analysis Using Multiple Kinetic Isotope Effects: Mechanisms of Enzymatic and Non-enzymatic Glycoside Hydrolysis and Transfer. *Adv. Phys. Org. Chem.* **2002**, *37*, 239–314.

(139) Berti, P. J. Determining Transition States from Kinetic Isotope Effects. *Methods Enzymol.* **1999**, *308*, 355–397.

(140) Whittaker, V. P.; Adams, D. H. A Method for Determining the Ratio of the Michaelis Constants of an Enzyme with Respect to Two Substrates. *Nature* **1949**, *164*, 315–316.

(141) McCann, J. A. B.; Berti, P. J. Transition-State Analysis of the DNA Repair Enzyme MutY. *J. Am. Chem. Soc.* **2008**, *130* (17), 5789–5797.

(142) Schramm, V. L. Enzymatic transition states and transition state analog design. *Annu. Rev. Biochem.* **1998**, *67* (1), 693–720.

(143) Miles, R. W.; Tyler, P. C.; Furneaux, R. H.; Bagdassarian, C. K.; Schramm, V. L. One-Third-the-Sites Transition-State Inhibitors for Purine Nucleoside Phosphorylase. *Biochemistry* **1998**, *37* (24), 8615–8621.

(144) Kline, P. C.; Schramm, V. L. Purine Nucleoside Phosphorylase. Catalytic Mechanism and Transition-State Analysis of the Arsenolysis Reaction. *Biochemistry* **1993**, *32* (48), 13212–13219.

(145) Sauve, A. A.; Cahill, S. M.; Zech, S. G.; Basso, L. A.; Lewandowicz, A.; Santos, D. S.; Grubmeyer, C.; Evans, G. B.; Furneaux, R. H.; Tyler,

P. C.; et al. Ionic States of Substrates and Transition State Analogues at the Catalytic Sites of *N*-Ribosyltransferases. *Biochemistry* **2003**, *42* (19), 5694–5705.

(146) Kicska, G. A.; Long, L.; Hörig, H.; Fairchild, C.; Tyler, P. C.; Furneaux, R. H.; Schramm, V. L.; Kaufman, H. L. Immucillin H, a powerful transition-state analog inhibitor of purine nucleoside phosphorylase, selectively inhibits human T lymphocytes. *Proc. Natl. Acad. Sci. U. S. A.* **2001**, *98* (8), 4593–4598.

(147) Shi, W.; Ting, L. M.; Kicska, G. A.; Lewandowicz, A.; Tyler, P. C.; Evans, G. B.; Furneaux, R. H.; Kim, K.; Almo, S. C.; Schramm, V. L. *Plasmodium falciparum* Purine Nucleoside Phosphorylase: CRYSTAL STRUCTURES, IMMUCILLIN INHIBITORS, AND DUAL CATALYTIC FUNCTION. *J. Biol. Chem.* **2004**, *279* (18), 18103–18106.

(148) Thomas, K.; Haapalainen, A. M.; Burgos, E. S.; Evans, G. B.; Tyler, P. C.; Gulab, S.; Guan, R.; Schramm, V. L. Femtomolar Inhibitors Bind to 5′-Methylthioadenosine Nucleosidases with Favorable Enthalpy and Entropy. *Biochemistry* **2012**, *51* (38), 7541–7550.

(149) Tu, C. K.; Paranawithana, S. R.; Jewell, D. A.; Tanhauser, S. M.; LoGrasso, P. V.; Wynns, G. C.; Laipis, P. J.; Silverman, D. N. Buffer Enhancement of Proton Transfer in Catalysis by Human Carbonic Anhydrase III. *Biochemistry* **1990**, *29* (27), 6400–6405.

(150) Jiang, Y. L.; Ichikawa, Y.; Stivers, J. T. Inhibition of Uracil DNA Glycosylase by an Oxacarbenium Ion Mimic. *Biochemistry* **2002**, *41* (22), 7116–7124.

(151) Schowen, R. L. Mechanistic Deductions from Solvent Isotope Effects. *Prog. Phys. Org. Chem.* **1972**, *9*, 275–332.

(152) McCann, J. A. B. Mechanisms of *N*-Glycoside Hydrolysis, McMaster University, 2006.

(153) Pace, C. N.; Vajdos, F.; Fee, L.; Grimsley, G.; Gray, T. How to measure and predict the molar absorption coefficient of a protein. *Protein Sci.* **1995**, *4* (11), 2411–2423.

(154) Tataurov, A. V.; You, Y.; Owczarzy, R. Predicting ultraviolet spectrum of single stranded and double stranded deoxyribonucleic acids. *Biophys. Chem.* **2008**, *133* (1-3), 66–70.

(155) Beynon, R. J.; Easterby, J. S. *Buffer Solutions: The Basics*; BIOS Scientific Publishers, 1996.

(156) Thomas, L.; Yang, C. H.; Goldthwait, D. A. Two DNA Glycosylases in *Escherichia coli* Which Release Primarily 3-Methyladenine. *Biochemistry* **1982**, *21* (6), 1162–1169.

(157) Tu, C.; Silverman, D. N.; Forsman, C.; Jonsson, B. H. Role of Histidine

64 in the Catalytic Mechanism of Human Carbonic Anhydrase II Studied with a Site-Specific Mutant. *Biochemistry* **1989**, *28* (19), 7913–7918.

(158) Goldberg, J. M.; Kirsch, J. F. The Reaction Catalyzed by *Escherichia coli* Aspartate Aminotransferase Has Multiple Partially Rate-Determining Steps, While That Catalyzed by the Y225F Mutant Is Dominated by Ketimine Hydrolysis. *Biochemistry* **1996**, *35* (16), 5280–5291.

(159) Toney, M. D.; Kirsch, J. F. Direct Brønsted Analysis of the Restoration of Activity to a Mutant Enzyme by Exogenous Amines. *Science* **1989**, *243* (4897), 1485–1488.

(160) Go, M. K.; Amyes, T. L.; Richard, J. P. Rescue of K12G Triosephosphate Isomerase by Ammonium Cations: The Reaction of an Enzyme in Pieces. *J. Am. Chem. Soc.* **2010**, *132* (38), 13525–13532.

(161) Eliot, A. C.; Kirsch, J. F. Pyridoxal Phosphate Enzymes: Mechanistic, Structural, and Evolutionary Considerations. *Annu. Rev. Biochem.* **2004**, *73*, 383–415.

(162) Roday, S.; Amukele, T.; Evans, G. B.; Tyler, P. C.; Furneaux, R. H.; Schramm, V. L. Inhibition of Ricin A-Chain with Pyrrolidine Mimics of the Oxacarbenium Ion Transition State. *Biochemistry* **2004**, *43* (17), 4923–4933.

(163) Schärer, O. D.; Nash, H. M.; Jiricny, J.; Laval, J.; Verdine, G. L. Specific Binding of a Designed Pyrrolidine Abasic Site Analog to Multiple DNA Glycosylases. *J. Biol. Chem.* **1998**, *273* (15), 8592–8597.

(164) Schowen, K. B.; Schowen, R. L. Solvent Isotope Effects of Enzyme Systems. *Methods Enzymol.* **1981**, *87*, 551–606.

(165) O'Brien, P. J.; Ellenberger, T. Human Alkyladenine DNA Glycosylase Uses Acid-Base Catalysis for Selective Excision of Damaged Purines. *Biochemistry* **2003**, *42* (42), 12418–12429.

(166) Dawson, R. M. C. *Data for Biochemical Research*; Oxford University Press, 1989.

(167) Keenholtz, R. A.; Mouw, K. W.; Boocock, M. R.; Li, N.-S.; Piccirilli, J. A.; Rice, P. A. Arginine as a General Acid Catalyst in Serine Recombinase-mediated DNA Cleavage. *J. Biol. Chem.* **2013**, *288* (40), 29206–29214.

(168) Balón, M.; Carmona, M. C.; Muñoz, M. A.; Hidalgo, J. The Acid-Base Properties of Pyrrole and Its Benzologs Indole and Carbazole - a Reexamination From the Excess Acidity Method. *Tetrahedron* **1989**, *45* (23), 7501–7504.

(169) Hu, W.; Cross, T. A. Tryptophan Hydrogen Bonding and Electric Dipole Moments: Functional Roles in the Gramicidin Channel and

Implications for Membrane Proteins. *Biochemistry* **1995**, *34* (43), 14147–14155.

(170) McCann, J. A. B.; Berti, P. J. Transition State Analysis of Acid-Catalyzed dAMP Hydrolysis. *J. Am. Chem. Soc.* **2007**, *129* (22), 7055–7064.

(171) Horenstein, B. A.; Parkin, D. W.; Estupiñán, B.; Schramm, V. L. Transition-State Analysis of Nucleoside Hydrolase from *Crithidia fasciculata*. *Biochemistry* **1991**, *30* (44), 10788–10795.

(172) Singh, V.; Luo, M.; Brown, R. L.; Norris, G. E.; Schramm, V. L. Transition-State Structure of *Neisseria meningitides* 5′-Methylthioadenosine/*S*-Adenosylhomocysteine Nucleosidase. *J. Am. Chem. Soc.* **2007**, *129* (45), 13831.

(173) Singh, V.; Lee, J. E.; Núñez, S.; Howell, P. L.; Schramm, V. L. Transition State Structure of 5‘-Methylthioadenosine/*S*-Adenosylhomocysteine Nucleosidase from *Escherichia coli* and Its Similarity to Transition State Analogues. *Biochemistry* **2005**, *44* (35), 11647–11659.

(174) Lee, J. E.; Singh, V.; Evans, G. B.; Tyler, P. C.; Furneaux, R. H.; Cornell, K. A.; Riscoe, M. K.; Schramm, V. L.; Howell, P. L. Structural Rationale for the Affinity of Pico- and Femtomolar Transition State Analogues of *Escherichia coli* 5 -Methylthioadenosine/*S*-Adenosylhomocysteine Nucleosidase. *J. Biol. Chem.* **2005**, *280* (18), 18274–18282.

(175) Drohat, A. C.; Stivers, J. T. *Escherichia coli* Uracil DNA Glycosylase: NMR Characterization of the Short Hydrogen Bond from His187 to Uracil O2. *Biochemistry* **2000**, *39* (39), 11865–11875.

(176) Loverix, S.; Geerlings, P.; McNaughton, M.; Augustyns, K.; Vandemeulebroucke, A.; Steyaert, J.; Versées, W. Substrate-assisted Leaving Group Activation in Enzyme-catalyzed *N*-Glycosidic Bond Cleavage. *J. Biol. Chem.* **2005**, *280* (15), 14799–14802.

(177) Desiraju, G. R. The C-H•••O Hydrogen Bond: Structural Implications and Supramolecular Design. *Acc. Chem. Res.* **1996**, *29* (9), 441–449.

(178) Scheiner, S.; Kar, T.; Gu, Y. Strength of the $C^{\alpha}H$••O Hydrogen Bond of Amino Acid Residues. *J. Biol. Chem.* **2001**, *276* (13), 9832–9837.

(179) Scheiner, S.; Kar, T.; Pattanayak, J. Comparison of Various Types of Hydrogen Bonds Involving Aromatic Amino Acids. *J. Am. Chem. Soc.* **2002**, *124* (44), 13257–13264.

(180) Kaneda, T.; Tanaka, J. The Crystal Structure of the Intermolecular Complex between 9-Ethyladenine and Indole. *Bull. Chem. Soc. Jpn.* **1976**, *49* (7), 1799–1804.

(181) Ishida, T.; Shibata, M.; Fujii, K.; Inoue, M. Inter- and Intramolecular

Stacking Interaction between Indole and Adeninium Rings. *Biochemistry* **1983**, *22* (15), 3571–3581.

(182) Versées, W.; Loverix, S.; Vandemeulebroucke, A.; Geerlings, P.; Steyaert, J. Leaving Group Activation by Aromatic Stacking: An Alternative to General Acid Catalysis. *J. Mol. Biol.* **2004**, *338* (1), 1–6.

(183) Versées, W.; Decanniere, K.; Pellé, R.; Depoorter, J.; Brosens, E.; Parkin, D. W.; Steyaert, J. Structure and Function of a Novel Purine Specific Nucleoside Hydrolase from *Trypanosoma vivax*. *J. Mol. Biol.* **2001**, *307* (5), 1363–1379.

(184) Vandemeulebroucke, A.; Versées, W.; Steyaert, J.; Barlow, J. N. Multiple Transients in the Pre-Steady-State of Nucleoside Hydrolase Reveal Complex Substrate Binding, Product Base Release, and Two Apparent Rates of Chemistry. *Biochemistry* **2006**, *45* (30), 9307–9318.

(185) Slonczewski, J. L.; Rosen, B. P.; Alger, J. R.; Macnab, R. M. pH homeostasis in *Escherichia coli*: Measurement by ^{31}P nuclear magnetic resonance of methylphosphonate and phosphate. *Proc. Natl. Acad. Sci. U. S. A.* **1981**, *78* (10), 6271–6275.

(186) Ugurbil, K.; Rottenberg, H.; Glynn, P.; Shulman, R. G. ^{31}P nuclear magnetic resonance studies of bioenergetics and glycolysis in anaerobic *Escherichia coli* cells. *Proc. Natl. Acad. Sci. U. S. A.* **1978**, *75* (5), 2244–2248.

(187) Neidhardt, F. C.; Curtiss, R. *Escherichia coli and Salmonella: Cellular and Molecular Biology*, 2nd ed.; ASM Press: Washington, D.C., 1996.

(188) Nelson, D. L.; Lehninger, A. L.; Cox, M. M. *Principles of Biochemistry*, 2nd ed.; Worth Publishers: New York, 1993.

(189) Bennett, B. D.; Kimball, E. H.; Gao, M.; Osterhout, R.; Van Dien, S. J.; Rabinowitz, J. D. Absolute metabolite concentrations and implied enzyme active site occupancy in *Escherichia coli*. *Nat. Chem. Biol.* **2009**, *5* (8), 593–599.

(190) Morohoshi, F.; Hayashi, K.; Munkata, N. *Bacillus subtilis alkA* Gene Encoding Inducible 3-Methyladenine DNA Glycosylase Is Adjacent to the *ada* Operon. *J. Bacteriol.* **1993**, *175* (18), 6010–6017.

(191) Memisoglu, A.; Samson, L. Cloning and characterization of a cDNA encoding a 3-methyladenine DNA glycosylase from the fission yeast *Schizosaccharomyces pombe*. *Gene* **1996**, *177* (1-2), 229–235.

(192) Chen, J.; Derfler, B.; Samson, L. *Saccharomyces cerevisiae* 3-methyladenine DNA glycosylase has homology to the AlkA glycosylase of *E. coli* and is induced in response to DNA alkylation damage. *EMBO J.* **1990**, *9* (13), 4569–4575.

(193) Lingaraju, G. M.; Davis, C. A.; Setser, J. W.; Samson, L. D.; Drennan, C. L. Structural Basis for the Inhibition of Human Alkyladenine DNA

Glycosylase (AAG) by 3,N^4-Ethenocytosine-containing DNA. *J. Biol. Chem.* **2011**, *286* (15), 13205–13213.
(194) Adhikary, S.; Eichman, B. F. Analysis of substrate specificity of *Schizosaccharomyces pombe* Mag1 alkylpurine DNA glycosylase. *EMBO Rep.* **2011**, *12* (12), 1286–1292.
(195) Wyatt, M. D.; Allan, J. M.; Lau, A. Y.; Ellenberger, T. E.; Samson, L. D. 3-Methyladenine DNA glycosylases: structure, function, and biological importance. *Bioessays* **1999**, *21* (8), 668–676.
(196) Drohat, A. C.; Kwon, K.; Krosky, D. J.; Stivers, J. T. 3-methyladenine DNA glycosylase I is an unexpected helix-hairpin-helix superfamily member. *Nat. Struct. Mol. Biol.* **2002**, *9* (9), 659–664.
(197) Lau, A. Y.; Wyatt, M. D.; Glassner, B. J.; Samson, L. D.; Ellenberger, T. Molecular basis for discriminating between normal and damaged bases by the human alkyladenine glycosylase, AAG. *Proc. Natl. Acad. Sci. U. S. A.* **2000**, *97* (25), 13573–13578.
(198) Evans, G. B.; Furneaux, R. H.; Lewandowicz, A.; Schramm, V. L.; Tyler, P. C. Synthesis of Second-Generation Transition State Analogues of Human Purine Nucleoside Phosphorylase. *J. Med. Chem.* **2003**, *46* (24), 5271–5276.
(199) Lou, M.; Gilpin, M. E.; Burger, S. K.; Malik, A. M.; Gawuga, V.; Popović, V.; Capretta, A.; Berti, P. J. Transition State Analysis of Acid-Catalyzed Hydrolysis of an Enol Ether, Enolpyruvylshikimate 3-Phosphate (EPSP). *J. Am. Chem. Soc.* **2012**, *134* (31), 12947–12957.
(200) Lou, M.; Burger, S. K.; Gilpin, M. E.; Gawuga, V.; Capretta, A.; Berti, P. J. Transition State Analysis of Enolpyruvylshikimate 3-Phosphate (EPSP) Synthase (AroA)-Catalyzed EPSP Hydrolysis. *J. Am. Chem. Soc.* **2012**, *134* (31), 12958–12969.
(201) Horrocks, D. L. *Applications of Liquid Scintillation Counting*; Academic Press Inc, 1974.
(202) Horrocks, D. A new method of quench monitoring in liquid scintillation counting: the H number concept. *Journal of Radioanalytical and Nuclear Chemistry* **1978**, *43* (2), 489–521.
(203) Lewandowicz, A.; Schramm, V. L. Transition State Analysis for Human and *Plasmodium falciparum* Purine Nucleoside Phosphorylases. *Biochemistry* **2004**, *43* (6), 1458–1468.
(204) Birck, M. R.; Schramm, V. L. Nucleophilic Participation in the Transition State for Human Thymidine Phosphorylase. *J. Am. Chem. Soc.* **2004**, *126* (8), 2447–2453.
(205) Schwartz, P. A.; Vetticatt, M. J.; Schramm, V. L. Transition State Analysis of Thymidine Hydrolysis by Human Thymidine Phosphorylase. *J. Am. Chem. Soc.* **2010**, *132* (38), 13425–13433.

(206) Silva, R. G.; Vetticatt, M. J.; Merino, E. F.; Cassera, M. B.; Schramm, V. L. Transition-State Analysis of *Trypanosoma cruzi* Uridine Phosphorylase-Catalyzed Arsenolysis of Uridine. *J. Am. Chem. Soc.* **2011**, *133* (25), 9923–9931.

(207) Zhang, Y.; Luo, M.; Schramm, V. L. Transition States of *Plasmodium falciparum* and Human Orotate Phosphoribosyltransferases. *J. Am. Chem. Soc.* **2009**, *131* (13), 4685–4694.

(208) Luo, M.; Li, L.; Schramm, V. L. Remote Mutations Alter Transition-State Structure of Human Purine Nucleoside Phosphorylase. *Biochemistry* **2008**, *47* (8), 2565–2576.

(209) Zhang, Y.; Schramm, V. L. Ground-State Destabilization in Orotate Phosphoribosyltransferases by Binding Isotope Effects. *Biochemistry* **2011**, *50* (21), 4813–4818.

(210) Bron, J.; Stothers, J. B. Carbon-13 kinetic isotope effects. V. Substituent effects on k_{12}/k_{13} for alcoholysis of 1-phenyl-1-bromoethane. *Can. J. Chem.* **1969**, *47* (13), 2506–2509.

(211) Werner, R. M.; Stivers, J. T. Kinetic Isotope Effect Studies of the Reaction Catalyzed by Uracil DNA Glycosylase: Evidence for an Oxocarbenium Ion−Uracil Anion Intermediate. *Biochemistry* **2000**, *39* (46), 14054–14064.

(212) Ramnarine, A. Towards the Transition State Structure of AlkA-Catalyzed *N*-Glycoside Hydrolysis using Kinetic Isotope Effects, McMaster University, 2008.

(213) Birck, M. R.; Schramm, V. L. Binding Causes the Remote [5‘-^{3}H]Thymidine Kinetic Isotope Effect in Human Thymidine Phosphorylase. *J. Am. Chem. Soc.* **2004**, *126* (22), 6882–6883.

(214) Nakano, S. I.; Kirihata, T.; Fujii, S.; Sakai, H.; Kuwahara, M.; Sawai, H.; Sugimoto, N. Influence of cationic molecules on the hairpin to duplex equilibria of self-complementary DNA and RNA oligonucleotides. *Nucleic Acids Res.* **2006**, *35* (2), 486–494.

Appendix 1. Calculation of Intrinsic SDKIE on Buffer-Catalyzed Hypoxanthine Excision by AlkA

The y-intercept of the $v_0/[E]_0$ vs. [phosphate] plot represents the rate of the reaction at 0 mM phosphate (in other words, the buffer-independent rate). The contribution from buffer catalysis increases as the buffer concentration increases. Therefore, the observed SDKIE at each buffer concentration is a function of two intrinsic SDKIEs: $\text{SDKIE}_{\text{buffer}}$, the intrinsic SDKIE on the buffer-catalyzed reaction, and $\text{SDKIE}_{\text{acid}}$, the intrinsic SDKIE on the non-buffer-catalyzed reaction. The two factors f_{buffer} and f_{acid} account for the contribution to the observed SDKIE from buffer catalysis and acid catalysis, respectively.

$$\text{SDKIE}_{\text{obs}} = f_{\text{buffer}}\text{SDKIE}_{\text{buffer}} + f_{\text{acid}}\text{SDKIE}_{\text{acid}}$$

SDKIEs and rates at [IB25] = 2 μM and pH 7 were used to calculate $\text{SDKIE}_{\text{acid}}$ and $\text{SDKIE}_{\text{buffer}}$. From linear extrapolation, $\text{SDKIE}_{\text{acid}} = 0.63$. The observed rate at 75 mM phosphate was 0.022 min^{-1} and the extrapolated rate at 0 mM phosphate was 0.0074 min^{-1}, so f_{buffer} and f_{acid} were calculated as follows.

$$f_{\text{buffer}} = \frac{0.022\,\text{min}^{-1} - 0.0074\,\text{min}^{-1}}{0.022\,\text{min}^{-1}} = 0.664$$

$$f_{\text{acid}} = \frac{0.0074\,\text{min}^{-1}}{0.022\,\text{min}^{-1}} = 0.336$$

From $\mathrm{SDKIE}_{\mathrm{acid}}$, f_{buffer}, f_{acid}, and $\mathrm{SDKIE}_{\mathrm{obs}} = 1.42$, $\mathrm{SDKIE}_{\mathrm{buffer}}$ can be calculated.

$$\mathrm{SDKIE}_{\mathrm{obs}} = f_{\mathrm{buffer}}\mathrm{SDKIE}_{\mathrm{buffer}} + f_{\mathrm{acid}}\mathrm{SDKIE}_{\mathrm{acid}}$$

Therefore,

$$\mathrm{SDKIE}_{\mathrm{buffer}} = \frac{\mathrm{SDKIE}_{\mathrm{obs}} - f_{\mathrm{acid}}\mathrm{SDKIE}_{\mathrm{acid}}}{f_{\mathrm{buffer}}}$$

$$\mathrm{SDKIE}_{\mathrm{buffer}} = \frac{1.42 - (0.336)(0.63)}{0.664}$$

$$\mathrm{SDKIE}_{\mathrm{buffer}} = \frac{1.42 - (0.336)(0.63)}{0.664}$$

$$\mathrm{SDKIE}_{\mathrm{buffer}} = 1.8$$

Appendix 2. Calculation of pK_a of W272F AlkA

The difference in activation free energies ($\Delta\Delta G^{\ddagger}$) is related to the ratio of rates by the equation:

$$\frac{k_1}{k_2} = e^{\frac{-\Delta\Delta G^{\ddagger}}{RT}}$$

k_1 is the rate of WT-catalyzed Hx excision (0.022 min^{-1}) and k_2 is the rate of W272F-catalyzed Hx excision (0.001 min^{-1}) at 75 mM phosphate at pH 7.0. T is the temperature (310.15 K) and R is the ideal gas constant (8.314 J K^{-1} mol^{-1}).

Therefore,

$$\Delta\Delta G^{\ddagger} = -RT \ln \frac{k_1}{k_2}$$

$$\Delta\Delta G^{\ddagger} = -RT \ln \frac{k_{W272F}}{k_{WT}}$$

$$\Delta\Delta G^{\ddagger} = 7970 \text{ J/mol}$$

$$\Delta\Delta G^{\ddagger} = 7.97 \text{ kJ/mol}$$

Therefore, the activation free energy change in W272F AlkA is 8 kJ/mol greater than in WT AlkA. Because proton transfer is rate-limiting at pH 7, the proton-transfer equilibrium is 8 kJ/mol less favourable in W272F AlkA than in WT AlkA.

$$\Delta\Delta G = \Delta G_{WT} - \Delta G_{W272F}$$

$$\Delta\Delta G = -7970\ \text{J/mol}$$

The equilibrium constant of a reaction is related to its free energy change by the following equation:

$$\Delta G = -RT\ln K$$

Two equilibrium constants are related to the difference in free-energy changes between the two reactions:

$$e^{\frac{-\Delta\Delta G}{RT}} = \frac{K_1}{K_2}$$

Therefore, for acid-base equilibria:

$$e^{\frac{-\Delta\Delta G}{RT}} = \frac{K_{\mathrm{a}1}}{K_{\mathrm{a}2}}$$

For acid-base equilibria in W272F and WT AlkAs:

$$e^{\frac{-\Delta\Delta G}{RT}} = \frac{K_{\mathrm{a,W272F}}}{K_{\mathrm{a,WT}}}$$

$$-\log e^{\frac{-\Delta\Delta G}{RT}} = -\log\frac{K_{\mathrm{a,W272F}}}{K_{\mathrm{a,WT}}}$$

$$-\log e^{\frac{-\Delta\Delta G}{RT}} = -(\log K_{\mathrm{a,W272F}} - \log K_{\mathrm{a,WT}})$$

$$-\log e^{\frac{-\Delta\Delta G}{RT}} = -\log K_{\mathrm{a,W272F}} - (-\log K_{\mathrm{a,WT}})$$

$$-\log e^{\frac{-\Delta\Delta G}{RT}} = \mathrm{p}K_{\mathrm{a,W272F}} - \mathrm{p}K_{\mathrm{a,WT}}$$

$$\log e^{\frac{-\Delta\Delta G}{RT}} = \mathrm{p}K_{\mathrm{a,WT}} - \mathrm{p}K_{\mathrm{a,W272F}}$$

$$\log e^{\frac{-\Delta\Delta G}{RT}} = \mathrm{p}K_{\mathrm{a,WT}} - \mathrm{p}K_{\mathrm{a,W272F}}$$

$$\log e^{\frac{-(-7970\mathrm{J/mol})}{RT}} = \mathrm{p}K_{\mathrm{a,WT}} - \mathrm{p}K_{\mathrm{a,W272F}}$$

$$1.34 = \mathrm{p}K_{\mathrm{a,WT}} - \mathrm{p}K_{\mathrm{a,W272F}}$$

$$\mathrm{p}K_{\mathrm{a,W272F}} = \mathrm{p}K_{\mathrm{a,WT}} - 1.34$$

If the rate is slower at pH 7 with W272F, then the predicted pK_a of W272F is 4.36.

The Henderson-Hasselbalch equation relates the pH and the pK_a to the ratio of an acid to its conjugate base.

$$\mathrm{pH} = \mathrm{p}K_{\mathrm{a}} + \log\frac{[\mathrm{B}]}{[\mathrm{BH}^+]}$$

From this equation, the fraction of the total that is represented by protonated species can be calculated.

$$10^{\mathrm{pH}-\mathrm{p}K_{\mathrm{a}}} = \frac{[\mathrm{B}]}{[\mathrm{BH}^+]}$$

$$f_{\mathrm{BH}^+} = \frac{1}{1+\frac{[\mathrm{B}]}{[\mathrm{BH}^+]}}$$

$$f_{\mathrm{BH}^+} = \frac{1}{1+10^{\mathrm{pH}-\mathrm{p}K_{\mathrm{a}}}}$$

$$f_{\mathrm{BH^+,WT}} = \frac{1}{1+10^{7-5.7}}$$

$$f_{\mathrm{BH^+,WT}} = 0.0477$$

$$f_{\mathrm{BH^+,W272F}} = \frac{1}{1+10^{7-4.36}}$$

$$f_{\mathrm{BH^+,W272F}} = 0.00229$$

$f_{\mathrm{BH+}}$ for the WT at pH 7 (pK_a = 5.7) is 0.0477. $f_{\mathrm{BH+}}$ for W272F at pH 7 with the predicted pK_a of 4.36 is 0.00229. The protonated fraction is 21-fold greater in the WT than in W272F. The difference in rates between the WT and W272F under identical conditions is 22-fold.